HANDBOOK

AND

PROCEEDINGS

OF THE

TENNESSEE JUNIOR

ACADEMY OF SCIENCE

2013

Sponsored by the
Tennessee Academy of Science

Edited by Jack Rhoton, Director
Tennessee Junior Academy of Science
P.O. Box 70301
East Tennessee State University
Johnson City, TN 37614
RhotonJ@etsu.edu

TENNESSEE JUNIOR ACADEMY

OF SCIENCE

ANNUAL MEETING

Belmont University

Nashville, Tennessee

Friday, April 19, 2013

Sponsored by the

TENNESSEE ACADEMYOF SCIENCE

TABLE OF CONTENTS

TENNESSEE ACADEMY OF SCIENCE OFFICERS: 2013

Mandy Carter-Lowe……..…..…….. … President
Columbia State Community College, Columbia

Kim Cleary Sadler..…….…… ...President-Elect
Middle Tennessee State University, Murfreesboro

William H. Andrews ..…….....Immediate Past President
Oak Ridge National Laboratory, Oak Ridge

Teresa Fulcher…….…….……. …….Secretary
Pellissippi State Technical Community College, Knoxville

C. Steven Murphree…….…….…….…….Treasurer
Belmont University, Nashville

Abigail M. Goosie……..…….Assistant Editor
Tennessee Academy of Science Journal, *Walter's State Community College*

TENNESSEE JUNIOR ACADEMY OF SCIENCE
Sponsored by the
TENNESSEE ACADEMY OF SCIENCE

Jack Rhoton…..……..…..Director, Tennessee Junior Academy of Science
East Tennessee State University, Johnson City

READING COMMITTEE 2012-2013

Jack Rhoton..…….…….East Tennessee State University

Gary Henson..…..……..……..East Tennessee State University

Timothy McDowell..…..…….East Tennessee State University

Chih-Che Tai..…..…….East Tennessee State University

JUDGES

M. Gore Ervin..…..……Middle Tennessee State University

E. Lewis Myles....……..…….Tennessee State University

Preston J. MacDougall..…..……...Middle Tennessee State University

James English..……..……..Lipscomb University

LOCAL ARRANGEMENTS

C. Steven Murphree..…...…….Belmont University

INSTRUCTIONS FOR PARTICIPATION IN THE
TENNESSEE JUNIOR ACADEMY OF SCIENCE

Purpose. The Tennessee Junior Academy of Science (TJAS) is designed to further the cause of science education in Tennessee high schools by providing an annual program of scientific atmosphere and stimulation for capable students. It is comparable to scientific meetings of adult scientists. The Junior Academy supplements other efforts in the encouragement of able students of science by providing one venue of stimulation and expression

Rewards and Prizes. The student's primary rewards are the honor of being selected to appear on the program, experience in presenting his/her paper, opportunity to discuss this work with other students of similar interests, membership in the Tennessee Junior Academy of Science, and publication of his/her paper in the *Handbook and Proceedings of the Tennessee Junior Academy of Science.* However, the top two student writers will receive $500 each from the Tennessee Academy of Science, and other top writers will receive $200 for each paper published in the *Handbook.* In addition, the TAS will award $500 to each of the top two writers to participate in the Annual Meeting of the American Junior Academy of Science (AJAS). The AJAS meeting is held in a different city each year. All students who present papers to the TJAS are encouraged to enter their papers in other competitive programs, such as the Westinghouse Science Talent Search and the International Science and Engineering Fair. Students are also encouraged to solicit scholarships from individuals, companies, or institutions.

Preparation of the Report. The report should be an accurate presentation of a science or mathematics project completed by the student. It should be comprehensive, yet avoid excessive verbosity. Maximum length should be 1500 words. The report and the project it describes must be original with the student, not just a review of another article. It should be obvious that the experimentation and/or observations have been scientifically made. The paper should reflect credit on the writer and the school represented.

Visual aids such as slides, mock-ups, and charts may be used in presentation of the report. **PLEASE NOTE THE FOLLOWING: ILLUSTRATIONS WITHIN THE REPORT MUST BE RESTRICTED TO TABLES AND/OR SIMPLE LINE DRAWINGS. These must be done in BLACK ON 8 ½ X 11 WHITE PAPER. COLORED FIGURES CANNOT BE PRINTED IN THE HANDBOOK. Total width of the illustration itself cannot be more than 7". Illustrations submitted with the paper MUST be originals, NOT COPIES, and MUST be BLACK AND WHITE.**

The report must be **DOUBLE-SPACED** on 8 ½" by 11" paper. Give careful attention to spelling and grammar. **IT IS VERY IMPORTANT that YOU prepare a COVER SHEET** for the report, giving **ALL** the required information as specified, INCLUDING YOUR HOME TELEPHONE NUMBER **AND E-MAIL ADDRESS.** IF YOUR PAPER SHOULD BE SELECTED FOR PUBLICATION, IT MAY BE NECESSARY FOR OUR EDITORS TO CONTACT YOU. FAILURE TO PROVIDE CONTACT INFORMATION COULD PREVENT YOUR PAPER FROM BEING PUBLISHED. The cover sheet included with this material may be duplicated as needed. Prepare an abstract to accompany your paper (not more than 100 words). **NO PAPER WILL BE CONSIDERED UNLESS IT IS ACCOMPANIED BY AN ABSTRACT.**

Scientific or Technical Report Writing. A very important phase of the research of a scientist is the effective reporting of the research project attempted and completed. The technical report is different from other kinds of informative writing in that it has a single, predetermined purpose: to investigate an assigned

subject for particular reasons. Technical reporting is done in the passive voice. Use of personal pronouns should be avoided except in rare instances. The telling portion of the research job is often underrated. Thus, communication is a very necessary part of research work. Any breakdown in communication means that the report has failed. The following functional analysis of the parts of the report is suggested to aid in organizing and presenting the results of scientific and experimental efforts.

I. Introduction
   A. Purpose of the investigation (why the work was done)
   B. How the problem expands/clarifies knowledge in the general field
   C. Review of related literature

II. Experimental procedure (how the work was done)
   A. Brief discussion of experimental apparatus involved
   B. Description of the procedure used in making the pertinent observations and obtaining data

III. Data (what the results were)
   A. Presentation of specific numerical data in tabulated or graphic form
   B. Observations made and recorded
   C. Any and all pertinent observations made that bear on the answer to the problem being investigated

IV. Conclusions (final contributions to knowledge)
   A. General contributions the investigations have made to the answer to the problem
   B. Further investigation suggested or indicated by the work

V. References –should be the **WORKS CITED ONLY** (the literature sources that are ACTUALLY **CITED** in the paper)
   A. Items arranged alphabetically by author's surname
      1. Author (surname, with initials only)
      2. Date, in parentheses
      3. Title, capitalize first work only
      4. Source: (periodical) (NO ABBREIVATIONS)
         (book) city, state of publication, publisher.

Each item in the Works Cited **MUST ALSO BE CITED WITHIN THE TEXT** of the student paper, using the parenthetical format of the APA Style Manual. Plagiarism is a serious offense, and is **not** limited to direct quotations. Any word, thought, statement, or instruction written by another author and used in the student paper must be appropriately cited in the student paper presented to the Junior Academy.

Submission of the Report. Each report must bear an OFFICIAL COVER SHEET, which may be obtained in advance from:

Director of the Tennessee Junior Academy of Science
Dr. Jack Rhoton
East Tennessee State University
Box 70301
Johnson City, TN 37614
E-mail: Rhotonj@etsu.edu

The ORIGINAL COPY of the report should arrive on or before **March 1, 2014**. The parts of each report should be stapled or clipped, not bound. Heavy covers increase the cost of postage. The student should keep a copy of the report; the original cannot be returned. (We **MUST** have the **ORIGINAL** of all papers –and illustrations- for publication.)

Selection of the Report. Each report submitted must be endorsed by a local science or mathematics teacher. The teacher should approve the report as the first member of a selection committee. IT SHOULD BE APPROVED ONLY IF IT IS OF HIGH QUALITY AND REPRESENTS THE STUDENT'S OWN WORK IN RESEARCH AND PREPARATION. The science or math faculty submitting two or more papers in a given category will be asked to serve as judges for those papers and rate them in the order of 1, 2, 3, 4, etc., according to merit before submission to the Tennessee Junior Academy of Science for final judging. The report will then be read by a committee of two or more additional scientists in the field appropriate to the report. Reports will be selected on the basis of research design (30 points), creative ability (20 points), analysis of results (20 points), grammar and spelling (20 points), and general interest (10 points).

TENNESSEE JUNIOR ACADEMY OF SCIENCE CALENDAR FOR 2014

March 1	Final Date for Receiving Reports
March 20	Completion of Report Evaluation
March 30	Mailing of Invitations
April 25	Annual Meeting – Nashville

RESEARCH GRANTS FOR SCIENCE PROJECTS BY HIGH SCHOOL STUDENTS

The Tennessee Academy of Science has available a limited number of small research grants ($100-$300 per student) to assist high school students involved in developing scientific projects for the TJAS program. These grants are intended to be need-based. That is, we want to support good proposals from motivated students of adequate ability, where lack of some outside financial support might result in a poor project or possibly no project at all. These grants should not be regarded as competitive merit awards for outstanding proposals or outstanding students, and should not be given to students whose families, or whose project mentors, can readily provide the resources needed. For instance, a project being conducted under the mentorship of a university professor would not, in general, be a good choice for a TAS grant, no matter how able the student and how good the proposed project. It is intended that the TAS research grants program create opportunities for adequately motivated students with access to limited resources to conduct significant, competitive projects. The Tennessee Academy of Science will depend on the

sponsoring science or math teachers to provide input into the decision-making process as it concerns the need of applying students and worthiness of their proposed projects.

The application form for the TAS research grant included in these materials may be duplicated as needed. Please note the deadline for receiving grant applications is ***NOVEMBER 15, 2013***. However, the earlier grant applications are received, the sooner grant application funds can be distributed. If you desire further information concerning the TAS research grants program, please write to Dr. Jack Rhoton, Division of Science Education, Box 70684, East Tennessee State University, Johnson City, TN 37614 or E-mail: Rhotonj@ETSU.edu.

TENNESEE JUNIOR ACADEMY OF SCIENCE
SPRING MEETING – 2014

The 69th Annual Meeting of the Tennessee
Junior Academy of Science will be held in
Nashville (Belmont University) on Friday, April 25, 2014

All Tennessee high schools are invited to participate in the TJAS program leading up to the spring meeting. The program provides state-wide and national recognition for high school students' investigative or research-type science projects

TENNESSEE JUNIOR ACADEMY OF SCIENCE REGULATIONS

The following regulations have been developed to govern the Tennessee Junior Academy meeting by the Standing Committee on Junior Academies of the Academy Conference. Papers must be of a research problem type, with evidence of creative thought. Papers presented should be suitable for publication (typewritten, double-spaced, one side of paper only, name and address on each sheet) and between 1000 and 1500 words in length. Oral presentation will be limited to 10 minutes. Projectors and other audiovisual equipment will be available. Questions on paper presentation will be limited to 3 minutes. All papers should be postmarked **NO LATER THAN MARCH 1, 2014**, and sent to Dr. Jack Rhoton, PO Box 70684, East Tennessee State University, Johnson City, TN 37614. Certificates will be presented to all participants. Sponsoring schools or clubs should have insurance coverage to protect school participants. The Tennessee Junior Academy of Science can assume no responsibility in this matter.

WHAT YOU CAN DO NOW

If there is no science club at your high school, why not start one? A science club will provide many opportunities to work on problems that will be fun and relaxing. The ready, mutual exchange of ideas can provide a challenging experience in proposing, designing, and completing research into the unknown. Begin now to work on a scientific project to present at the next annual meeting of your local, state, and national Junior Science Clubs. For further information on the Junior Academy program, contact:

Tennessee Junior Academy of Science
Dr. Jack Rhoton, Director
PO Box 70301
East Tennessee State University
Johnson City, TN 37614
Phone: 423-439-7589
E-mail: Rhotonj@etsu.edu
Fax: 423-439-7530

PURPOSE OF THE ACADEMIES OF SCIENCE

The purpose of the various state and municipal Junior Academies is to promote science as a career at the secondary school level. The basic working unit is the science club or area in each school where the extracurricular science projects and activities are supervised by science teachers/sponsors. The American Junior Academy serves a state or city organization much the same as do the professional societies, and it functions in a similar manner; e.g., holding annual meetings for presenting research papers. The parent sponsor of a Junior Academy of Science is the State Academy of Science. The primary activity of the American Junior Academy of Science is the Annual Meeting held with the Annual Meeting of the American Association for the Advancement of Science and the Association of Academies of Science. Top young scientists in each state or city academy are encouraged to present papers and exchange research ideas at the national level. Tours and social hours are also arranged.

DIRECTORS OF THE TENNESSEE JUNIOR ACADEMY OF SCIENCE

1942-2013

The Tennessee Academy of Science has been the sponsor of the Tennessee Junior Academy of Science since its initial organizational meeting on the Vanderbilt University campus in 1942.

The Directors of the Junior Academy of Science since 1942 are as follows:

Dr. Frances Bottom – 1942-1955…….. George Peabody College
Nashville

Dr. Woodrow Wyatt – 1955-1958……...The University of Tennessee
Knoxville

Dr. Myron S. McCay – 1958-1963……..The University of Tennessee
Knoxville

Dr. Robert Wilson – 1963-1965……..The University of Tennessee
Chattanooga

Dr. John H. Bailey – 1965-1976…….East Tennessee State University
Johnson City

Dr. William N. Pafford – 1976-1992……..East Tennessee State University
Johnson City

Dr. Jack Rhoton – 1992-present…….….East Tennessee State University
Johnson City

TENNESSEE JUNIOR ACADEMY OF SCIENCE
Sponsored by the
TENNESSEE ACADEMY OF SCIENCE
Annual Meeting

Belmont University
Nashville, Tennessee
Friday, April 19, 2013

PROGRAM

9:00 –9:30 a.m.	Registration
9:30 – 9:40 a.m.	Welcome
9:40 –11:30 a.m.	Paper Presentations
11:35 a.m.	Special Presentations
12:00 –1:00 p.m.	Lunch
1:30 –4:00 p.m.	Paper Presentations
4:00 p.m.	Adjournment

TENNESSEE JUNIOR ACADEMY OF SCIENCE

Papers to be Presented at Annual Meeting
Title of Paper, Student's Name, School, City

A FILTER TODAY DEEPS POLLUTANTS AWAY: A STUDY OF NANOFIBER BASED STORMWATER FILTRATION — **Environmental Management**

Darby Schumacher
Baylor School, Chattanooga

BIOMASS TO BIOFUELS: NEW SOURCES TO MAKE ETHANOL IN THE PLACE OF CORN — **Environmental Management**

Rachel Baker
Camden Central High School, Camden

THE EFFECTS OF HIGH CHLORINE ON THE FIVE SENSES BEFORE AND AFTER PHYSICAL ACTIVITY — **Chemistry**

Jada Hampton
Cleveland High School, Cleveland

THE ROLE OF THE α_aMANNOSE RECEPTOR AND TOLL-LIKE RECEPTOR 2 in TNFά AND IL-6 PRODUCTION — **Cell Biology**

Elizabeth Li, Michelle Lu, Oge Onuh, & Shu Zhang
School for Science and Math at Vanderbilt, Nashville

GENETIC AND FUNCTIONAL CHARACTERIZATION OF ß-GLUCOSIDASE IN FUNGAL SPECIES UNDER ASSORTED CONDITIONS — **Biology**

Qiaozhi Guo, Tiannan Zhou, Jennifer Peek, & Michael Kessler
School for Science and Math at Vanderbilt, Nashville

A POSSIBLE CONFIRMATION OF A PLANET ORBITING STAR K015475431 — **Astronomy**

Benjamin D. Firth
Sullivan South High School, Kingsport

BIODEGRADATION OF QUATERNARY AMMONIA COMPOUNDS BY BIOFILM AND FREE-LIVING BACTERIA — **Microbiology**

Zheer Ahmed
Martin Luther King Academic Magnet High School, Nashville

DETERMINING PLANT SPECIES BY USE OF AN ANDROID APPLICATION — **Computer Science**

Reeta Bandyopadhyay, Angelica Coleman, Young-Hun Kim, & Brennan Steele
School for Science and Math at Vanderbilt, Nashville

WATER QUALITY IN SELECTED WATERSHEDS IN BENTON COUNTY, TENNESSEE — **Environmental Management**

Sam Hedge
Camden Central High School, Camden

ALLELOPATHIC EFFECTS OF THE *Juglans nigra* (BLACK WALNUT) ON THE PEA PLANT — **Botany**

Megan Gerstner & Katie Swaringen
Pope John Paul II High School, Hendersonville

THE EFFECTS OF TEMPERATURE ON INSECT ACTIVITY DURING FLESH DECOMPOSITION — **Forensics**

Chloe Kirkpatrick & Emily McRen
Pope John Paul II High School, Hendersonville

REMOTE SENSING OF CARBON DIOXIDE IN THE LOWER ATMOSPHERE — **Environmental Science**

Ryan Dunaway, Jackson Ferrell, Rob Edwards, & Nathan Beeten
School for Science and Math at Vanderbilt, Nashville

NATURAL ANTIBIOTIC RESISTANCE IN CAVE STREAM BACTERIAL COMMUNITIES — **Microbiology**

Petra Byl & Diana Neculcea
Hume-Fogg High School, Nashville

THE EFFECTS OF L ITHIUM CHLORIDE ON THE FEEDING HABITS OF THE ELIMIA SNAIL — **Zoology**

Victoria Dolan & Jordan Lee
Pope John Paul II High School, Hendersonville

THE GOOD AND BAD EFFECTS OF FERTILIZER ON SUNFLOWERS — **Botany**

Taylor Cook
Northwest High School, Clarksville

THE EFFECTS OF ANGLE OF ATTACK ON THE LIFT CREATED BY AN AIRFOIL — **Physics**

Lachlan Hassman & Eliza Gooding
St. Andrew's-Sewanee School, Sewanee

WATER TURBIDITY HAS NO EFFECT ON PHEROMONE COMMUNICATIONS IN AQUATIC FLATWORMS — **Zoology**

Kathryn Pickrell & John Crenshaw
Hume-Fogg High School, Nashville

THE EFFECTS OF VARYING GLUCOSE CONCENTRATIONS ON CELLULAR GLYCOLYTIC RATES — **Engineering**

Regan Givens
Pope John Paul II High School, Hendersonville

THE LONG-TERM EFFECTS OF AIRPORT RUNOFF ON URBAN STREAM QUALITY AND HABITABILITY IN NASHVILLE, TENNESSEE — **Environmental Science**

Jansen Gibson, Thomas Metke, Sabrina Brewer & Cristian Vera
School for Science and Math at Vanderbilt, Nashville

TESTING THE EFFECTIVENESS OF LUMINOL IN THE DATING OF SKELETAL REMAINS — **Chemistry**

Katherine Watson & Skyler Cochrane
School for Science and Math at Vanderbilt, Nashville

Students Who Submitted Papers to the Tennessee Junior Academy of Science

Ahmed, Zheer; Martin Luther King Academic School, Nashville
Baker, Rachel; Camden Central High School, Camden
Bandyopadhyay, Reeta; School for Science and Math at Vanderbilt, Nashville
Beeten, Nathan; School for Science and Math at Vanderbilt, Nashville
Bilbrey, Emma; School for Science and Math at Vanderbilt, Nashville
Brewer, Sabrina; School for Science and Math at Vanderbilt, Nashville
Byl, Petra; Hume-Fogg High School, Nashville
Cochrane, Coleen; School for Science and Math at Vanderbilt, Nashville
Coleman, Angelica; School for Science and Math at Vanderbilt, Nashville
Cook, Taylor; Northwest High School, Indian Mound
Crenshaw, John; Hume-Fogg High School, Nashville
Dolan, Victoria; Pope John Paul II High School, Hendersonville
Dunaway, Ryan; School for Science and Math at Vanderbilt, Nashville
Edwards, Nathanael; Pope John Paul II High School, Nashville
Edwards, Rob; School for Science and Math at Vanderbilt, Nashville
Ferrell, Jackson; School for Science and Math at Vanderbilt, Nashville
Firth, Benjamin; Sullivan South High School, Kingsport
Gerstner, Megan; Pope John Paul II High School, Gallatin
Gibson, Jansen; School for Science and Mat at Vanderbilt, Nashville
Givens, Regan; Pope John Paul II High School, Hendersonville
Gooding, Eliza; St. Andrew's-Sewanee School, Sewanee
Guo, Qiaozhi; School for Science and Math at Vanderbilt, Nashville
Gutierrez, Hector; Cleveland High School, Cleveland
Hampton, Jada; Cleveland High School, Cleveland
Harris, Sarah; Camden Central High School, Camden
Hassman, Lachlan; St. Andrew's- Sewanee School, Sewanee
Hedge, Sam; Camden Central High School, Camden
Kessler , Michael; School for Science and Math at Vanderbilt, Nashville
Kilpatrick, Chloe; Pope John Paul II High School, Goodlettsville
Kim, Young-Hun; School for Science and Math at Vanderbilt, Nashville
Kondor, John; Cleveland High School, Cleveland
Lee, Jordan; Pope John Paul II High School, Mt. Juliet
Lew, Lauren; Hume-Fogg High School, Nashville
Li, Elizabeth; School for Science and Math at Vanderbilt, Nashville
LoMonaco, Elizabeth; St. Andrew's-Sewanee School, Sewanee
Lu, Michelle; School for Science and Math at Vanderbilt, Brentwood
McRen, Emily; Pope John Paul II High School, Henderson
Metke, Thomas; School for Science and Math at Vanderbilt, Hermitage
Neculcea, Diana; Hume-Fogg High School, Nashville
Neenan, Baker; Hume-Fogg High School, Nashville
O'Dell, Natalie; School for Science and Math at Vanderbilt, Nashville
Onuh, Oge; School for Science and Math at Vanderbilt, Nashville
Peek, Jennifer; School for Science and Math at Vanderbilt, Nashville
Pickrell, Kathryn; Hume-Fogg High School, Nashville
Schumacher, Darby; Baylor School, Hixson
Steele, Breenan; School for Science and Math at Vanderbilt, Antioch

Swallow, Sophie; St. Andrew's-Sewanee School, Sewanee
Swaringen, Katie; Pope John Paul II High School, Hendersonville
Tyus, David; Hume-Fogg High School, Nashville
Vera, Christian; School for Science and Math at Vanderbilt, Hermitage
Watson, Katherine; School for Science and Math at Vanderbilt, Nashville
Yang, Yenny; Hume-Fogg High School, Brentwood
Zhang, Shu; School for Science and Math at Vanderbilt, Nashville
Zhou, Tiannan; School for Science and Math at Vanderbilt, Nashville

Papers of Excellence

A Filter Today Keeps Pollutants Away: A Study of Nanofiber Based Storm Water Filtration

Darby Schumacher
Baylor School, Chattanooga

Abstract

Pollution of both inland and coastal waterways is a worldwide issue adversely affecting both aquatic life and human safety. Urbanization and land development have increased hard surface run-off and water sustainability has been negatively affected. The EPA estimates that 30% of all known water pollution is attributable to storm water runoff. This storm water runoff from airports, agriculture, roads, construction, and other non-point source pollution sites contributes to high levels of pathogens, heavy metals, sediments, and chemical pollution. This project engineered and analyzed an innovative, low cost nanofiber based water filter designed to mitigate water pollution within current storm water runoff infrastructure. Two nylon polymer nanofiber and activated carbon based filters with differing densities were prototyped and built. Thorough water testing determined that the filter incorporating activated carbon and nanofiber material with a density of 2 grams per square meter had minimal water flow rate reduction of 15% and high pollution mitigation efficiency, reducing pollutant levels 51-100%. This novel filter is a practical, cost effective solution for storm water runoff pollution and reduces pollutant and pathogen levels below EPA recreational water use limits. Further research and filter engineering has led to the expansion of the potential uses of the filtration system to include clean residential water capture via downspout, rain barrel filtration, possible portability in emergency situations, and commercial use within the City of Chattanooga, Tennessee so that businesses can operate in a sustainable and socially responsible manner by practicing environmental stewardship.

Introduction

Pollution of our waterways has been, and is currently, an important issue. Water pollution not only adversely affects aquatic life, but also human safety during recreational uses of the water. Storm water runoff from roads, constructions sites, agriculture, and other non-point pollution is a main factor in high nutrient, pathogen, metal, sediment, and chemical levels. Fifteen percent of all surface waters in the Middle Tennessee-Chickamauga Watershed are listed as impaired according to the Clean Water Act of 1998. A significant source of this impairment is from storm drain runoff. Ninety five percent of storm water runoff in Chattanooga flows untreated into the Tennessee River, contaminating my favorite place to spend time during the summer months. Too many local waterways are unsafe for human and aquatic life. This is why I chose to build a filter to fit inside, or around, storm drain outfalls to decrease the amount of sediment, excessive nutrients, metals, pathogens, and various other pollutants that can make water harmful to aquatic life and humans.

Citico Creek in Chattanooga

Several years ago I became interested in Storm water pollution after volunteering with a pollutant monitoring program called First Flush in the Monterey Bay area. I designed and built a water filter that mitigated the amount of pollutants that flowed directly from the storm drain system into the Pacific Ocean. I tested an activated carbon filter, a sand filter, and a foam filter in that project, and found carbon to be the filter material that worked most efficiently for reducing the levels of nutrients harmful to aquatic life in high concentrations, such as phosphates and nitrates.

For this project, I decided to design and build a more complex filter that should mitigate storm water pollutant levels at a higher percentage rate, as it is a significant issue in Chattanooga. I also wanted to expand the scope of my testing beyond my previous testing for nutrient reduction and perform tests measuring the change in turbidity, E. Coli and coliform. From previous testing, I knew that activated carbon was a factor I wanted to use in my filter, but another, more advanced filtration material was needed to improve pollutant reduction. To further develop this water filter, I chose to add nanofiber materials.

Nanofibers: Nanofibers are part of the new, rapidly growing field of nanotechnology. They are fibers that have diameters smaller than 1000 nanometers. They are prepared through an innovative

electrospinning technique. Synthetic nanofibers are produced from a variety of polymer materials such as nylon, acrylic, and polycarbonate. Nanofibers are created through a process known as electrospinning, where electrical charges are used to draw fine fibers from a liquid. New nanofiber water and air filters are on the market because nanofibers are an optimal medium for filtration. This is due to their small size of between 20-200 nanometers, about 1,000 times thinner than a human hair, and their high surface area-to-mass ratio. Nanofiber materials are measured in grams of nanofibers per square meter (gsm), and the higher the gsm, the more surface area of nanofibers are on the material, making it a less permeable textile.

The two nanofiber materials acquired for this experiment were provided by an innovative nanotechnology company in Chattanooga, eSpin Technologies. Both nanofiber materials were electrospun from nylon polymers in a 150 nanometer range. The nanofibers were spun onto a polyester material that gives it structural stability and mechanical strength. One of the nanofiber materials is composed of a top layer of 2 gsm of nanofibers, and the other is 10 gsm. The 2 gsm nanofiber material is projected to eliminate particles 0.3 microns or greater at a 40% efficiency, and the 10 gsm nanofiber material is projected to eliminate particles 0.3 microns or greater at a 99.999% efficiency, according to Dr. Jayesh Doshi, founder and owner of eSpin Technologies. Two different materials were tested because it was believed there could be a water flow rate issue with the denser nanofiber material due to its plastic-like properties, and less permeable nature.

Objective: The objective of this experiment is to test each of the water filters on their filtering efficiency of polluted storm water runoff that would otherwise flow untreated into our very own Chattanooga creeks and rivers. I hope that the conclusions from this project will serve as an aid to our local storm water management practices and will help our city leaders in determining a way to reduce water pollution because "A Filter Today Keeps Pollutants Away."

Hypothesis: The hypothesis is that nanofiber filters will significantly reduce the nutrient, pathogen, sediment, heavy metal, and pollutant levels in storm water when compared to the unfiltered water from storm drain outfall locations. Filter B, made with both activated carbon and the thicker, 10 gsm layer of nanofiber material is predicted to decrease the turbidity and all tested contaminant levels the most because of the higher density of nanofibers spun onto the polyester medium. Filter A, made with both activated carbon and the thinner, 2 gsm, layer of nanofiber material, is predicted to also decrease turbidity and pollutant levels, but not as significantly as Filter B because of the larger pore sizes in this filter, due to less nanofibers overlapping on the surface.

Materials and Methods

Materials: Items used in constructing the filter models were the following: 4 flexible rubber pipe couplings (3in. by 2in.), a filter sock for pipes (purchased at Lowes), scissors, a sewing machine, thread, a permanent marker, needles, activated carbon, 2 12.5cm nylon polymer 150-nanometer range 2 gsm nanofiber circles, 2 12.5cm nylon polymer 150-nanometer range 10 gsm nanofiber circles, pipe sock material, masking tape, 4 17.3cm flexible window screening circles, 4 15cm flexible window screening circles, a 2-decimal place electronic balance, and 1 3in. diameter PVC pipe (approximately 30cm long). To test flow rate, a one-gallon jug and a hose were used, as well as a stopwatch. To sterilize collection jars, a pot, a stove, water, and glass jars were used. To collect samples, a cooler, ice packs, the sterilized collection bottles, rubber gloves, a Vernier portable LabQuest, a Vernier temperature probe, a timer, and paper towels were used. To test for nutrients, turbidity, pH, and carbonate hardness, the following were used: distilled water, refrigerator, 1 cup measuring cup, a Vernier LabQuest USB cable, 10 sterilized plastic pipettes, a timer, a computer, the LoggerPro software interface, a Vernier portable LabQuest, a Vernier turbidity sensor kit, a Vernier ammonium ion-selective electrode kit, a Vernier nitrate ion-selective electrode kit, an API Reef Master kit Aquarium edition, an API Reef Master kit Marine edition, pH strip tests, and paper towels. To test for heavy metals, the following were used: distilled water, 3 sterilized wide mouth beakers, 3 small sterilized beakers, a timer, SenSafe heavy metal dip strips, a Copper 1000 ppb solution metal standard, and a Trace Metals Standard (500 ppm aluminum, 250 ppm vanadium, 100 ppb zinc, arsenic, beryllium, chromium, cobalt, copper, iron, lead, manganese, nickel, zinc). To test for E. Coli and Coliform bacteria, the following were used: distilled water, 10 IDEXX Quanti-trays, 4 sterilized quantitative 10mL pipette shafts, an orange pipette bulb, 10 IDEXX reagent packets, 10 sterilized 100mL bottles, a Quanti-tray rubber sealing tray, a Quanti-tray MPN table, a biohazard disposal bag, a black light, and an incubator.

Procedure: Nanofiber materials were obtained from eSpin, the manufacturer in Chattanooga. Other filter materials and water test kits were purchased at Lowes and a local pet shop. The SenSafe heavy metal dip strips were ordered from FilterWater.com. Water collection and testing materials and equipment came from my house or were borrowed from my high school's lab.

I organized a box of water collection and testing equipment in preparation for an appropriate rainfall event and stored it all in a large container with a lid for easy access. It included: umbrella, container of distilled water, 2 sterilized collection jars for each sample location, stopwatch, notebook, pen, rubber gloves, ice or blue ice blocks (kept in freezer until leaving for water sample collection),

cooler, rain boots, rain gear, flashlight, a charged Vernier LabQuest, a temperature probe, camera (to document the sampling).

Filter Design: My water filters were redesigned several times and finally looked like the picture to the left. To build the filter, I cut 4 circles with 17.3cm diameter and 4 circles with 15cm diameter out of the metal screening. I then cut 2 circles with 12.5cm diameter out of the 2 gsm nanofiber material and did the same with the 10 gsm nanofiber material. I cut four sections of the pipe sock material, each about 17cm long. I traced the inner diameter of the narrower end of the pipe coupling onto the center of each piece of pipe filter sock. Using the electronic balance, I massed out four quantities of 20.00 grams of activated carbon and set each aside. Using a sewing machine, I stitched around the traced circle, leaving a small opening so I could fill it with activated carbon. I then hand stitched the pouch shut. I made four of these pouches. To assemble a filter, I unscrewed the metal fastener on the narrower end of the pipe coupling and removed it. I placed the smaller diameter metal screening directly on top of the 2in. hole on the pipe coupling. I layered an activated carbon pouch on top, ensuring that the carbon circle was centered within the pipe opening, and then placed a 2 gsm nanofiber circle over the activated carbon pouch with the "sticky and rough" side facing towards the carbon pouch. Then I added the large metal screening circle and pushed the metal fastener back on and tightened it. I made another 2 gsm filter and then I made two 10 gsm nanofiber material filters in the same way.

Model of Filter Design

Figure A

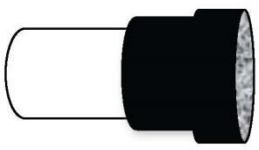

Figure A: The black coupling attaches to the pipe to secure the filter and withstand pressure. The larger end of the coupling contains the material components of the filter.

Figure B

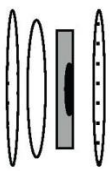

Figure B: The order of layers in the filter. Water flows from left to right. The water passes through metal screening, followed by nanofiber material, an activated carbon pouch, and a final layer of screening.

Collection: I monitored the weather until there were 3-4 dry days followed by a significant rainfall event of greater than one half inch. When this rainfall occurred, I put the box of equipment in the car, drove to the predetermined water collection sites, collected the water samples, measured the temperature, put the samples on ice in the cooler and returned home.

Citico Creek Watershed Water Sampling Locations

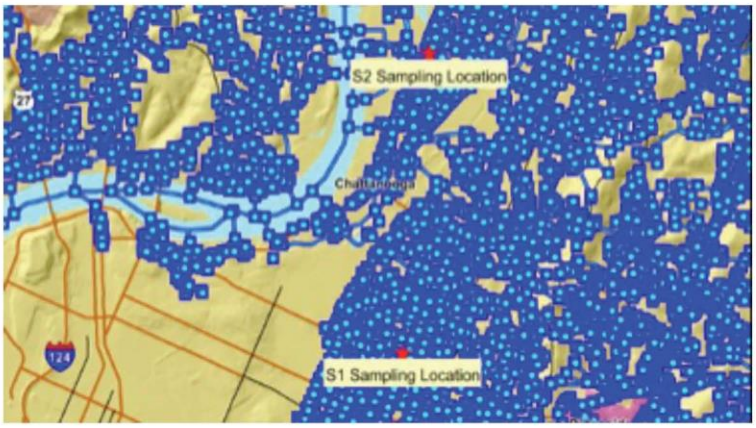

Testing: Within the required 24 hours, I filtered the polluted Citico Creek water with each of the nanofiber filters and tested all the samples for turbidity, ammonium, nitrates, ammonia, phosphates, carbonated hardness, and nitrites being careful to follow correct testing protocols.

Testing with the Vernier Probe

Testing with the API Reef Test Kit

The next day I packed the original and filtered water samples on ice and drove to the Tennessee-American Water Chemical Laboratory to complete the E. Coli, Coliform, and heavy metal tests.

Water Samples Prepared for Testing

Utilizing Quanti-trays and following all laboratory testing and safety protocols I prepared the water samples for incubation with the help of Kim Durham, one of the laboratory technicians. I also mixed a 10% dilution of both S1 samples in case the Coliform and E. Coli levels were too high in undiluted samples to discern any appreciable filter effectiveness. I put all the Quanti-trays into a 34.9-degree incubator for 24 hours.

I then gathered the materials needed for heavy metals testing: SenSafe Heavy Metals Strips, clean beakers, paper towels, a bottle of trace metals standard, a bottle of copper standard, pH strips, rubber gloves, and goggles. Following the SenSafe package directions, I tested a 20mL sample of trace

metals standard before and after running it through each of my nanofiber filters, making sure to use a new sample for each filter. After thoroughly cleaning the filters with distilled water, I repeated the procedure with 1000 ppb copper standard. Then, because the results seemed skewed, I tested the acidity of both metals standards using pH strips.

Testing filter for Heavy Metals Mitigation

I returned to the Tennessee-American Water Chemical Laboratory 24 hours later to read the Quanti-tray test results. I brought the cooler with ice and unfiltered and filtered water samples in case any testing needed to be repeated or new testing was required. I counted the yellow squares on each Quanti-tray test and recorded the results. Since the Coliform levels were so high, the E. Coli and Coliform testing had to be repeated with more diluted water samples. The same safety and testing protocols were followed and the Quanti-trays were again put into the 34.9 degree incubator for 24 hours. I returned to the Tennessee-American Water Chemical Laboratory to count the yellow squares on the Quanti-Trays and calculate the results taking into account the dilution factor.

Quanti-trays showing very high Coliform levels

Results

The two nanofiber-based filters designed in this project were tested for their water flow rate impairment and contaminant mitigation efficiency and also their percentage decrease of pollutants in comparison to the unfiltered storm water from S1 and S2.

Phosphates: Filter A decreased the phosphate level by 50% and Filter B decreased it by 75% in the tests for the S1 location. S2 results were a constant 0.25 ppm for the unfiltered, Filter A, and Filter B water.

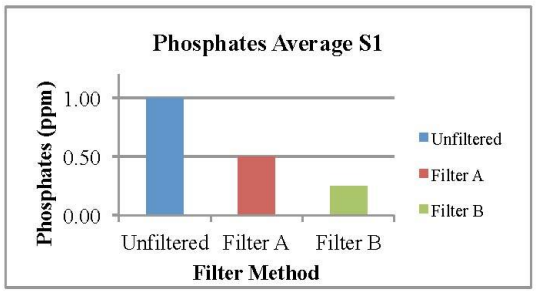

Ammonium: For the storm water outfall location S1, Filter A decreased the ammonium level by 46% and Filter B decreased it by 54%. In the S2 testing, Filter A decreased the ammonium level by 55% and Filter B decreased it by 80%.

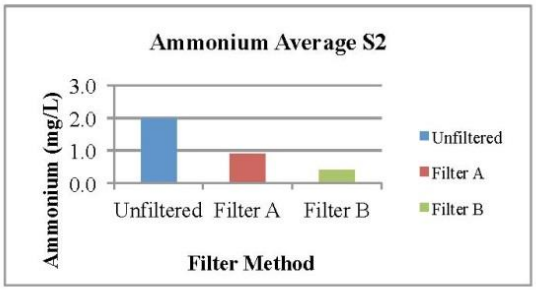

Nitrates: For the storm water samples collected for S1, Filter A decreased the nitrate level by 24% and Filter B decreased it by 45%. For storm water samples collected from S2, Filter A decreased the already low nitrate level by 41%, and Filter B decreased it by 47%.

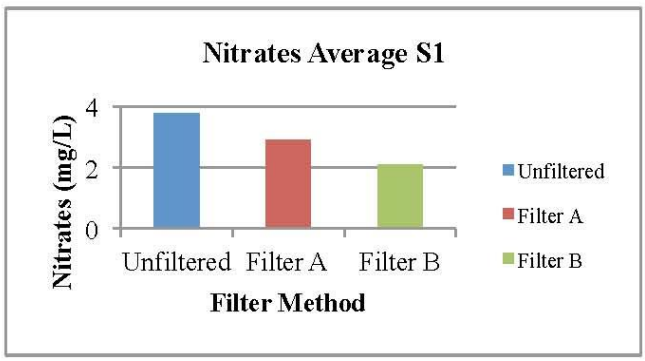

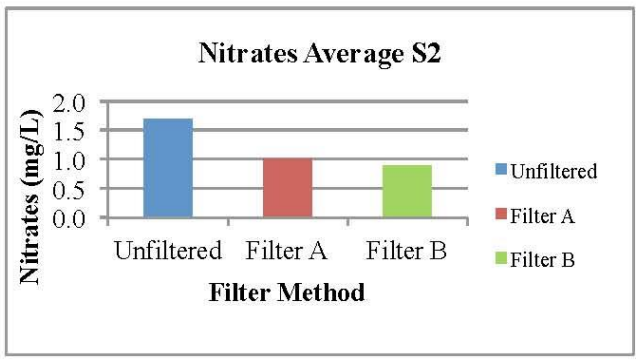

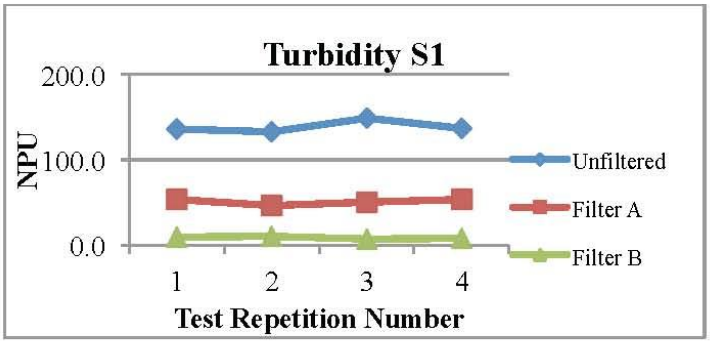

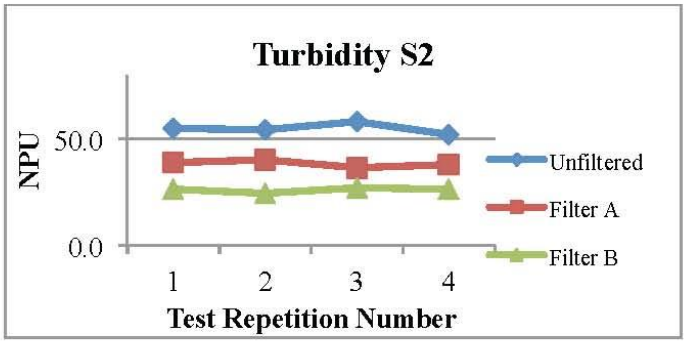

Turbidity: Before filtration, the water was a murky brown, and there were so many tiny particles that in a glass jar, something on the other side of the jar was not visible. For the S1 storm water, Filter A eliminated 63% of the particles, and Filter B eliminated 94%. For the S2 storm water, where the unfiltered water was not nearly as murky or turbid as S1, Filter A reduced the turbidity by 30%, and Filter B reduced it by 52%.

Carbonate Hardness: Carbonate hardness is the measure of alkalinity in water and is tested by the presence of carbonate and bicarbonate ions. Using a home aquarium test kit, both filtered and unfiltered water from S1 and S2 were tested. The carbonate hardness level for S1 was 89.5 ppm for unfiltered storm water, and the level for Filter A did not change. The level dropped to 71.6 ppm when filtered through Filter B. The unfiltered S2 storm water had a carbonate hardness level of 35.8 ppm. Filter A increased this level to 53.7 ppm, and Filter B also increased the level, but to 71.6 ppm.

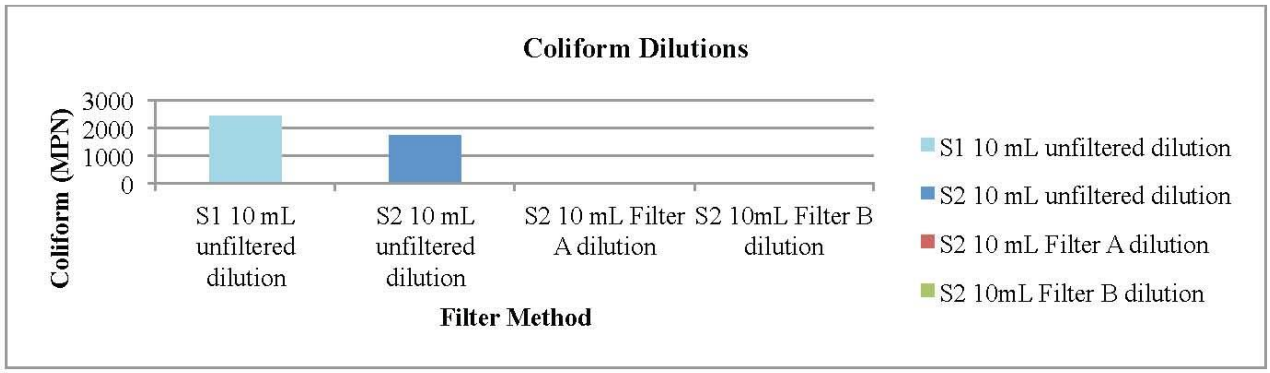

Coliform: The IDEXX tests used to determine coliform were Quanti-trays that are read by counting yellow squares on two different sections of each tray and then matched on a table to get the amount of coliform in the water. Because the unfiltered, Filter A, and Filter B water for S1 and S2 storm water all had Quanti-trays where each square was yellow, the tests were repeated with dilution factors of 10. The 10mL dilution of S1 still had a full reading, which matches up to greater than 2419.6 MPN, which exceeds the highest readings that a Quanti-tray can accurately measure. The 10mL dilution of S2 was

1733 MPN, meaning that not all squares were yellow, so this test can be considered accurate. The S2 Filter A and Filter B water was also used in a 10mL dilution. After incubation, Filter A had a reading of 10.0 MPN and Filter B had a reading of 30.0 MPN. This demonstrates that Filter A mitigated 99.4% of coliform and Filter B mitigated 98.3%.

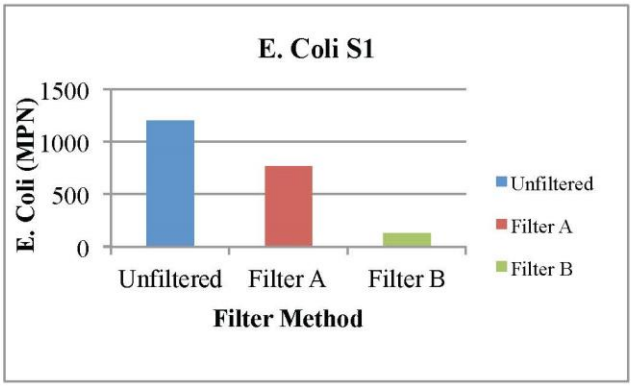

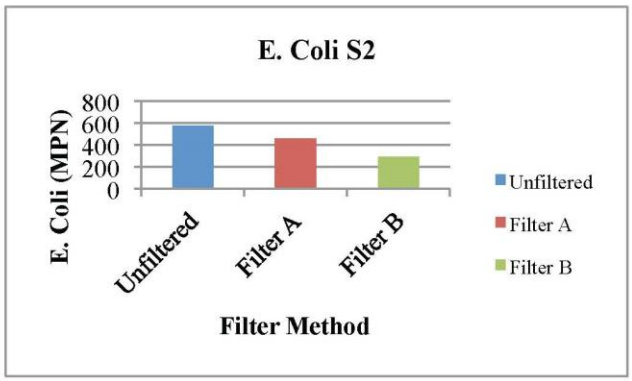

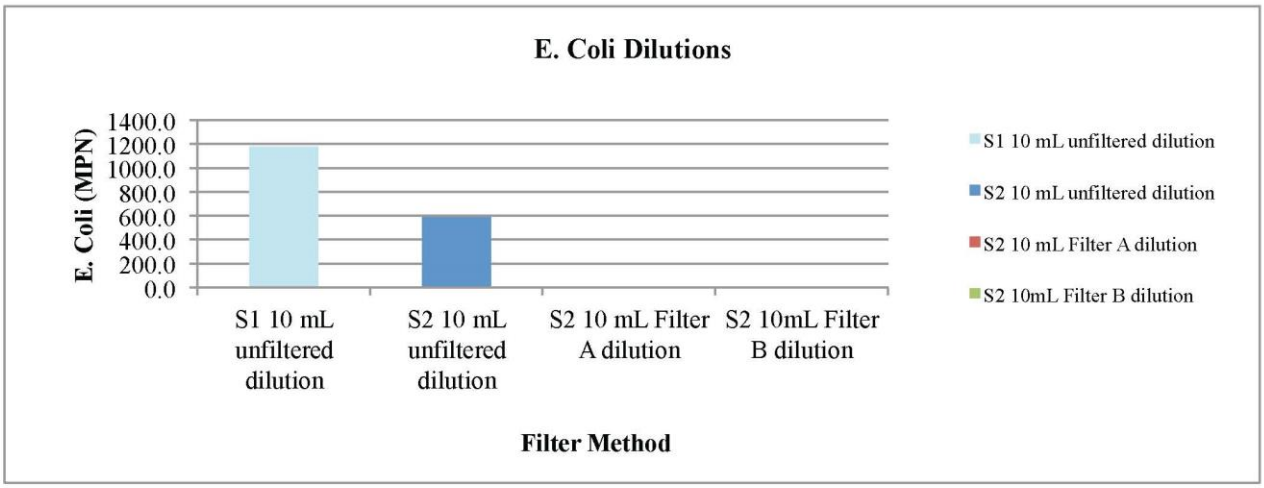

E. Coli: E. Coli was tested in the same Quanti-trays as the coliform, but was detectable under a black light. If a square fluoresced, it was an indicator than E. Coli was present. For the S1 location, Filter A reduced this high level by 36%, and Filter B reduced it by 89%. Using samples taken from the S2 location, the unfiltered E. Coli level was 579.4 MPN. Filter A reduced this level by 20%, and Filter B reduced this level by 50%. The 10mL dilutions were also placed under the black light to record E. Coli levels. The 10mL dilution of unfiltered S1 storm water was 1178.0

E Coli detection revealed under blacklight

MPN. The 10mL dilution of unfiltered S2 storm water indicated that 591.0 MPN on E. Coli was present in 100mL. When the 10mL dilutions of Filter A and Filter B for the S2 locations were placed under the black light, neither Quanti-tray fluoresced, indicating no presence of E. Coli.

pH: The S1 location had a pH of 7.6 when left unfiltered. Filter A changed this level to 7.2, but Filter B did not, and the test result was the same as the unfiltered water, a pH of 7.6. The S2 location unfiltered pH was 7.0. The S2 storm water filter through Filter A also had a pH of 7.0, but the storm water filtered through Filter B had a pH of 6.8.

Nitrites: Unfiltered, Filter A, and Filter B water for the S1 location had readings of 0.0 ppm. Unfiltered, Filter A, and Filter B water for the S2 location had readings of 0.0 ppm.

Ammonia: The unfiltered storm water from S1 had 0 ppm of ammonia. Filter A and Filter B for S1 also had 0 ppm. For the S2 location, unfiltered, Filter A, and Filter B water all had readings of 0.25 ppm.

Heavy Metals: A Trace Metal Standard was poured through the filters to determine if nanofiltration was a practical way for reducing heavy metal particles. Using the SenSafe Heavy Metals strips, the Trace Metal Standard had a reading of between 50 and 100 ppb. This solution was poured through Filter A and the color of the tab that should be compared to the color chart, was a rusty brown, which read at between 200 and 400 ppb. The same test through Filter B produced a similar rusty brown color, although lighter than the Filter A strip, showing that the heavy metal level was between 200 and 300 ppb.

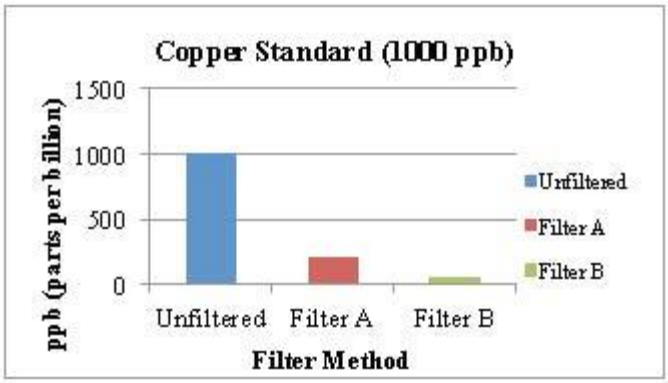

Heavy metals testing with SenSafe Strip

Copper: Another metal standard was used to test the heavy metal filtration of both Filter A and Filter B. This solution was a 1000 ppb copper metal standard. The color tab registered as 1000 ppb on the color chart. When poured through Filter A, the filtered solution produced a reading of 200 ppb, which is an 80% reduction of copper. When poured through Filter B, the reading was 50 ppb, which is a 95% reduction of copper.

Discussion

The results from this experiment showed that both Filter A and Filter B did mitigate nutrient and contaminant levels in stormwater through a number of tests of nutrient, bacteria, and sediment levels. On average, Filter A reduced pollutant or excessive nutrient levels by 51% and Filter B reduced pollutant or excessive nutrient levels by 73%.

Nutrients and other water quality factors: The phosphate testing results show that both Filter A and Filter B had a mitigating effect on the phosphate level on the S1 sample, but not on the S2 sample. In the S2 testing, the unfiltered level was so low that the home test kit was most likely not able to read such slight changes because the unfiltered S2 storm water read at the lowest detectable level. The S1 results show that filtration of phosphates was possible with a nanofiber based filter design. The ammonium test results show that Filter A and Filter B had an effect on ammonium levels for both the S1 and S2 samples. The Vernier probes used were able to detect small amounts at a consistent level, proving to be a reliable testing option. Even at such low levels, as S1 and S2 had unfiltered levels of 2.0 mg/L or less, the nanofiber based filters showed a high mitigation percentage rate, demonstrating their filtering potential. The nitrates test results show that Filter A and Filter B decreased nitrate levels for both the S1 and S2 samplesl. For the S2 sample, Filter A and Filter B decreased the nitrate level significantly, even when the nitrate level was already low enough to meet the drinking water standard. In the turbidity testing, the water was very murky before filtration for both sample locations. For S1 in particular, the water exceeded the "dirty" standard in the testing kit, and after filtration in Filter B, the water was as clear as tap water. Turbidity was the most noticeable test of filtration, as it was possible to not only have quantitative results, but the color change was also a visible, qualitative result. These test results demonstrate a huge advance in sediment and particle filtration, showing that nanofibers' small pore size is its greatest filtration factor. To test carbonate hardness, a home aquarium test kit was used, and the results were questionable. For the S1 sample, the level did not change when filtered through Filter A, but dropped when filtered through Filter B. These results show a decrease in alkalinity when Filter B was used for the S1 storm water, but for the S2 storm water the results diverted from this pattern. For the S2 sample, Filter A increased the level, as did Filter B. Because the same filters did not follow a consistent pattern for S1 and S2, there must be other underlying factors that contributed to these results. The pH
was tested to ensure that the storm water was of a neutral pH and also to ensure that the filters did not alter the pH of the storm water, turning it basic or acidic. The pH did not stay constant for the S1 stormwater or the S2 stormwater, meaning that either the activated carbon, nanofiber materials, or metal

screening altered the pH, or other underlying factors were involved. In one test, Filter A altered the pH and in the other Filter B altered the pH, but the pH still remained in the neutral range. A nitrites test was performed, but all results were negative for S1 and S2, so a nanofiber-based filter's nitrite filtration efficiency could not be determined due to non-applicable testing. For ammonia testing, the unfiltered S1 water had 0 ppm of ammonia. Filter A and Filter B for S1 also had 0 ppm, and were tested as controls to ensure the filter did not introduce new pollutants into the water. For the S2 sample, the color registered as the lowest detectable level for unfiltered, Filter A, and Filter B. Because of such low levels, Filter A and Filter B's mitigation of ammonia cannot be determined, as the color levels were either undetectable, or so faint that no difference was discernable.

Coliform and E. Coli: The IDEXX Quanti-trays proved to be a reliable and simple way to test for both Coliform and E. Coli bacteria. The unfiltered, Filter A, and Filter B samples for S1 and S2 storm water all had completely yellow Quanti-trays, meaning the Coliform bacteria level was too high for the method used for testing. Because of this, the tests were repeated with dilution factors of 10. While the 10mL dilution of S1 was completely yellow and exceeded result constraints, the 10mL dilution of S2 was 1733 MPN, meaning that not all squares were yellow, so this test could be considered for analysis. Because of this valid reading, the S2 samples using Filter A and Filter B were tested in a 10mL dilution. After incubation, very few squares were yellow, showing a significantly lower Coliform level for both Filter A and Filter B, as both reduced the level by over 98%. Both Filter A and Filter B in the S2 coliform dilution tests brought the coliform level below the maximum allowable level of 200 MPN per 100mL in Tennessee. The coliform tests show not only the extreme levels of coliform in storm water runoff in Chattanooga, but also the potential for almost complete mitigation of coliform bacteria when filtered through nanofiber materials and activated carbon. E. Coli was also tested using the same Quanti-trays as the coliform. For the S1 sample, the unfiltered storm water had 6 times the maximum EPA E. Coli standard of 200 MPN per 100mL. Filter B decreased E. Coli levels so much that the filtered water abided by EPA standards at S1. The 10mL dilutions were also placed under the black light to record E. Coli levels. The 10mL dilution of unfiltered S1 storm water was 1178.0 MPN, showing consistency in testing because the non-diluted unfiltered S1 storm water had a reading of 1203.3 MPN. The nearly identical results demonstrate the reliability of this form of testing. The 10mL dilution of unfiltered S2 stormwater indicated that 591.0 MPN of E. Coli was present in 100mL, which also is comparable with the non-diluted reading of the same water. When the 10mL dilutions of Filter A and Filter B for the S2 samples were placed under the black light, neither Quanti-tray fluoresced, indicating a complete

mitigation of E. Coli bacteria. Filter A and Filter B showed a 100% decrease in E. Coli when the water was diluted.

Heavy Metals and Copper: A Trace Metal Standard was poured through the filters because the heavy metal strips had negative readings for the S1 and S2 samples. Both Filter A and Filter B produced readings that were rusty brown, and not the projected red or orange. Both nanofiber-based filters increased the heavy metal levels, rather than decrease them. The pH of the Trace Metal Standard solution was taken, and proved to be very acidic. This pH test result confirmed the suspicion that the metal from the screening was leeched in filtration, because the nanofiber material should reduce the heavy metal levels. This demonstrates that the heavy metal solution that was used skewed the results because the acidic nature of the solution leeched aluminum from the metal screening that holds the layers of the filter together. A separate, neutral pH, specific 1000 ppb copper heavy metal test was performed following this testing. When tested with the SenSafe strips, the color tab registered as 1000 ppb on the color chart. This demonstrates the accuracy of the heavy metal strips that were used. Filter A and Filter B both had a high reduction rate of the heavy metal copper, as both were over 80%.

Errors: Systematic errors are errors in measurement that lead to skewed data or results. In this project possible systematic errors were that the various probes used were not correctly calibrated, or the Vernier probes used did not correctly measure the nutrients in each water sample. During the turbidity testing, the water added could have not been exactly 5mL, causing the light refraction method of testing to be skewed due to an inconsistent amount of liquid. The large gaps between measurements in the home test kits also could have contributed to possible errors, as the colors of the test results do not always directly match with a certain shade on the color matching charts. Other systematic errors could have come from the IDEXX Coliform testing. The correct amount of water might not have been put in each sterile plate for testing, or an incorrect amount of reagent could have been added. There were many possible random errors in this experiment. Different size drops from the reagent bottles in the pH, ammonia, nitrites, and carbonate hardness test could have skewed data. Other random errors include not holding the Vernier nutrient probes in the water correctly, using an incorrect number of drops in tests, or not waiting the correct amount of time to read results.

Conclusions

In this project, the filtration efficiency of a novel storm drain outfall filter using nanofiber materials in combination with activated carbon was tested on storm water. The hypothesis was that both of the filters designed with variations of those two components would mitigate a large percentage of the pollutants. Filter B, the filter designed with a thicker, less permeable 10 gsm nylon polymer nanofiber material was hypothesized to have a greater impact on the levels of heavy metals, turbidity, and excessive nutrients than Filter A, with the thinner, 2gsm material, because the former has a higher density of nanofibers covering the surface to trap pollutants. After a thorough analysis of the results produced through field-testing, lab testing, and model testing, the data was concluded to support the original hypothesis.

In all tests with applicable data, Filter B outperformed Filter A, except in the coliform 10mL dilution tests. Filter B consistently had the highest percentage reduction as predicted, but both filters showed a considerable decrease in many harmful pollutants and excessive nutrients. The testing for pH was questionable because of fluctuations in pH when filtered, but the pH levels remained in the neutral pH zone of 5.5-7.5 that is healthy for fish and safe for humans.

While Filter B seems like the "best" option because of the higher reduction rates, for practical purposes Filter A was concluded to be the best filter to be used to reduce pollution flowing into the Tennessee River via storm water outfalls due to its more optimal flow rate. When tested for flow rate, water poured through Filter A took only 36.9 seconds to fill up a gallon jug, whereas Filter B's flow rate was one gallon per 74 minutes. While Filter B proved to be a great pollutant mitigator, its impracticality limits its future in storm drain filtration. Filter A only reduced the flow rate by 15%, while still filtering an average of 51.3% of the contaminants from the unfiltered storm water. By using this filter, over 50% of pollution could be easily reduced, while still maintaining a steady flow rate.

The question of the practicality of a filter design such as this in terms of cost was also addressed. Both filter designs are low-cost options, whereas most other filtration options, especially which reduce upwards of 85% of pathogens like these filters, are expensive. The nanofiber material used in Filter A costs $0.50 per square foot. With the nanofiber being the main filter medium, this stormwater filtration system not only is efficient in regards to reducing contaminant levels and maintaining the water flow rate, but also is a cost-effective option.

The goal of this experiment was to test the effects of nanofiltration on storm water, and to try to determine the practicality and future use of nanofiber based filters. I believe this research and experiment shows others how important it is to filter stormwater, and the practicality of installing a

larger model of Filter A on an actual storm drain outfall. I hope that the results of this testing show that there are inexpensive, practical options to reduce storm water pollution that currently flows untreated into the Tennessee River.

Future Recommendations: If this project were to be repeated in the future, several aspects of testing could be improved, changed, or added. More in-depth and specific heavy metal testing could be done to investigate whether the nanofiber based filter could eliminate most heavy metals, similar to Filter B's 95% reduction of copper. The heavy metals would need to be tested with known standard levels like what was done in this research, in order to test the filter's ability at a high concentration, rather than using a water sample. This use of known standard levels could be done with all of the nutrient tests, and this would eliminate the negative readings of ammonia and nitrites. Probe-based testing should replace the subjective testing like color-based matching. In this project, the color match tests were kept to a minimum, but if they could be eliminated and replaced by more exact quantitative readings, the results would be more exact. A test that could be added would be for total suspended solids (TSS), as this is the EPA standard for sediment testing, and is a test used in rating water pollutant filters. One possible extension experiment would be to test nanofiber based filters' ability to mitigate pharmaceutical drugs in water, as ways to do this now are very costly and lengthy. These pharmaceutical tests were planned to be included in this experiment, but the testing machinery was unavailable for use in this experiment, and too costly to purchase. Regarding the filter design, an experiment to test the lifespan of a filter with buildup of pollutants could be designed to monitor the frequency of clogging and backup to occur. All of these changes could further the development of the design of an inexpensive nanofiber and activated carbon based filter for not only storm water filtration, but that also could be applied to other water impurity issues. Currently, the filter is being developed to be used attached to down spouts on gutters of rain barrels as a way to have a sustainable resource of water for home irrigation or other non-potable water needs. The potential drinkability of the water that exits the filter is being examined. Because of the low-cost design of the filter, it has potential applications for use in emergency situations when water is needed such as floods or water line breaks. Currently, the filter is being used in part with the University of Tennessee at Chattanooga in a concrete filter test bed that monitors the flow rate decrease after filtration and is hooked up to a storm drain system under ground. The lifespan and longevity of the filter will be tested in this manner, and the design can be further designed to accommodate a high flow rate. These changes made to the experimentation and process and filter design will further both the efficiency and practicality of using a nanofiber based filter for water pollution.

Work Cited

"After the Storm." U.S. Environmental Protection Agency, Jan. 2003. Web. 14 May 2012. <http://water.epa.gov/action/weatherchannel/stormwater.cfm>.

"City of Chattanooga GIS Maps." *City of Chattanooga*. Web. 15 Mar. 2012. <http://www.chattanooga.gov/general_government/62_124.htm>.

"City of Chattanooga Land Distribution Requirements." *Hamilton County*. Hamilton County, 3 Mar. 2011. Web. 18 Jan. 2012. <http://www.hamiltontn.gov/waterquality/bmps/2.1.pdf>.

"Environmental Technology Verification Report." U.S. Environmental Protection Agency, Sept. 2003. Web. 9 May 2012. <http://www.epa.gov/etv/pubs/09_vr_kleen.pdf>.

"Middle Tennessee-Chickamauga Watershed." U.S. Environmental Protection Agency, 13 May 2012. Web. 14 May 2012. <http://cfpub.epa.gov/surf/huc.cfm?huc_code=06020001>.

"Nanofibers." *ESpin*. Web. 15 Mar. 2012. <http://www.espintechnologies.com/about/about-nanofibers.html>.

"National Pollutant Discharge Elimination System (NPDES)." U.S. Environmental Protection Agency, 24 May 2006. Web. 12 May 2012. <http://cfpub.epa.gov/npdes/stormwater/menuofbmps/index.cfm?action=factsheet_results>.

Pitt, Robert. "Sources of Stormwater Pollutants." University of Alabama, 12 Aug. 2003. Web. 19 Jan. 2013. <http://rpitt.eng.ua.edu/SLAMMDETPOND/WinSlamm/Ch3/M3.html>.

"Protect the Environment Through Stormwater Management." *Bureau of Water*. South Carolina Department of Health and Environmental Control, Sept. 2011. Web. 14 May 2012. <http://www.scdhec.gov/environment/water/swater/pollutants.htm>.

"Sediment." Clean Water Education Partnership. Web. 14 May 2012. <http://www.nccwep.org/stormwater/sources/sediment.php>.

Sohn, Pam. "Stormy Challenge for Water Quality." *Times Free Press*. 6 June 2010. Web. 15 Mar. 2012. <http://www.timesfreepress.com/news/2010/jun/06/stormy-challenge-for-water-quality/>.

"Source Water Protection Practices Bulletin." U.S. Environmental Protection Agency, Aug. 2010. Web. 13 May 2012. <http://www.epa.gov/safewater/sourcewater/pubs/fs_swpp_stormwater.pdf>.

"Storm Drain Outfall Monitoring." Baltimore County Maryland, 1 Mar. 2011. Web. 9 May 2012. <http://www.baltimorecountymd.gov/Agencies/environment/monitoring/outfalls.html>.

"Stormwater Management Plan." Pennsylvania Department of Environmental Protection, 21 June 2012. Web. 14 Jan. 2013. <http://files.dep.state.pa.us/water/Watershed%20Management/WatershedPortalFiles/StormwaterManage ment/SpringCreekWhole.pdf>.

"Virginia Stormwater Management Handbook." Virginia Department of Conservation and Recreation,

Sept. 2012. Web. 10 Jan. 2013.
<http://www.dcr.virginia.gov/stormwater_management/documents/smhbdrft07.pdf>.

Walch, Marianne. "Evaluation of the Performance of Four Catch Basin Inserts." Delaware Department of Transportation NPDES Program, Nov. 2002. Web. 15 Jan. 2013.
<http://www.deldot.gov/stormwater/pdfs/StormCon04_Walch.pdf>.

"Waterbody Quality Assessment Report: Citico Creek Watershed." *United States EPA*. Environmental Protection Agency. Web. 12 Apr. 2012.

"Water Quality Criteria." *Environmental Protection Agency*. Web. 15 Mar. 2012.
<http://water.epa.gov/scitech/swguidance/standards/criteria/index.cfm>.

"Water Quality Division: Permits: Stormwater." Arizona Department of Environmental Quality. Web. 14 May 2012. <http://www.azdeq.gov/environ/water/permits/stormwater.html>.

Acknowledgements

I would like to thank Dr. Dawn Richards for providing me with Vernier probes to test my samples and being open to answer any environmental or water quality related question. Dr. Jayesh Doshi of eSpin Tehcnologies for providing me with proprietary nanofiber materials, giving me advice, and providing me with so much nanofiber knowledge. Mark Heinzer, a City of Chattanooga drainage and flood control specialist, and storm water expert for providing me answers to countless questions. Much thanks to Susan Holmes, a water quality specialist at Tennessee American Water, for sponsoring the materials cost and providing expensive water testing equipment for the E. Coli and Coliform testing of my project and allowing me access to her lab, and also to Kim Durham, for working alongside me in the lab and teaching me how to use IDEXX and heavy metal testing.

Appendix

Filter Model

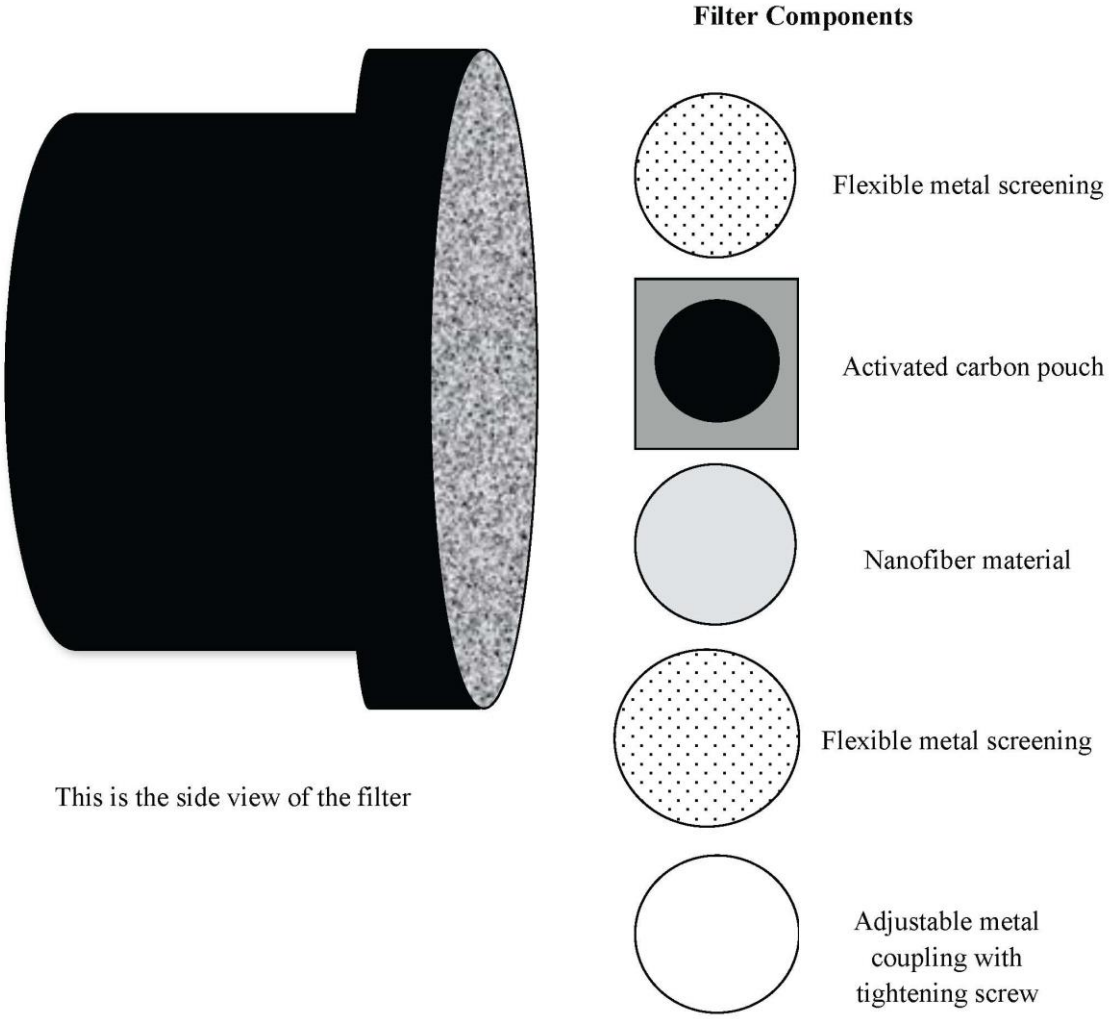

This filter is composed of four separate parts. The first layer is a piece of flexible screening to give the filter structural stability and to help withstand heavy flow rates. The next layer is a pouch made out of nylon webbing, filled completely with activated carbon. Layered on that is a sheet of nanofiber material, and then to finish the filter, a second, larger, piece of flexible screening is put in place to hold all of the filter components together.

This filter is practical, not only because of the high reduction percentages, but also because it is cheap. The nanofiber used in Filter A only costs $0.50 per square foot. With the nanofiber being the main filter medium, this stormwater filtration system not only is efficient in regards to reducing contaminant levels and steadying the flow rate, but also is a cost-effective option.

The Role of Bio-film on the Biodegradation of Quaternary Ammonia Compounds

Zheer Ahmed
Martin Luther King High School, Nashville TN

Abstract

Quaternary Ammonia Compounds (QAC) are ubiquitous and commonly used in industrial, domestic, agricultural, and healthcare related fields. QACs are used in surfactants, fabric softeners, disinfectants and even pesticides. One consequence of its widespread use, however, is that 75% of these compounds are discharged into wastewater and little is known about their environmental fate or consequence to ecosystems. Despite their strong bactericide characteristics, QACs are vulnerable to the process of biodegradation. The objective of this project was to determine the role of surface area and biofilm development on biodegradation rates of QACs (didecyl dimethyl ammonium chloride and dimethyl benzyl ammonium chloride). To achieve this objective, bacteria resistant to QACs were collected from a WNS decontamination station at Mammoth Cave saturated with QACs. An experiment was designed to test whether bacteria provided approximately 2.6 times (527 cm^2) more surface area for biofilm development were more efficient at biodegrading QACs than free-living bacteria. Previous research has shown that biofilm formation enhances certain biodegradation pathways. The microcosms containing QAC solution and bacteria were allowed to equilibrate for 4 weeks to account for sorption and the attachment of bio-film. Then negligibly sized samples were taken periodically to assess biodegradation rates under the different conditions. Preliminary results show that the microcosms with 2.6 times more surface area improved degradation rates with a 48% reduction as opposed to a 38% reduction over a two week period. The results indicated that providing more surface area for biofilm development is something that wastewater engineers should consider if they are targeting biodegradation of QACs.

Introduction

Quaternary ammonia compounds are ubiquitous in our daily lives with applications in agriculture, healthcare, and industry. QACs are one of the more widely used organic compounds; used in surfactants, fabric softeners, disinfectants, and even pesticides. One consequence, however, of their widespread use is that they are often transported into streams, lakes and groundwater systems. This not only produces direct harm to indigenous species and aquatic organisms, but also introduces selection pressure to native bacteria at the dumping sites (McBain, Ledder, Moore, Catrenich, Gilbert). This is problematic due to the fact that QACs are classified as toxic High

Production Volume (HPV) chemicals and are produced in millions of pounds per year (Tezel 2009).

QACs are primarily classified as organic compounds. QAC structures consist of a central nitrogen ion bonded covalently to four functional groups- methyl, benzyl, and chained alkyl groups (Tezel 2009). Due to their organic complexity, however, the toxicity, half-life, and mechanisms for degradation of QACs are widely unknown and have only recently come to be studied. Moreover, these compounds are known to be able to absorb to a wide variety of other compounds and products such as sediments, clays, sulfides, oxides, sulfates, and halides through a process known as sorption (Tezel). Because of the unintended consequences of QACs on non-target aquatic organisms, it is critical that a better understanding of the factors that play a role in the biodegradation of quaternary ammonia be developed.

Hypothesis and Methodology

The purpose of this study was to assess the role of the development of bio-film and free-living bacterial communities on the efficiency of QAC biodegradation. The method of developing this bio-film was primarily through increasing surface area within the test chamber. Previous research had established that greater biofilm area had no effect on biodegradation rate of toluene as compared to free-living bacteria from a karst aquifer (Painter, Kochary and Byl, 2006); however, no such experimentation had been conducted with QACs and it could be inferred that there is a significant biological difference between toluene and QACs. Understanding the role of biofilm versus free-living bacteria in the biodegradation of QACs would allow us to optimize the design of QAC treatment facilities. The general methodology of this experiment used a bio-film developed from bacteria collected at a QAC-contaminated site at Mammoth Cave. The free-living bacteria were collected from the same area, but were not provided surface area for attachment in the microcosms. To assess this role, relative concentrations of QAC were taken from separate microcosms held under similar conditions and temperatures periodically over a period of 8 weeks. Furthermore, slides of bacteria were taken from all six microcosms, replications being used primarily for accuracy and trial, and viewed under a microscope to ensure the presence of bacteria in the actual system.

The bacteria were also given four weeks to equilibrate to account for sorption of QAC and the attachment of bacteria to the surfaces (ie. Biofilm development).

Experimentation and Procedures

Bacteria resistant to QACs and thought to biodegrade compounds were collected from a WNS decontamination station at Mammoth Cave in Kentucky. The bacterial culture environments were held constant throughout the experimentation and were sealed off from air, thereby not allowing any foreign bacteria into the microcosms. To test our hypothesis, six sterile 500-mL Erlenmeyer flasks were set aside and filled with approximately 250 mL of the solution containing the indigenous bacteria and QAC. Seventy- five marbles with a radius of 0.75 cm were then added to three of the flasks (which will be referred to as replicates “A”, “B”, and “C” throughout this report) to allow for a greater amount of surface area. Flasks “D”, “E”, and “F” had no marbles, and therefore lacked that surface area. The surface area of each marble was calculated using geometry and multiplied by the number of marbles used (75). . The resulting ratio of surface area in flasks “A”, “B”, and “C” compared to flasks “D”, “E”, and “F” was approximately 2.6 to 1, respectively. All six flasks were then sealed off from any possible contamination and placed in a temperature controlled rotating shaker-incubator.

The incubator was then held at a constant temperature (25 C) and set to 75 rotations per minute to provide some mixing in the microcosms, preventing stagnant areas within the microcosms and keeping it aerated. Even though glass marbles are not efficient sorption surfaces, the weak Van der Waals force between the QAC and marble surfaces would still remove some of the QAC from solution. The microcosms were allowed to equilibrate for 4 weeks to allow this weak sorption to come to equilibrium and for a good biofilm to develop on the surface of the marbles. After the set up of the flasks and period of equilibration, negligible samples of bacteria (less than 0.1% by volume) were taken from all flasks and viewed directly under a light microscope at 500x and 1000x magnification. The marbles used in the experiment were also viewed under a microscope to confirm that an actual bio-film layer was in place during the study.

To evaluate the concentration of QAC during different periods of experimentation, a UV vis-spectrophotometer was used. The model was a Hach DR5000. The method of measuring concentration was through light absorption and with the wavelength set for 575 nano-meters (Abs 575nm). Fifty micro-liters of solution containing QAC were collected from each microcosm after known incubation times. These 50 µL aliquots were diluted with 25 mL of de-ionized water (dilution factor of 500x). The solution was gently mixed with a Hach's QAC reagent 1 powder pillow and followed with Hach's QAC reagent 2 powdered pillows. The solution was then allowed to settle for a period of two minutes. The solution changed to various shades of magenta – purple, depending on the quantity of QAC in solution. The resulting solutions were transferred to quartz cuvettes to minimize the diffraction of light, placed in the spectrophotometer and the absorbencies of QAC were recorded for each respective sample (ie. "A", "B", "C", "D", "E", and "F"). The absorbencies measured, however, were unit-less data that merely provided a measure of light absorbed by the colored water in the cuvettes based on how much QAC was present. To determine the actual concentration in mg/L, stock solutions with known concentrations of QAC was taken, tested with QAC reagents 1 and 2, measured in the spectrophotometer and a regression curve was set-up to establish a direct correlation between absorbency and concentration (Figure 1).

Results

The goal of this project was to determine if biofilms were more efficient than free-living bacteria at biodegrading QACs. Marbles provided 2.6 times more surface area and biofilm development

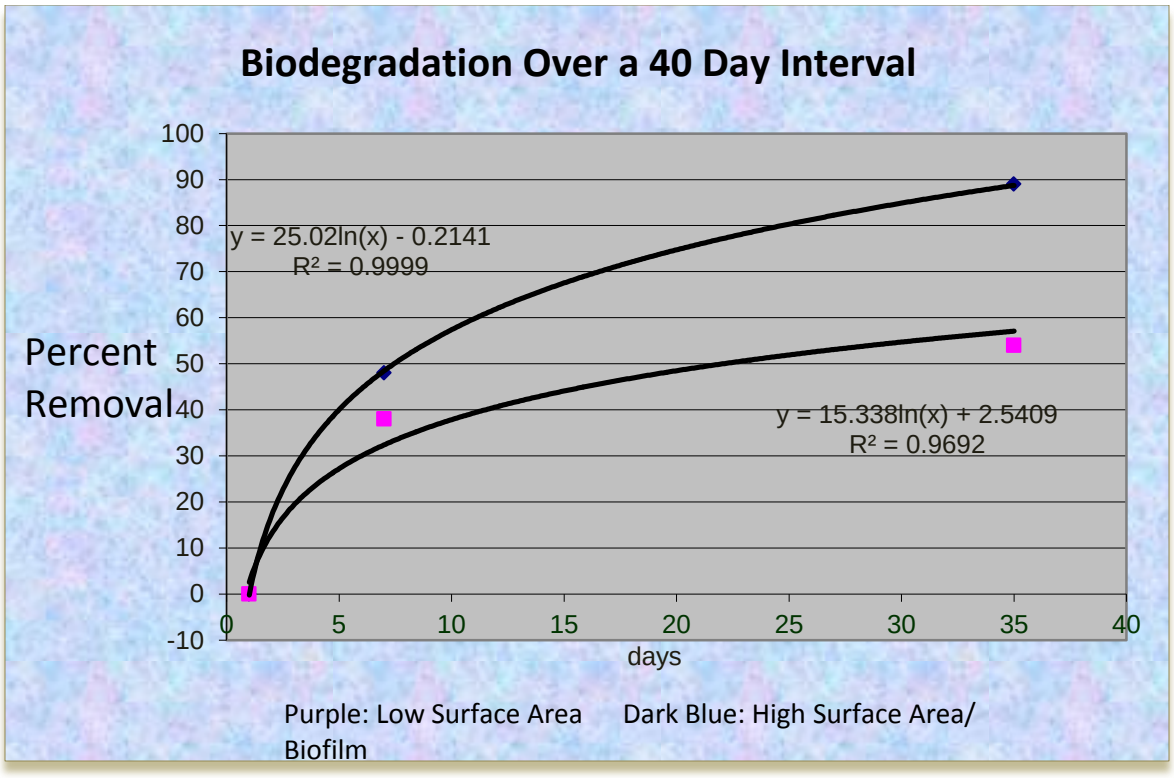

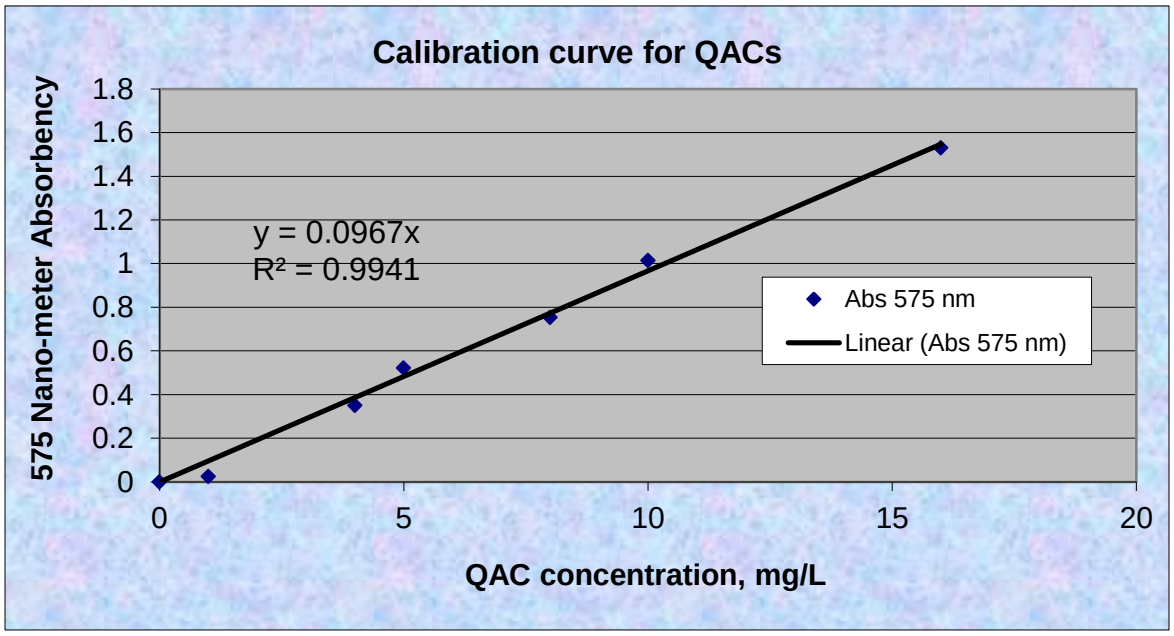

Figure 1. QAC calibration curve; used to convert Abs_{575nm} readings into QAC concentrations.

Concentrations of QAC Throughout the Analysis				
treatment	week	Abs	QAC, mg/L	mg/L (Before Dilution)
A	11-Jan	0.044	0.455	228
B	11-Jan	0.052	0.538	269
C	11-Jan	0.049	0.507	253
D	11-Jan	0.082	0.848	424
E	11-Jan	0.025	0.259	129
F	11-Jan	0.075	0.776	388
A	18-Jan	0.04	0.414	207
B	18-Jan	0.021	0.217	109
C	18-Jan	0.015	0.155	78
D	18-Jan	0.017	0.176	88
E	18-Jan	0.041	0.424	212
F	18-Jan	0.055	0.569	284
A	26-Feb	0.006	0.062	31
B	26-Feb	0.009	0.093	47
C	26-Feb	0.001	0.010	5
D	26-Feb	0.021	0.217	109
E	26-Feb	0.022	0.228	114
F	26-Feb	0.041	0.424	212

Figure 2- Data collected

Analysis

After a degradation of approximately eight weeks, the bacteria produced surprising results. As opposed to the research conducted on BTEX (benzene, toluene, ethyl-benzene, and xylene), the presence of a bio-film had a significant effect on the biodegradation rate of quaternary ammonia. Microcosms containing 2.6 times more surface area degraded 35 percent more QAC than those without significant additional surface area. Although there were small fluctuations in data as can be seen from the concentrations of E from January 11 to January 18, the data ultimately provided accurate results. The calibration curve for converting absorbency to concentration had a 99.4% fit, as desired. What is interesting to note, however, is that the higher the initial concentration of QAC in a microcosm, the *faster* the rate of biodegradation. As can be

noted of microcosm C, which had a significant starting amount, the rate of QAC removal was very efficient with only 5mg/L remaining after over a month. Another characteristic of the biodegradation worth mentioning is the fact that the regression line of best fit exhibits a natural log decay rate. Although accurate over a certain interval, this function only approximates accurately the rate of decay to about 99%, which should theoretically then be constant. This also suggests that the removal of QAC by indigenous Mammoth Cave bacteria strictly follows a first order decay, which is expressed as an “klnx” curve or its inverse function “e^(kx)”. With a fit of over 96% per line, it can be reasonably inferred that the data is accurate and that the biodegradation model exhibits first order decay. Overall, the data strongly suggests that the development of a bio-film surface layer plays a critical role in breaking down of quaternary ammonia.

Bacterial Analysis

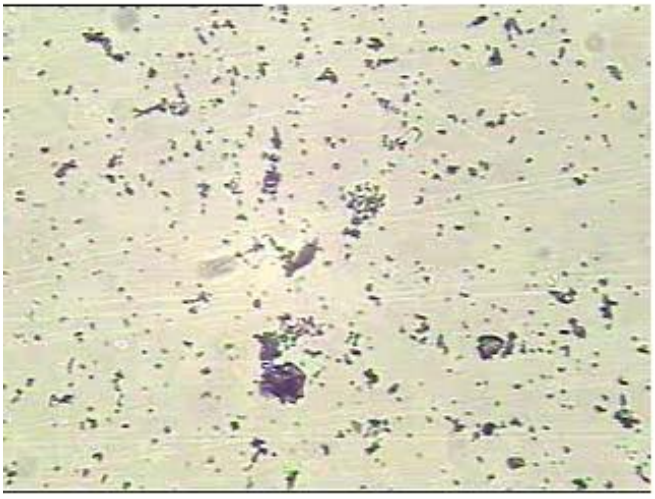

Figure 3-Free-living bacteria colony in Microcosm A

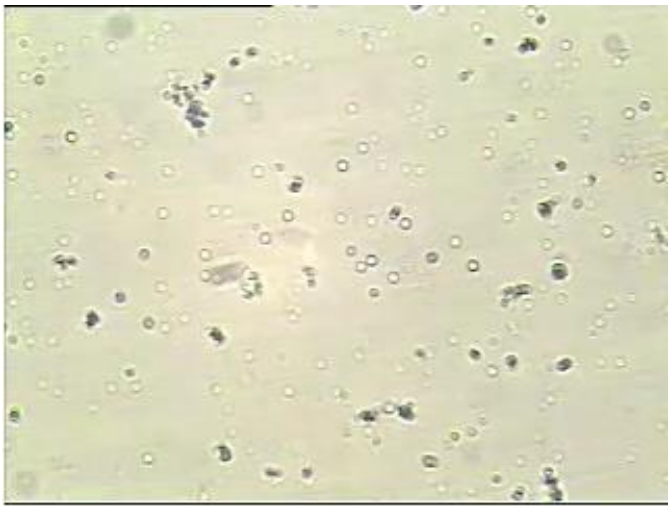

Figure 4-Free-Living Bacteria in Microcosm F

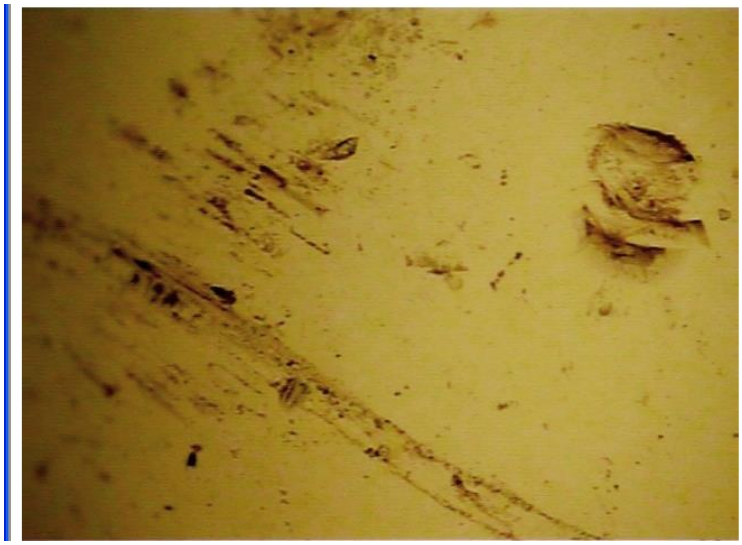

Figure 5-Attached bacteria (Taken directly from marble) on microcosm C

After the four week period of establishing equilibrium in the microcosms, samples were taken and directly viewed under a microscope. Using a Gram Stain Set, the bacteria were taken directly from each microcosm (“A”, “B”, “C”, etc.) and stained through a specific protocol. In order, a crystal violet stain was applied and rinsed with de-ionized water, then a gram of iodine, decolorizing solution, and safarin stain was applied to each (and subsequently rinsed). This allowed the transparent bacteria to be directly viewed under a microscope. The significance of the staining of the bacteria was that it allowed for a method of classification. In the test, a crystal violet stain was applied

to each bacterium. The result of this was that the bacteria could either be “gram positive” or “gram negative”. Bacteria may either reject the stain and therefore not retain that violet color or absorb it and be tested as “gram positive”. The former proved to be true of the bacteria that were tested in our lab. This suggests that the bacteria tested in our QAC analysis had an impenetrable membrane and were resistant to anti-bodies. This also goes on to suggest that the bacteria used in the lab had distinct lipopolysaccharide layers that protected them from any pathogenic intrusion which accords with the fact that these bacteria can biodegrade QACs. In order to determine the actual identity of the bacteria, however, the individual bacterium must be analyzed for shape and organizational structure. Although no such tests were conducted to actually determine the identity of these unknown bacteria, it is apparent that the bacteria are rod-shaped (bacillus) (see Figure 4) and most likely belong to the family of Pseudomonas, which are common throughout groundwater soil and known to biodegrade many contaminants.

Conclusion

In an ever-increasing industrial society where QACs are becoming more and more ubiquitous, it is pivotal that methods be developed to effectively treat the wastewater in streams and rivers. The result of this research suggests that the development of bio-film is of great importance in biodegrading Quaternary Ammonia as evidenced by the 35% increase in degradation rate. Although this research offers a path for future experimentation, much is unknown about the methods of biodegradation of QACs and many factors such as temperature and volume of the microcosms may significantly affect these rates. Perhaps efforts will be made in the future to address this problem in the form of bio-reactors specifically designed to optimally biodegrade QACs.

Work Cited

McBain, Andrew, Ruth Ledder, Louise Moore, Carl Catrenich, and Peter Gilbert. "Effects of Quaternary-Ammonium-Based Formulations on Bacterial Community Dynamics and Antimicrobial Susceptibility." *Applied and Environmental Microbiology*. 70.6 (2004): n. page. Web. 27 Feb. 2013. <http://aem.asm.org/content/70/6/3449.full

Tezel, Ulas. "Fate and Effect of Quaternary Ammonium Compounds in Biological Systems." 2009.

Acknowledgments

First and foremost I would like to thank Dr. Tom Byl, Professor of Environmental Engineering at TSU, for his mentorship and Tennessee State University for the use of their facilities. This ongoing analysis would not have been possible without the mentorship and help of Dr. Byl. I would also like to thank my parents for supporting me throughout and providing transportation to conduct this research. Last but not least, I would like to thank the administration of Martin Luther King Magnet High for allowing me to conduct this research, including my principal Dr. Turner in particular for excusing absences otherwise spent working on this project and my science instructor Mr. Andrew Beld.

Genetic and Functional Characterization of β-glucosidase in Fungal Species under Assorted Conditions

Qiaozhi Guo, Michael Kessler, Jennifer Peek, Tiannan Zhou
School for Science and Math at Vanderbilt, Nashville

Abstract

β-glucosidase is a key enzyme in ethanol production from lignocellulosic biomass, a potential source for alternative energy. It converts cellobiose into glucose, and many fungi contain this enzyme for decomposing biomass. This study compared β-glucosidase activity among domesticated and indigenous fungi and among different fungal structures. P-nitrophenyl glucopyranoside was used as an artificial substrate to measure β-glucosidase activity. The optimal conditions of this enzyme were determined from 11 samples, and the results showed that β-glucosidase activity was most efficient at a pH of 5, temperature of 37°C, high substrate and enzyme concentrations, and the activity levels were greatest in the gills of fungi. The enzymes from the fungi *Coriolus versicolor* and *Trametes pubescens* yielded the greatest enzymatic activity and withstood temperatures of up to 70°C. In addition, the β-glucosidase gene was amplified and sequenced from *Daedaleopsis confragosa* using a primer pair designed from homologous sequences. The established Internal Transcribed Spacer (ITS) primer was used as a control for the DNA templates. The gene sequence can be used to investigate the homology of this enzyme among different fungi and can also be used in the bioengineering of this enzyme for industrial ethanol production.

1. Introduction

Lignocellulosic materials are currently the most abundant biomass on the planet and have great potential as an abundant renewable energy source in the production of ethanol. The process for ethanol production is a two-step process: the hydrolysis of cellulose to glucose and the fermentation of glucose to ethanol. This process utilizes costly enzymes [1]. One of these enzymes is β-glucosidase, an enzyme used in the first step of ethanol production that converts cellobiose, a disaccharide, into glucose.

Many fungi contain β-glucosidase for the decomposition of cellulosic biomass. The amount of glucose produced correlates with the efficiency of the fungi's enzymes or the concentration of β-glucosidase present. In order to determine the fungal species with the highest concentration of or most efficient β-glucosidase and to optimize the conditions of this enzyme, this study compares β-glucosidase among various mushroom species, establishes the optimal pH, temperature, substrate concentration, and enzyme

concentration, and compares the enzyme efficiency among the different fungal structures. It was hypothesized that the efficiency of β-glucosidase differs among fungal species. Due to the difficult process of accurately quantifying glucose, an artificial substrate, p-nitrophenyl glucopyranoside, was used. When β-glucosidase cleaves a covalent bond within p-nitrophenyl glucopyranoside, β-glucose and a molecule of p-nitrophenol are produced, inducing a quantifiable colorimetric change. This study also determines the genetic characterization of β-glucosidase from the species that displayed high enzyme activities. Optimizing the conditions for β-glucosidase can potentially reduce the cost of using this enzyme in ethanol production. A better genetic characterization of β-glucosidase is beneficial as the homology of this enzyme among different fungi species can be examined, and it can be used in bioengineering.

1. Experimental procedures

2.1. Materials

β-glucosidase was obtained from *Agaricus bisporus*, a store bought mushroom, and the wild mushrooms *Guepinia spathularia, Schizophyllum commune, Daedaleopsis confragosa, Ganoderma lucidum, Coriolus versicolor, Lycoperdon pyriforme, Stereum ostrea, Hygrophorus tennesseenis, Ganoderma applanatum,* and *Tramete pubescens*. The mushrooms were identified using spore prints, microscopic analyses of gill patterns, and the book *A Field Guide to Mushrooms: North America*. The substrate p-nitrophenyl glucopyranoside, pure β-glucosidase, 1x stop solution, 1x resuspension buffer, extraction buffer, and the Nucleic Acid Extraction Module were all obtained from the company Bio-Rad. The plasmid vector pUC was obtained from the company Agilent.

2.2. Characterization of β-glucosidase

To characterize the efficiency of enzymes under different conditions, mushroom enzyme extracts were made by grinding raw mushroom tissue with extraction buffer (Bio-Rad). Standard dilutions were made with known concentrations of p-nitrophenyl so that absorbance values at 410 nm collected using a spectrophotometer could be converted to nM of p-nitrophenol. To determine the optimal conditions for the β-glucosidase, the enzyme activity was measured at a variety of pH and temperature

conditions. Samples with high or low enzyme concentrations were reacted with high or low (3.0 mM and 1.5 mM) substrate concentrations. The pH values tested were 5, 6.3, and 8.6; the temperatures tested were 0˚C, 22˚C, and 37˚C (with the additions of 48˚C, 70˚C, and 80˚C for *Coriolus versicolor* and *Trametes pubescens).* Finally, the efficacies of the enzyme extracts were tested over time, and enzyme activities were measured using a spectrophotometer at 1, 2, 4, 6, and 8 minutes. Adding a basic solution to the products of the enzymatic reaction removes an H+ from the hydroxyl group on p-nitrophenol, producing a yellow colorimetric change that can be quantified and correlated to enzyme activity. After the reaction was stopped with the addition of 1x stop solution, β-glucosidase activity was measured. All of the absorbance values obtained were then converted to nM using the standard curve. These values were analyzed in order to elucidate the optimal conditional factors that induce higher enzyme activity and more efficient β-glucosidase. Moreover, the experiments delineate whether an increased or decreased pH value, temperature, or amount of time would maximize the productivity of enzymes such as β-glucosidase.

2.3. Sequencing the β-glucosidase Gene

2.3.1 Extraction

DNA was extracted from *C. versicolor, D. confragosa, S. commune, G. lucidum, T. pubescens, G. applanatum* using the Biorad Nucleic Acid Extraction Module according to the manufacturer's instructions.

2.3.2 Amplification

The β-glucosidase Gene was amplified by Polymerase Chain Reaction. Two pairs of primers were used: designed primers and the established Internal Transcribed Spacer primers (ITS). The pair of primers used to amplify the unknown β-glucosidase gene was designed based on the sequences of this gene from the genus Amanita that were closely related to the experimental mushrooms. A pair of established Internal Transcribed Spacer (ITS) primers [2] was used as a control for the DNA templates. The ITS primers amplify the ITS region, which is located between two conserved sequences that code for ribosomes in many fungi. The sequences obtained from these primers

were compared to other sequences on GenBank to confirm the species identification or to contribute to the existing database. Primer Sequences are:

Amanita	Forward:	GARATYRCATAYSACGAAGGYGC
Amanita	Reverse:	GCGGGTCCAGTTGTCGATGAC
ITS-1-	Forward:	CTTGGTCATTTAGAGGAAGTAA
ITS-4-	Reverse:	TCCTCCGCTTATTGATATGC

Key to Symbols: R=A+G, Y=C+T

The PCR conditions used were 95˚C for 1 minute for denaturation; 56˚C for 1 minute for primer annealing; and 72˚C for 1 minute for extension. This process was repeated for 39 cycles. Gel electrophoresis was used to confirm the presence and purity of PCR products, which was then extracted from the gel and ligated to the plasmid vector pUC. The ligated products were transformed into *E. coli* cells and cloned. The plasmids were extracted from the *E. coli* cells and restriction enzyme digestion was performed to confirm the integration of the PCR products into the plasmids using the BglII enzyme. The lengths of the DNA products were tested using gel electrophoresis. The DNA cloned from *D. confragosa* amplified using the designed and ITS primers and from *C. versicolor* amplified using the ITS primers were sent for sequencing, and the obtained sequences were analyzed.

Results

3.1 Functional Characterization

In the experiment measuring the change in p-nitrophenol over time, enzymes from *C. versicolor* had the highest enzyme efficiency of the mushrooms tested, producing an average of 13.9 nM of p-nitrophenol per minute (Fig. 1). The line of best fit for *C. versicolor*'s data points has a R-squared value of 0.985. In comparison, *S. astrea*, the mushroom that was the next most efficient, produced p-nitrophenol at an average rate of 8.92 nM per minute (R-square value: 0.972). For the remaining fungi, the following is the order of p-nitrophenol yield from greatest to least: *S. commune, A. bisporus, H. tenneseenis, G. spathularia, L. pyriforme, D. confragosa,* and *G. lucidum*.

In the experiment measuring enzyme efficiency in relation to temperature, *C. versicolor* was shown to be most efficient at 70˚C, producing a total of 418 nM after two minutes of reaction (Fig. 2). In comparison, *T. pubescens* was most efficient at 48˚C,

producing 430 nM after two minutes of reaction. The experiment measuring the effect of pH on enzymatic activity shows that for several species, enzymatic efficiency changes when the mushroom extract and, subsequently, β-glucosidase, is exposed solutions of different pHs (Fig. 3a). The range of pH tested was 5, 6.3, and 8.6, which includes both acidic and basic conditions. The ANOVA shows delineation between each of the pH distributions. There is no indication of a significant difference between the pH of 6.3 and a pH of 5 or 8.3; however, the graph does signal a significant difference in the enzyme efficiency between a pH of 5 and 8.6 (Fig. 3b).

The experiment on fungal structure showed that within the same species, β-glucosidase from gills had the highest efficiency (Fig. 4a). Of the mushrooms *A. bisporus, H. tennesseensis,* and *G. lucidum*, β-glucosidase from *A. bisporus* was the most efficient, followed by that of *H. tennesseensis* and *G. lucidum* (Fig. 4a). This result corroborates the results of the time test. The ANOVA test shows that β-glucosidase from the caps was the least efficient, with an average of 11.92 nM over a span of two minutes, while β-glucosidase from the gills were the most efficient, with an average of 20.42 nM over a span of two minutes (Fig. 4b).

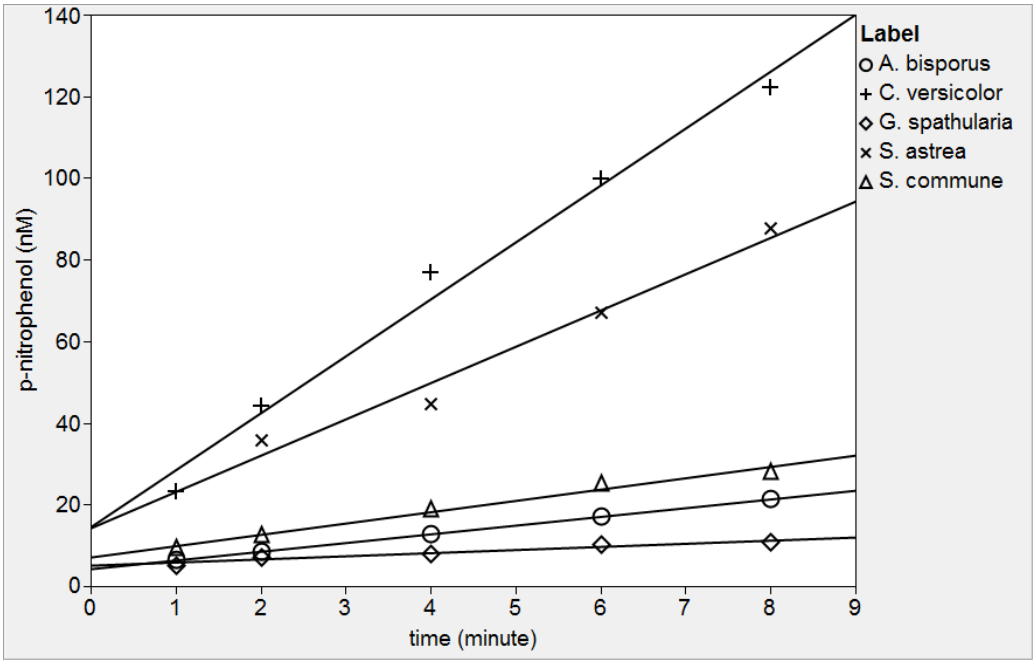

Figure 1 - Comparison of β-glucosidase activity among select mushroom species.

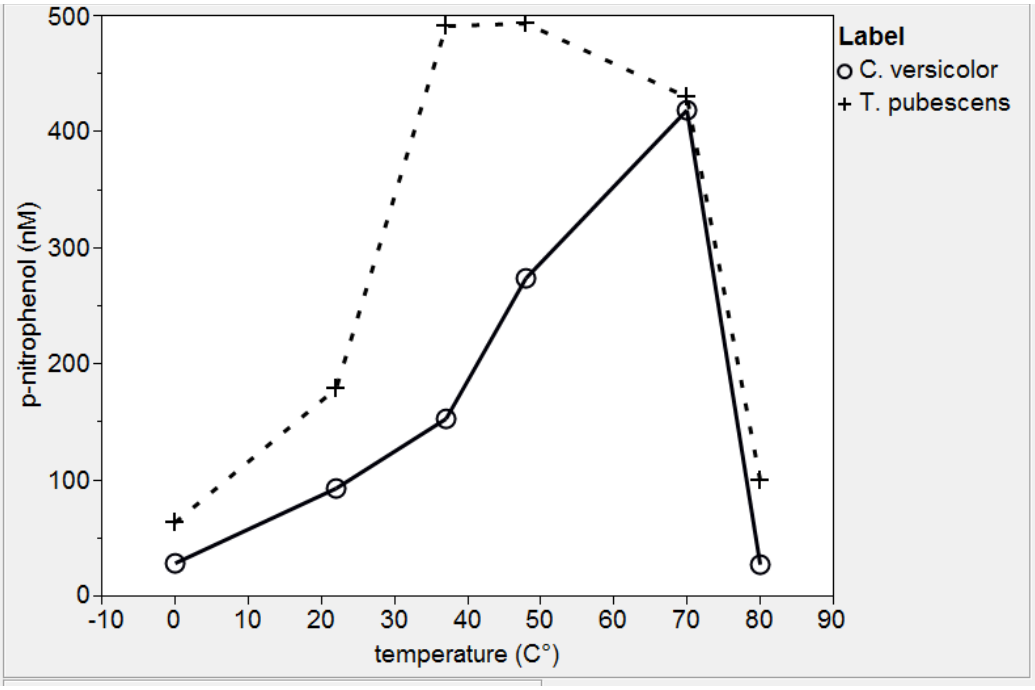

Figure 2 - Effect of temperature on amount of p-nitrophenol produced in *C. versicolor* and *T. pubescens*.

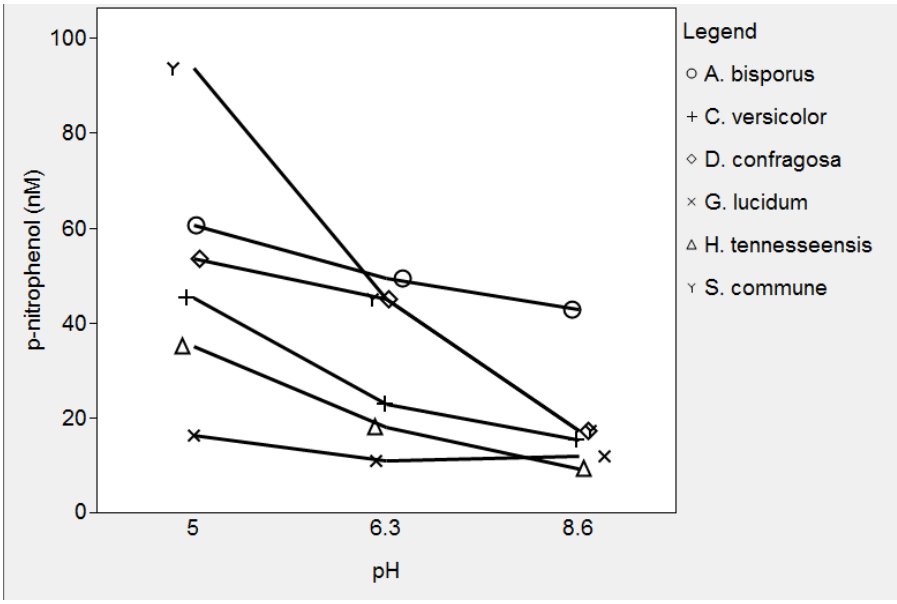

Figure 3a - Effect of pH on the amount of p-nitrophenol produced.

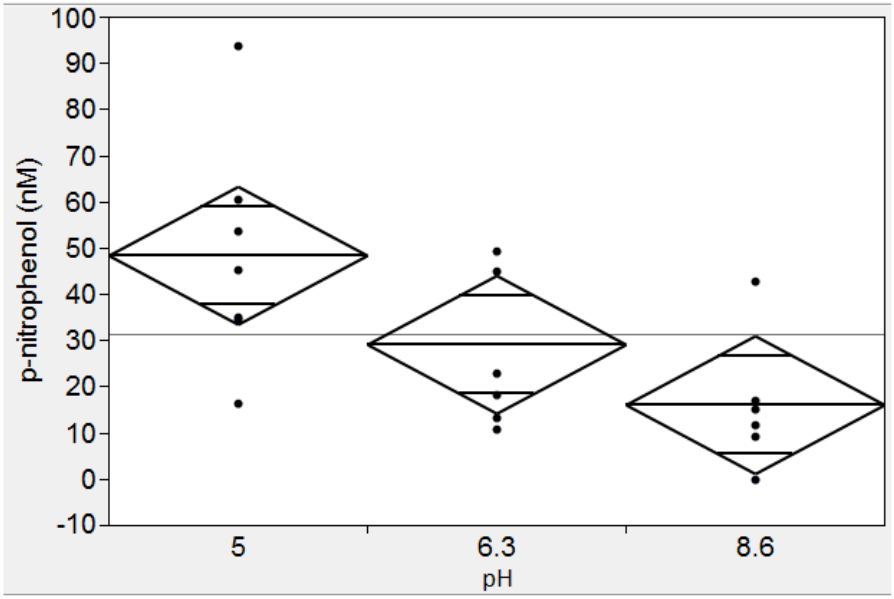

Figure 3b - ANOVA test on pH experiment data.

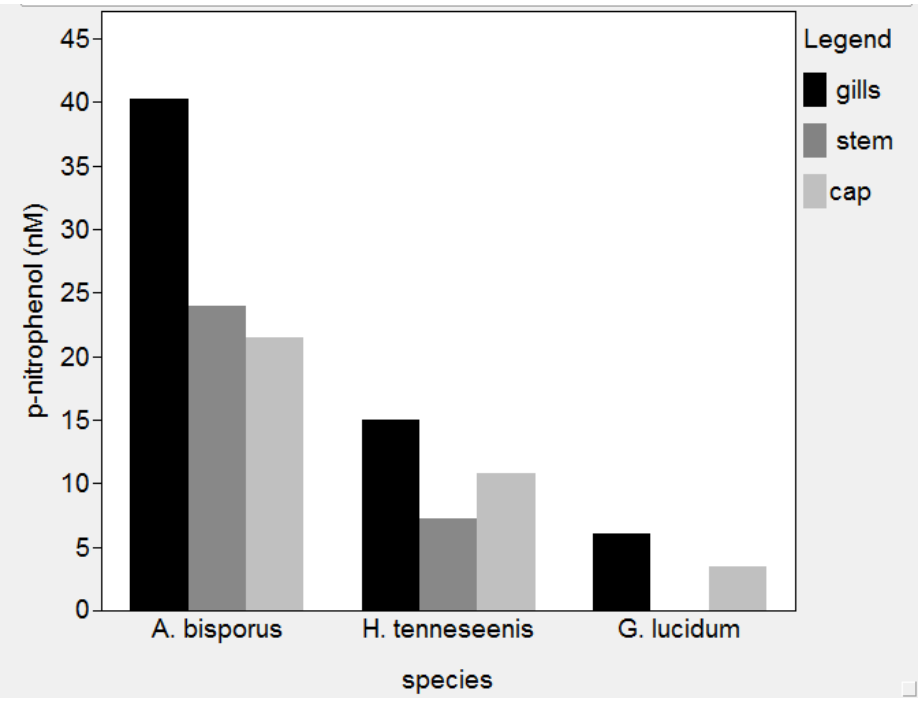

Figure 4a - Variation in p-nitrophenol yield in relation to fungal structure by species.

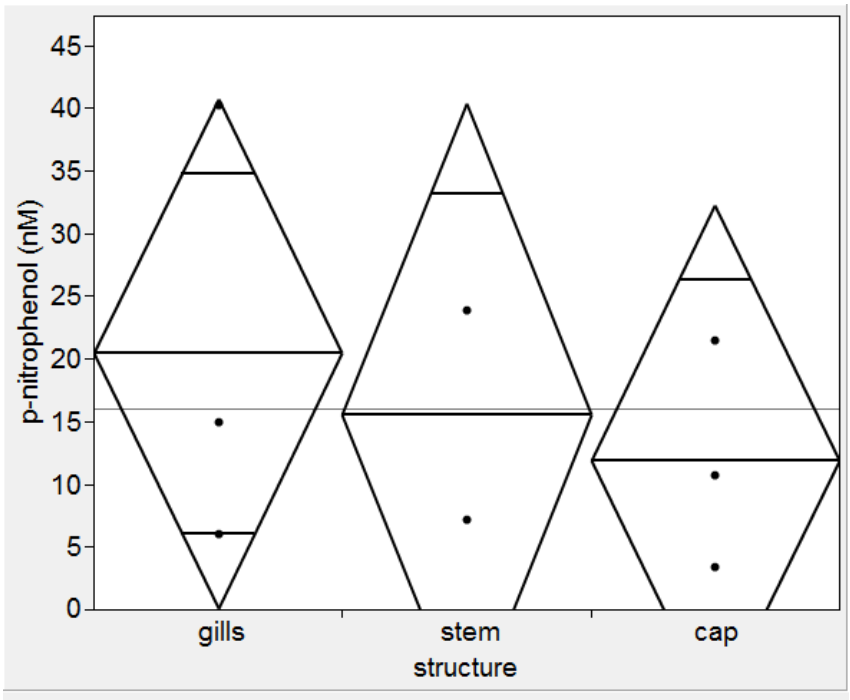

Figure 4b -ANOVA test of p-nitrophenol yield by fungal structure.

3.2. Genetic Characterization of β-glucosidase

DNA was extracted from several fungal species that showed high enzymatic activity levels. The β-glucosidase gene was amplified using designed β-glucosidase primers based on DNA sequences from closely related fungi; the ITS primers were used as control to confirm the identities of the mushroom species. The PCR products were cloned, and a BglII restriction enzyme digestion followed by a gel electrophoresis was performed to identify the positive clones. The results showed that only DNA from *D. confragosa* (amplified with both primers) and *C. versicolor* (amplified with the ITS primer) displayed two bands, indicating that the DNA amplified from these species using designated primers were successfully cloned.

The gene from *D. confragosa* amplified with the designed primers and the ITS primers and the gene from *C. versicolor* amplified with the ITS primers were sequenced. After the obtained sequences were analyzed, it was found that for both species, the DNA amplified with the ITS primers matched a sequence from *C. versicolor* with a query coverage of 100% and a max identity of 99%. This indicates that the DNA sample from *D. Confragosa* was contaminated and that *C. versicolor* was correctly identified. For the sequence obtained from *D. confragosa* and amplified with the primer

pair designed to amplify the region coding for β-glucosidase, it was found that the gene matched a sequence that codes for β-glucosidase from the fungus *Postia placenta* with a query coverage of 60% and a max identity of 71% (Figure 5). This indicates that the primer successfully amplified part of the β-glucosidase gene. Other top results for this sequence included sequences from the genus Amanita, which were used to design the primers.

Sequences producing significant alignments:

Accession	Description	Max score	Total score	Query coverage	E value	Max ident
XM_002475939.1	Postia placenta Mad-698-R hypothetical protein, mRNA	78.8	130	60%	2e-12	71%
XM_002474673.1	Postia placenta Mad-698-R beta-glucosidase, mRNA	75.2	130	60%	2e-11	71%
GU169871.1	Flammulina velutipes strain KACC 42777 isolate 25 putative	60.8	60.8	15%	5e-07	78%
XM_003032708.1	Schizophyllum commune H4-8 hypothetical protein, mRNA	41.0	41.0	7%	0.46	86%
JF707940.1	Volvariella volvacea GH family 3 beta-glucosidase gene, par	39.2	39.2	19%	1.6	71%
JF707919.1	Amanita sp. BEW-2011h GH family 3 beta-glucosidase gene	39.2	39.2	11%	1.6	76%
JF707916.1	Amanita solitaria GH family 3 beta-glucosidase gene, partial	39.2	39.2	19%	1.6	69%

Figure 5 - Top results from BLAST comparing the sequence obtained from *D. confragosa* and amplified with the designed primer with previously established sequences.

3. Conclusion/Discussion

In this study, β-glucosidase activity was compared among several fungi species and the optimal condition for this enzyme was established. It was shown that β-glucosidase obtained from *C. versicolor* had the highest enzymatic activity and produced 122.2 nM of p-nitrophenol. For all fungi, as the time increased, the amount of p-nitrophenol produced also increased.

Enzymatic activity was generally most efficient at a pH of 5 with high substrate concentration and high enzyme concentration. In general, the enzymatic activity increased with temperature. However, it should be noted that temperature tests were only conducted on 5 of the fungi due to a lack of time. Therefore, the verity of this conclusion is incomplete. The different structures of the fungi within the same organism yielded different levels of absorbance, with gills usually producing the greatest amount of product. However, it should be noted that *G. lucidum* did not have a stem, and therefore, there is no data for that structure in that fungi (Fig 4a). A possible reason for this is that gills are involved in the dispersion of spores and thus need much nutrition and energy from breaking down biomass. Indigenous fungi that were tested in general

produced larger amounts of p-nitrophenol than mushrooms grown for commercial use. This could be because commercially grown mushrooms are sometimes genetically modified, changing the efficiency/concentration of some enzymes. Also, wild mushrooms have undergone natural selection, thereby increasing the efficiency of the enzymes that provide them with energy sources.

As temperature increased from 70˚C to 80˚C, *T. pubescens*' enzymatic efficiency decreased from 430 nM after 2 minutes to 99 nM after 2 minutes while *C. versicolor* efficiency decreased from 418 nM after 2 minutes to 27 nM after 2 minutes. These drastic and consistent declines in enzyme efficiency correlate with the rise in temperature, suggesting that the denaturation temperature for β-glucosidase of both species occurs at some point between 70˚C to 80˚C. This is significant as ethanol production usually reaches high temperatures and it has been shown that β-glucosidase from these two species flourish at such temperatures [3].

The designed primer pair successfully amplified part of the gene that codes for β-glucosidase and the ITS primer pair successfully amplified the variable region between two conserved ribosomal regions for *C. versicolor.* However, it should be noted that because there was likely contamination of *D. confragosa* by *C. versicolor,* the β-glucosidase sequence obtained from the *D. confragosa* could possibly be the DNA from *C. versicolor.*

For future directions, the focus could be turned to producing ethanol from the *E. coli* cells that contain the gene that codes for β-glucosidase. In a similar study, R. K. Sukumaran et al. used the fungi *Richoderma reesei* and *Aspergillus niger* to examine the saccharification of sugar cane bagasse, rice straw and water hyacinth biomass to produce ethanol [4].

Acknowledgements

We would like to thank our instructors at the School for Science and Math at Vanderbilt for helping us. We would especially like to thank Dr. Angela Eeds for her invaluable guidance and support. Furthermore, we would like to thank Dr. Jason Slot at Vanderbilt University for helping us correctly identify the fungi. Finally, we would like to thank Shelby Bottoms Nature Center for graciously allowing us to collect fungi on their grounds.

Work Cited

[1] Sudipto Das, *et al.*, “Enzymatic hydrolysis of biomass with recyclable use of cellobiase enzyme immobilized in sol–gel routed mesoporous silica,” *Journal of Molecular Catalysis B: Enzymatic*, vol. 70, pp. 49–54, Jun. 2011.

[2] C. Schoch, *et al.*, “Nuclear ribosomal internal transcribed spacer (ITS) region as a universal DNA barcode marker for Fungi,” *Proc Natl Acad Sci U S A,* vol. 109, pp. 6241-6246, Mar. 2012.

[3] F. J. Castillo *et al.*, **“**Optimization of fermentation conditions for ethanol production from whey,” *Biotechnology Letters*, vol. 4, issue 9, pp. 567-572, Sept. 1982.

[4] Rajeev K. Sukumaran *et al.*, **“**Cellulase production using biomass feed stock and its application in lignocellulose saccharification for bio-ethanol production,” *Renewable Energy*, vol. 34, issue 2, pp. 421–424, Feb. 2009.

The Effects of Varying Glucose Concentrations on Cellular Glycolytic Rates

Regan Givens
Pope John Paul II High School, Hendersonville

Abstract

Cells use several cellular respiration pathways including glycolysis and oxidative phosphorylation, to convert glucose into ATP for the cell to use as energy. The optical redox ratio is a relative measure of the rates of glycolysis versus oxidative phosphorylation; yet, the optical redox ratio is poorly characterized in regards to sensitivity to metabolic inputs. Our objective was to determine the sensitivity of the redox ratio of cellular glucose concentrations. We hypothesized that as the concentration of media-glucose increased, so would the redox ratio. At increased media-glucose concentrations, we expected higher rates of glycolysis resulting in increased concentrations of NADH and decreased FAD concentrations. For this study, MCF7 cells were grown *in vitro* with media containing glucose at varying concentrations. Cellular NADH and FAD fluorescence was imaged by multi-photon fluorescence microscopy. The optical redox ratio, fluorescence intensity of NADH divided by the fluorescence intensity of FAD, compares the metabolic rates of the tumor cells across varying amounts of media glucose. The media containing no glucose, 0 mM, had the greatest effect on the glycolytic rates of cancer cells (p-value = .01).

Introduction

Our bodies are composed of trillions of cells that all play different parts within their respective locations. All cells use cellular respiration to make ATP (adenosine triphosphate) for the cells to use as energy. Mutations in DNA during replication, when cells divide into newer cells, can result in cancer cells. Approximately 30% of all cancer cases among American women are breast cancer ("U.S. Breast Cancer Statistics," 2012). Advances in health care and technology have allowed for extensive research into understanding this deadly disease. The current clinical therapies include chemotherapy, a process in which the chemotherapy drug attacks any cells that are rapidly dividing. Unfortunately, these non-specific drugs cannot distinguish between cancerous cells and healthy cells. ("How Does Chemotherapy Work?," 2011).

Researchers are looking for better treatments, or possible cures, for various types of cancer. Cancer cells *in vitro* which literally means taking place in a test tube, culture dish, or anywhere outside of a living organism, are used to test novel drug and

treatment Two-photon fluorescence microscopy utilizes a high power laser to excite tissue fluorescence. Fluorescence intensity is proportional to fluorophore concentration and can thus probe relative concentrations of biological molecules. Two endogenous fluorophores, nicotinamide adenine dinucleotide (NADH) and flavin adenine dinucleotide (FAD), are coenzymes of metabolism and report cellular metabolism health and efficiency. The redox ratio measures the glycolytic rates of the cells, as NADH is created in glycolysis, and FAD is used in oxidative phosphorylation (Chance, 1979). The redox ratio is sensitive to metabolic changes induced by malignancy and cancer treatments (Walsh et al. BOE, 2012); however, the sensitivity of the redox ratio to changes in available glucose has not been defined. The following experiments attempt to define the relationship between the redox ratio and cellular glucose concentrations. This knowledge is significant for the future of cancer research, because the results will further define the redox ratio, which is under-development as a biomarker of cancer therapy effectiveness.

Problem and Hypothesis

The challenge is to determine the sensitivity of the redox ratio to changes in cellular glucose concentrations. We hypothesized that as media-glucose concentrations increase, rates of glycolysis will increase, resulting in increased NADH concentrations and decreased FAD concentrations, which will result in a higher optical redox ratio.

Materials

We used the MCF-7 cell line, which is estrogen receptor positive (ER+), indicating the cells express the estrogen receptor and are able to process estrogen as they normally would *in vivo* ("MCF-7 Cells Human Breast," n.d.). To culture the MCF-7 cells, cell growth media (DMEM) was used with varying amounts of glucose and glutamine, such as 0 mM, 2.5 mM, 5 mM, 7.5 mM, 10 mM, 15 mM, 22.7 mM for glucose. The growth media was supplemented with 10% fetal bovine serum (FBS) and,

1% penicillin: streptomycin, an antibiotic/antifungal. Cells were cultured in an incubator, which maintained the temperature at 37^0C, the humidity at 95%, and the CO_2 at 5%.

Optical metabolic imaging interrogates the intrinsic fluorescence of NADH and FAD. Two-photon microscopy was performed on a customized multi-photon fluorescence microscope (Prairie Technologies) utilizing a titanium-sapphire laser (Chameleon, Coherent) tuned to 750 nm for NADH fluorescence and tuned to 890 nm for FAD fluorescence, as the excitation source. Two objectives, 40x and 20x (NA of 1.15, and 0.75, respectively), coupled the excitation and emission light in the epi-configuration. Two filters isolated 400-480 nm NADH emission and 500-600 nm FAD emission.

Methods

A time course was used to determine how length of time required for the MCF-7 cells to adjust their glycolytic rates to a new glucose concentration. The cells were imaged after exposure to 0, 5, and 27 mM glucose for 0, 3, 6, and 24 hours (as shown by the diagram in figure 1.1).

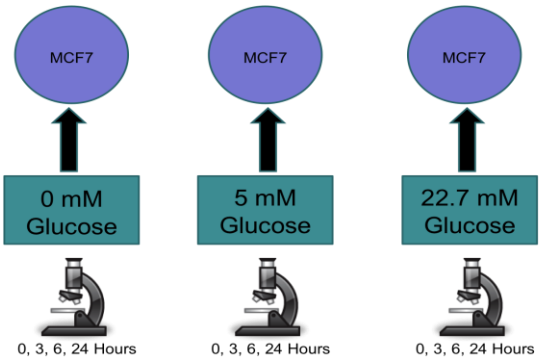

Figure 1.1 Time Course Methods

At each time interval, five different fields of view on each dish were imaged for repeated measurements. The images were analyzed by applying an intensity threshold to isolate cytoplasm fluorescence (ImageJ). Redox ratio values were obtained by diving the NADH image by the FAD image to acquire a redox ratio value for each pixel. Cellular redox ratio values were computed by averaging the cytoplasm pixels for each cell. Cell mean redox ratio values were averaged across the image.

To investigate additional glucose media concentrations, MCF7 cells were plated and placed in 22.7 mM glucose media (normal, high glucose DMEM), for 24 hours. After 24 hours, the media was exchanged with the media of the following concentrations of glucose: 0 mM, 2.5 mM, 5 mM, 7.5 mM, 10 mM, 15 mM, 22.7 mM. The cells were grown for another 24 hours to acclimate to the new media and its level of glucose. After that 24 hour time period, the cells were imaged and the images analyzed in the exact same way as the time course methods (above). The only difference was the use of a 20x objective (NA of 0.75) instead of the 40x objective.

Results

The time course data was normalized to the 22.7 mM solution, since that concentration of glucose was the standard high glucose media. The redox ratio was expected to decrease in cells exposed to the 0 mM concentration glucose media; however we observed no significant change in the redox ratio of the 0 mM and 5 mM after exposure for 24 hours (Figure 2.1). To validate metabolic interpretation from the redox ratio, the NADH and FAD fluorescence counts were examined separately. No change in NADH fluorescence was observed between the low-glucose media concentrations at any time point (Figure 2.2).

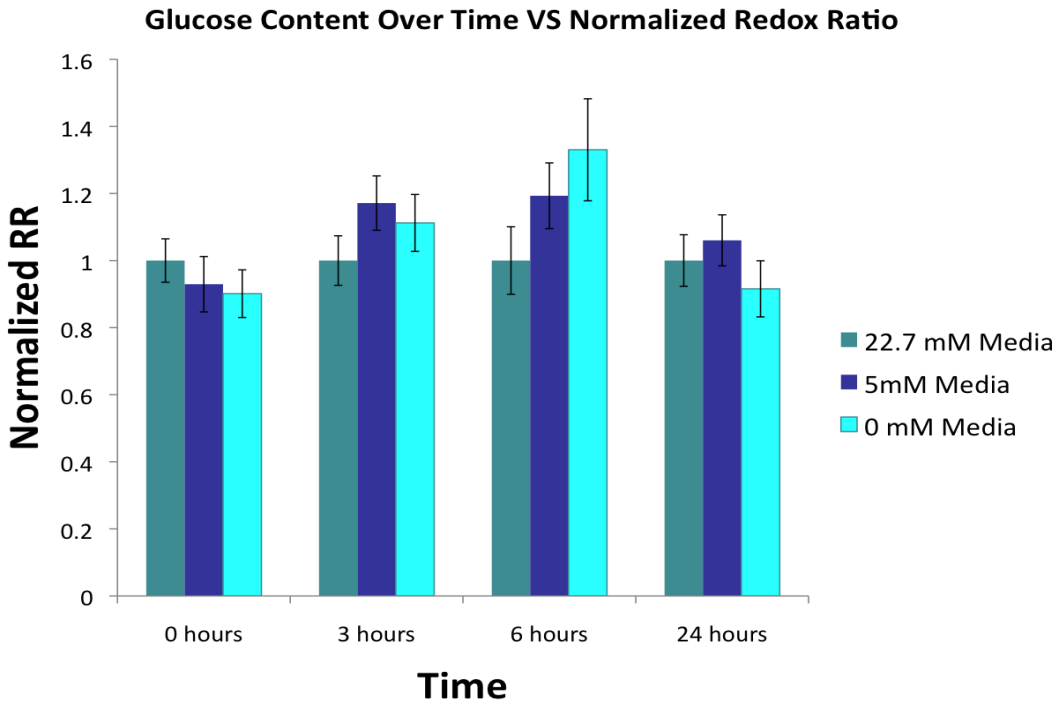

Figure 2.1: Time Course Redox Ratios for 22.7 mM, 5 mM, and 0 mM Media. All data is normalized to the 22.7 Media RR.

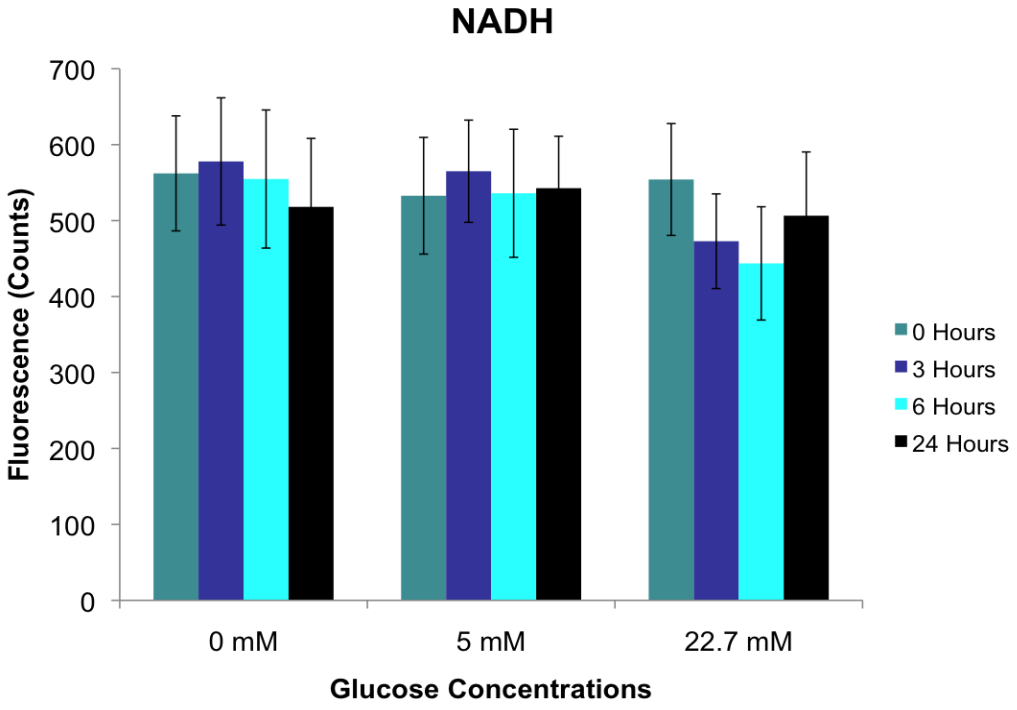

Figure 2.2: NADH Fluorescence counts from the Time Course Data

To determine the effect of the low metabolite concentrations on the redox ratio, both the glucose concentration and glutamine concentrations were varied. The redox ratios from cells with the glucose concentrations between 5 and 22.7 are statistically similar, with the exception of the 10 mM solutions. The cells grown in 0 mM glucose had a statistically significant decrease in the redox ratio (Figure 3.1). Without glucose, cells cease producing ATP through glycolysis and glucose-driven oxidative phosphorylation. Without glucose, the cells can use stored metabolites such as amino acids for metabolism, which may result in a decrease in the redox ratio.

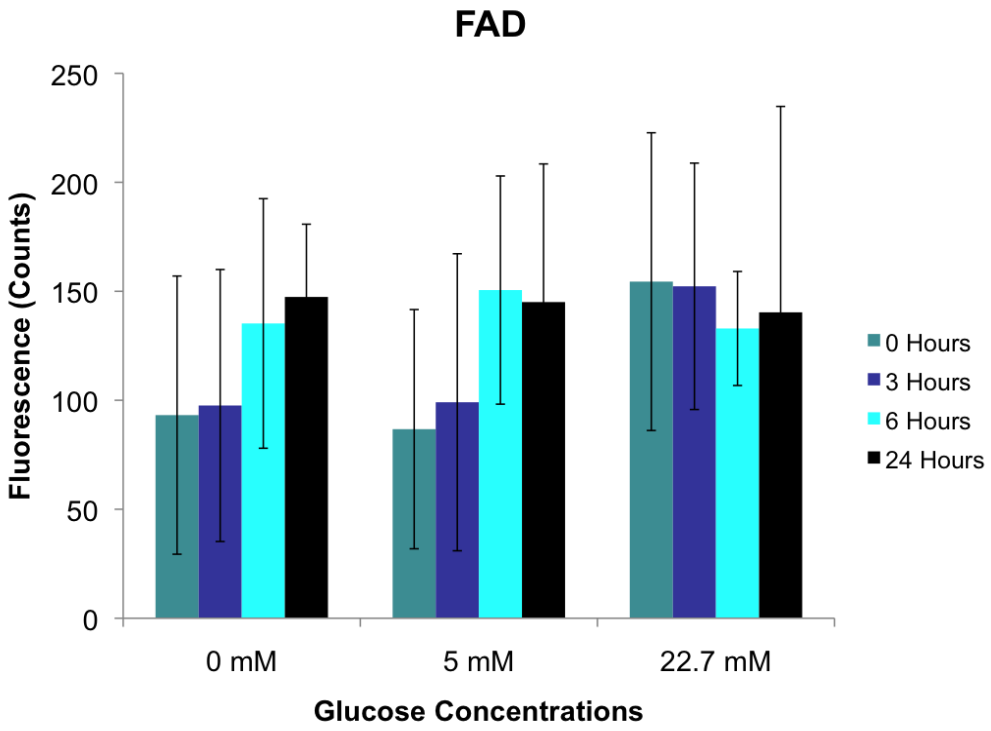

Figure 2.3: FAD Fluorescence counts from the Time Course Data

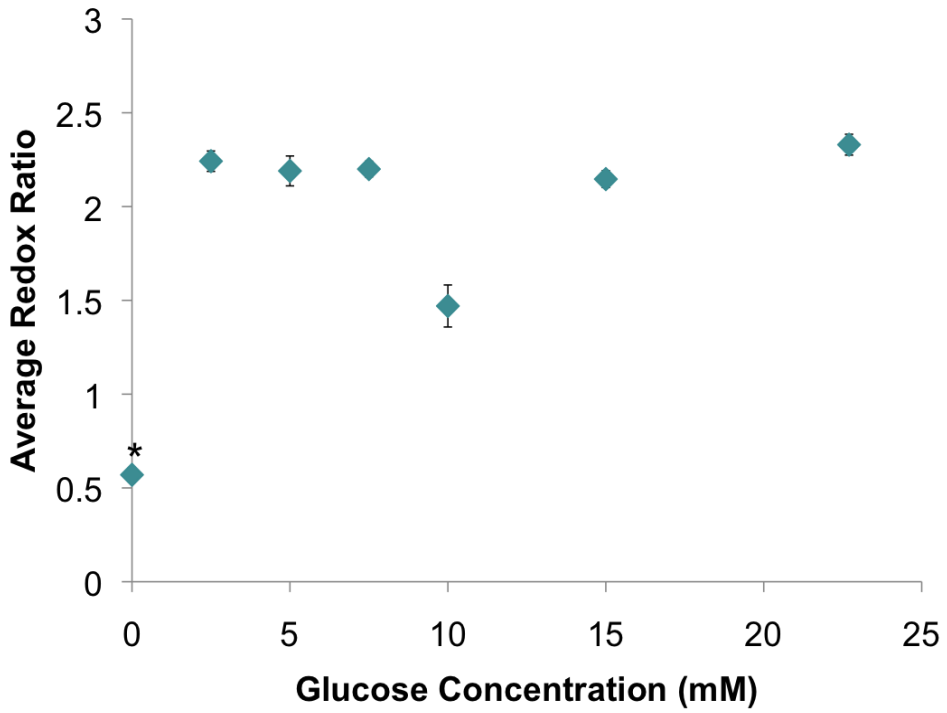

Figure 3.1: Scatter Plot of data from the Final Methods. The asterisk next to the 0 mM means that it is statistically significant using a student's T-test with a P-value of .01.

Conclusion and Discussion

Within the time course, the lack of change in redox ratio with decreased media glucose could be due to a metabolic stress effect from changing media or the presence of additional metabolites, such as glutamine, in the glucose. Glutamine can enter the oxidative phosphorylation pathway to produce ATP while generating FAD and consuming NADH (Oncogene, 2010). Increased glutamine metabolism may result in an increase in the redox ratio, which was observed in the low glucose, high glutamine media (Figure 2.1). For the FAD fluorescence, while not significant due to large error, an trend towards increased in FAD fluorescence was observed in the cells exposed to the low glucose concentration media at longer times, 6 and 24 hours (Figure 2.3). An increase in FAD fluorescence would suggest an increase in oxidative phosphorylation, consistent with increased glutamine metabolism.

While in the final method, the similar redox ratios among cells grown in media of glucose concentrations between 5 and 22.7 mM, could be attributed to either equal

reductions in glycolysis and oxidative phosphorylation rates or a low-glucose saturation level.

Overall, Increased media-glucose concentrations, above 2 mM, appeared to have no effect on cellular metabolism function. Future research efforts include experiments to test glucose concentrations between 0 mM to 2.5 mM and to allow an increased acclimation time in order to look at possible differences.

Work Cited

Biswas, S., Lunec, J., & Bartlett, K. (2012). Non-glucose metabolism in cancer cells-is it all in the fat? *Cancer Metastasis Rev*.

Chance B, Schoener B, Oshino R, Itshak F, Nakase Y. Oxidation-reduction ratio studies of mitochondria in freeze-trapped samples. NADH and flavoprotein fluorescence signals. J Biol Chem. 1979;254(11):4764-71.

DeBerardinis, R. J., & Cheng, T. (2010). Q's next: The diverse functions of glutamine in metabolism, cell biology and cancer. *Oncogene*, *29*, 313-324.

Heiden, V., Cantley, & Thompson. (2009). Understanding the Warburg effect: The metabolic requirements of cell proliferation. *Science*, *324*.

How does chemotherapy work? (2011, October 26). Retrieved October 30, 2012, from American Cancer Society website: http://www.cancer.org/treatment/treatmentsandsideeffects/treatmenttypes/chemotherapy/chemotherapyprinciplesanin-depthdiscussionofthetechniquesanditsroleintreatment/chemotherapy-principles-how-does-chemo-work

MCF-7 Cells human breast adenocarcinoma cell line. (n.d.). Retrieved November 18, 2012, from MCF-7 Cells website: http://www.mcf7.com/

Oncogene. 2010 January 21; 29(3): 313–324.Published online 2009 November 2. doi: 10.1038/onc.2009.358

U.S. Breast Cancer Statistics. (2012, October 30). Retrieved November 18, 2012, from Breast Cancer website: http://www.breastcancer.org/symptoms/understand_bc/statistics

Walsh A, Cook RS, Rexer B, Arteaga CL, Skala MC. Optical imaging of metabolism in HER2 overexpressing breast cancer cells. Biomed Opt Express. 2012;3(1):75-85. PMCID: 3255344.

Acknowledgement

The following research took place at Vanderbilt University in Nashville, Tennessee, as a part of the Research Experience for High School Students Program (from June 4th until July 13th). I would like to thank Vanderbilt University, The Center for Science Outreach at Vanderbilt, and Dr. Kimberly Mulligan for accepting my application into the REHSS program, Dr. Melissa Skala, Alex Walsh, Eli Brand, and the Biomedical Engineering Department at Vanderbilt for allowing me to use their technology, for their help with my project, and help with this very paper. Last but not least, I would like to thank Jennifer Dye and Jon Hall for their contributions and help with this research project.

Remote Sensing of Carbon Dioxide in the Lower Atmosphere

Nathan Beeten, Ryan Dunaway, Rob Edwards, Jackson Ferrell
School for Science and Math at Vanderbilt, Nashville

Abstract

Pollution caused by carbon dioxide, a greenhouse gas that is linked to global warming, has increased by 35% since the Industrial Revolution suggesting that a correlation between industrialization and CO_2 emissions exists. CO_2 concentration also changes with altitude and is distributed throughout the world's troposphere. The goal of this project was to create a simple mobile device that could compare CO_2 emissions in both rural and urban environments and changes in its concentration with altitude. The device consisted of a CO_2 sensor and an altimeter that were controlled by an Arduino microcontroller along with a camera and a cell phone (for GPS reception) placed in a polystyrene foam encasement. Code was written to allow the CO_2 sensor and altimeter to take measurements together and store the data in the microcontroller's internal memory. The box was suspended from a tethered helium-filled weather balloon and ascended into the atmosphere while its components took corresponding CO_2 and altitude readings. The data measured by this device can be used to observe changes in CO_2 emissions from rural and urban environments and with changes in altitude. After testing there was evidence to suggest that this can be a viable device for mobile CO_2 measurement.

Introduction

Concentrations of carbon dioxide (CO_2) are influenced by natural cycles of plant and animal respiration as well as human activities such as the burning of oil, coal, and natural gas. Urbanization has effectively increased and concentrated these human activities increasing the global CO_2 concentrations by 35% since the Industrial Revolution [1]. As a result of urbanization, CO_2 emissions are generally higher in industrial environments than in rural environments.

It was previously thought that CO_2 was evenly mixed to the point of equilibrium in the atmosphere, but with NASA's Atmospheric Infrared Sounder (AIRS) it has been shown that there are great amounts of seasonal variation of CO_2 values within the troposphere [2]. The concentrations of CO_2 throughout the troposphere are largely affected by jet streams as well as sizable weather systems[3]. Having the ability to track changes in the concentration of CO_2 values with changes in altitude would allow the scientific community to have a greater understanding of carbon dioxide's distribution in the earth's atmosphere.

In previous studies, such as *Differences between carbon dioxide levels over suburban and rural sites in Northern Spain,* a limitation was the CO_2 sensors ability to accurately collect data in an urban environment [1]. In this experiment, a sensor was mounted to the side of a building to collect data over time. Though the experiment presented in this article showed consistence with its steady carbon dioxide measurements at a set location, it was limited to one side of a building where much of the carbon dioxide in the urban area would not travel due to barriers in the city. This research was expanded upon by the use of a balloon and compact box to take measurements. It had a greater potential for risk, but it was more accurate in determining the CO_2 composition of the atmosphere in an area because it was free of obstructions.

Methods

A device was created that could take both CO_2 and altitude measurements. It was used to find the differences between CO_2 concentrations in urban and rural environments as well as observe changes in CO_2 concentration with increasing altitude. Points were taken around the city of Nashville, TN and the surrounding area. Emissions move from the source to the surrounding areas based on wind patterns as well as through general dispersion. The device was attached to a weather balloon which allowed for changes in altitude. It was designed so that it would be compact and mobile for effective assembly and data collection. It is a simple setup proved advantageous because several tests could be performed over the course of a single day, giving a more accurate picture of carbon dioxide dispersion.

Sensor Circuit Design

A K-30 1% infrared CO_2 sensor (CO_2Meter, Ormond Beach, FL) was used to take carbon dioxide measurements. The CO_2 measurement was referenced with an altitude measurement taken with an altimeter (Parallax, Rocklin, CA). These two sensors were programmed to run off of a single microcontroller (Arduino Duemilanove, SmartProjects, Italy). The circuit design, as shown in Figure 1, and microcontroller coding sampled the sensors every several seconds. These readings were written to the microcontroller memory that was then extracted and analyzed.

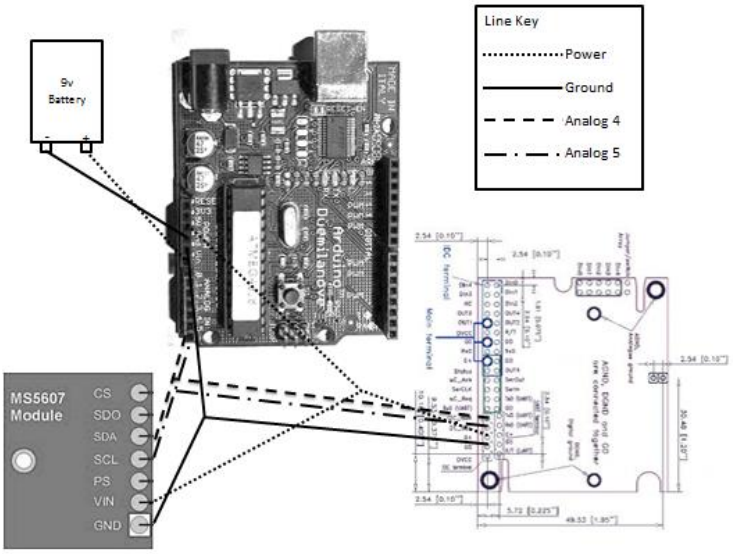

Figure 1. This diagram shows the wiring used to efficiently transmit the readings from the sensors to the controller. The wiring was done to utilize the I^2C interface that allows measurements to be taken from multiple devices over one connection.

A mobile phone (Motorola i290, Libertyville, IL) was used as a GPS tracking device. By downloading an Instamapper application to the phone, it was possible to see the coordinates of the package from the ground using online software. A camera (Canon Powershot 470, Lake Success, NY) was attached to the bottom of the package. The Canon Hacker Development Kit (CHDK) software package was uploaded to the camera's SD card. This added a variety of extra functions and manual controls to this specific model of Canon cameras. For this particular experiment the time-lapse photo function of CHDK was used, which takes a set amount of pictures with a set amount of time between each picture taken. These images were used to determine the composition of the terrain.

Encasement Design

The device was designed to provide a lightweight platform for the instruments. A polystyrene box was chosen to provide an insulated container for the instruments. Holes were carved in the side and bottom to provide a viewing angle for the camera and allowed air to flow to the CO_2 sensor. The altimeter and microcontroller were kept on the inside insulated from the weather.

It was calculated that 80 cubic feet of helium was needed to gain optimal lift of a 4 lb. package, (the actual device was approximately 11.5 oz.). The balloon was tethered to the ground

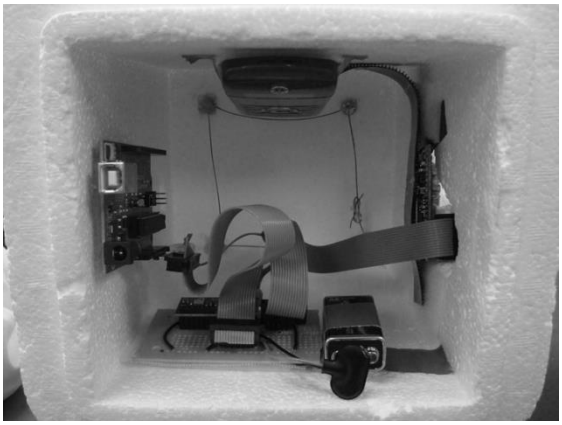

Figure 2. In the figure above the final configuration of the components is shown. Immediately before launch a heat source would be added to maintain core temperatures. The CO_2 sensor is mounted on the right wall inside the hole. The remaining features were

using two 500 feet 100 lb. test strength lines. This allowed controlled ascent and descent of the balloon and the Styrofoam box with all of the equipment inside. The final design is demonstrated in Figure 2.

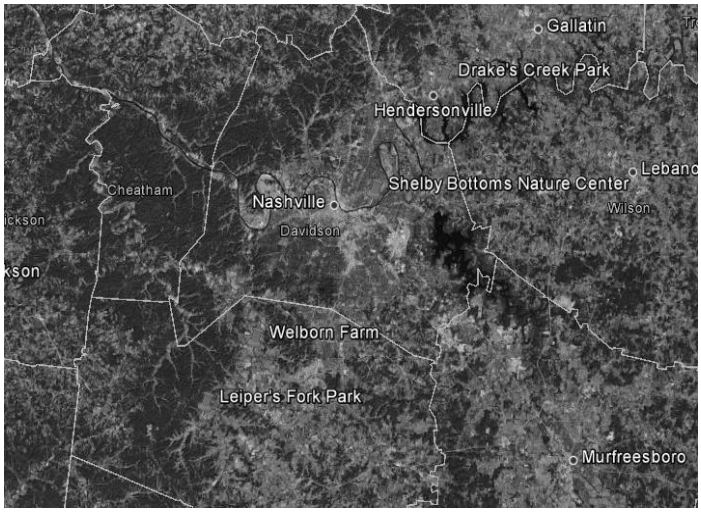

Figure 3. The launch sites were aligned along this common wind path so that the changes could be observed as CO_2 traveled with the wind through an urban environment. Areas were also chosen based upon proximity to the urban center, which was viewed as the main source of emissions.

Launch Procedure and Location Selection

To launch the balloon, a regulator was attached to a helium tank, and the balloon was filled to approximately 5 feet in diameter. The balloon was tethered using two 100 lb. test ropes and a metal carabiner to provide additional stability to the package. A parachute was added to provide security should the tethers break. The ideal launch sites were decided by a prevailing wind pattern of the Nashville area: from Southwest to Northeast through the city [2], as shown in Figure 3.

Results

Device Calibration

The consistency of the device was tested through a series of ground based field tests where the electronics remained at a stable altitude and data points were read directly into the computer from the microcontroller. Locations were referenced against a GPS coordinate to gain accurate altitude readings used to calibrate the altimeter. CO_2 data was also gathered at each site to visualize the typical fluctuations occurring at a stable altitude. The stability (low standard deviation from the average measurement) of both the altimeter and. This meant that the difference between predicted altitude and map altitude could easily be accounted *for* CO_2 Readings at Varying Altitudes and Locations.

Figure 4 shows how the measurements from this device can be used to see the dispersion of carbon dioxide from an urban center. This graph shows the higher levels of carbon dioxide at the site northeast of the city compared to those southwest of the city which were determined by anova test to be statistically different.

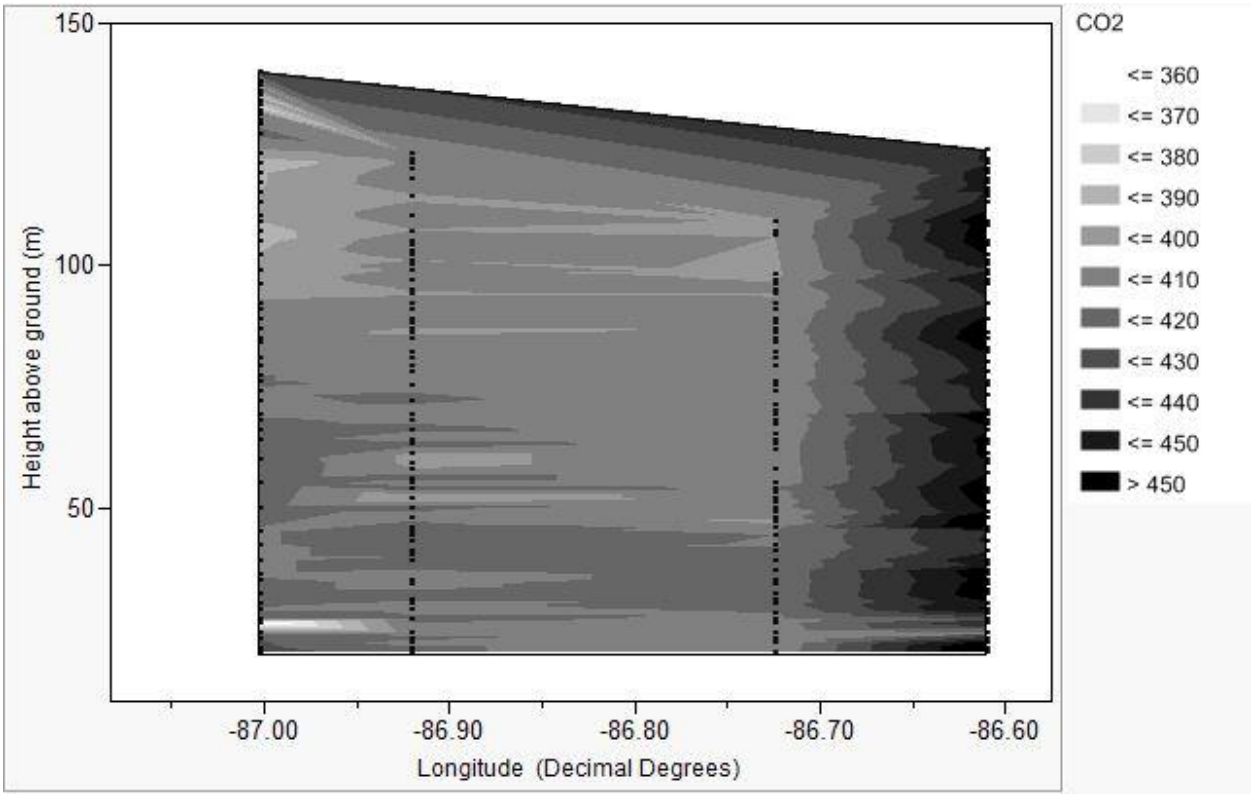

Figure 4. With downtown Nashville being located at approximately -86.78 longitude. The sites are analogous to those shown if Figure 3 (Leipers Fork, Welborn Farm, Shelby Bottoms Nature Center, and Drake's Creek from left to right)

Discussion

No conclusive results regarding the change in CO_2 levels across Nashville can be drawn from this data, but the experiment proved that this weather balloon device is a viable option for sensing particle concentration at a broad range of altitudes. There are many factors that could have potentially led to the lack of correlation in the field testing several of which are: Wind patterns, weather conditions, time of day, altitude, and the amount of tests taken. These tests were limited by the fact that two of the data points were taken on one day, and the other two were taken the following day. On the first day of testing (sites: Lieper's Fork, Welborn Farm) the wind was blowing to the southwest.

On the second day (sites: Drakes Creek, Shelby Bottoms Nature Center) the wind was blowing northeast. The tests were performed at different times during the day because the device was limited to one test site at a time. Another limitation of this project is that a tethered weather balloon is limited to an altitude of 500 feet, which may have been too low to determine significant changes in CO_2 concentrations. One way that could optimize the effectiveness of this experiment would be to simultaneously test several different sites. This would require the use of multiple balloons equipped with sensing devices. This method would be better suited than many alternatives because it is cost effective and provide readings which can be calibrated easily.

Conclusion

A device was created that can consistently measure CO_2 at different altitudes and locations. The design was validated through testing of both controlled and potential experimental settings. Going forward, an alignment of these balloons being deployed across the area of interest would allow a comprehensive map of CO_2 concentrations across the region. With more testing, data like the data collected by our device could conclusively show CO_2 dispersion away from the urban center on a city by city level without taking into account global mixing.

Work Cited

1. García, M. A., Sánchez, M. L., & Pérez, I. A. (2011). Differences between carbon dioxide levels over suburban and rural sites in Northern Spain. *Environmental science and pollution research international*, 1–8. Retrieved from http://www.springerlink.com/content/c51350218p2224l3/

2. "Wind & Weather Statistics North America North America Nashville Airport."*Windfinder.com*. N.p., n.d. Web. 29 Nov. 2012. < <http://www.windfinder.com/windstats/windstatistic_nashville_airport.htm> .

3. Chahine, M. T., L. Chen, P. Dimotakis, X. Jiang, Q. Li, E. T. Olsen, T. Pagano, J. Randerson, and Y. L. Yung(2008), Satellite remote sounding of mid-tropospheric CO2, Geophys. Res. Lett., 35, L17807, doi:10.1029/2008GL035022.

4. Miyazaki, K., P. K. Patra, M. Takigawa, T. Iwasaki, and T. Nakazawa (2008), Global- scale transport of carbon dioxide in the troposphere, J. Geophys. Res., 113, D15301, doi:10.1029/2007JD009557.

The Role of the Mannose Receptor and Toll-like Receptor 2 in TNFα and IL-6 Production

Elizabeth Y. Li, Michelle Lu, Oge Onuh, Shu Zhang
School for Science and Math at Vanderbilt, Nashville

Abstract

Macrophages are cells of the immune system that function through binding invading pathogens to their receptors. Though they are nonspecific immune responders, macrophages may affect specific immune responses through chemical signals, or cytokines that are produced from the binding of receptors. To study the activated signaling pathways and observe receptor responses through cytokine production, macrophage cells expressing the mannose receptor (MR) and Toll-like receptor 2 (TLR2) were incubated overnight in various cultures. After treating the cells with various ligands, TNFα and IL-6 were measured. It was found that the binding of ManLAM did not augment TNFα and IL-6 production. Moreover, pretreatment with an MR ligand prior to LPS treatment did not appear to stimulate MR-TLR2 interaction, as TNFα production was not increased through the binding of LPS to TLR2. Thus, it was inferred that the receptors may not interact in order to increase cytokine production and that the binding of ligands to these receptors do not significantly impact IL-6 and TNFα production.

Introduction

Macrophages are cells of the immune system that function against invading pathogens such as bacteria, viruses, and fungi. This process is initiated through the binding of the pathogen to a receptor on the surface of a macrophage. The receptors on these macrophages help fight against the pathogens by binding and then releasing various cytokines, which help create a specific immune response that either allows the cells to live and kills the invading pathogen, or allows the pathogen to take over the cell. The mannose receptor is a large protein that spans the cell membrane, with approximately 90% of the molecule on the outside and 10% on the cytoplasmic side (Figure 1). The mannose receptor (MR) can be activated by binding of a mannose-capped lipoarabinomannan sugar coated onto a polystyrene bead (ManLAM bead), acting as a pathogen, to the host MR.

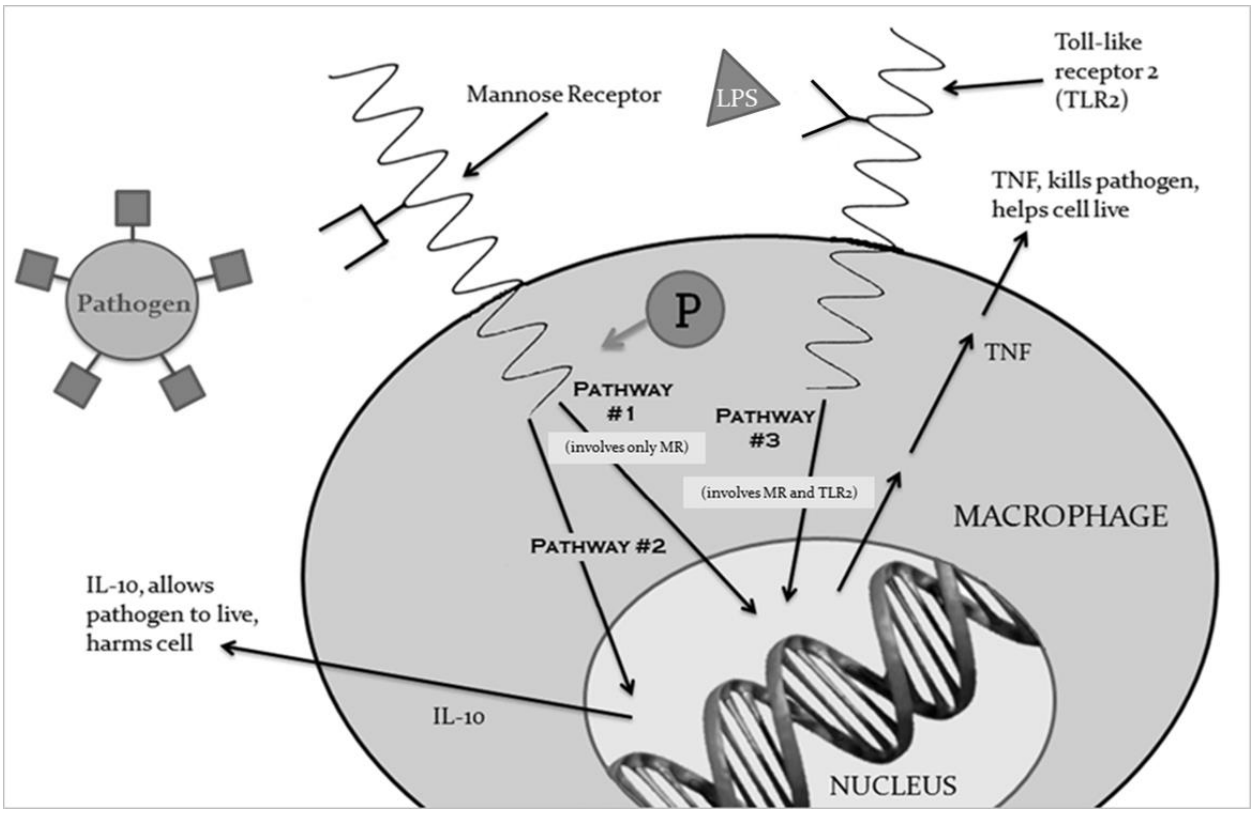

Figure 1. Diagram of a macrophage cell with two different receptors, the MR and TLR2, and three different possible pathways concerning IL-10 and TNFα. Pathway #1 involves only the MR and results in the production of TNFα through the binding of a pathogen. Pathway #2 likewise only involves the MR but results in the production of IL-6 through the binding of a pathogen. Pathway #3 involves both the MR and TLR2, with the pathogen initially binding to the MR and then leading to a conformational change, thus activating the TLR2 through LPS binding.

The purpose of this project was to research the cytokines that help eliminate the pathogen and allow the cell to live, such as TNFα and IL-6. This can occur by several possible pathways. The first potential pathway involves only the MR and might produce TNFα, a cytokine that helps in the cell's survival. The second pathway also involves only the MR. In this potential pathway, the pathogen binds to the MR, which results in the production of IL-10, a cytokine harmful to the host. The third pathway also produces TNFα; however, this involves both the MR and TLR2. In pathway three, multiple receptors work together to produce a response. Because TNFα can be produced in response to activation of the Toll-like 2 receptor (TLR2) on the macrophage, the MR and TLR2 were the main objects of investigation in this project. IL-6 was studied in conjunction with TNFα on the basis of deSchoolmeester's study indicating its increased response to binding of the MR [1]. It was hypothesized that ManLAM beads would bind to the MR and stimulate cells to produce tumor necrosis factor (TNFα) and interleukin-6

(IL-6), which would be released in an effort to protect the cell from the pathogen. This hypothesis was based on an article published Matthew L. deSchoolmeester supporting the production of IL-6 as a cytokine beneficial to the cell in response to MR stimulation. It was also hypothesized that pretreatment with an MR ligand prior to lipopolysaccharide (LPS) treatment would cause a conformational shift and stimulate interaction of the MR with TLR2, resulting in increased TNFα production through binding of LPS to TLR2. This was suggested because receptor interactions in other studies evidenced a positive correlation between TLR2 activity and TNFα production [2].

Methods

The macrophage hybridoma cell line (43MR cells) [3] used were grown in RPMI-1540 cell culture media supplemented with 1% pen-strep and 10% Fetal Bovine Serum. The cells were grown in a water jacketed CO_2 incubator at 37º C.

In order to verify receptor activity through the production of cytokines in these 43MR cells, sandwich ELISA assays were done on cells that were treated in a variety conditions (Table 1). These assays allowed the receptor response to be quantified through the production of cytokines TNFα and IL-6 (Figure 2).

Treatment Type	Description	Predicted Outcome
ManLAM beads	Beads coated with lipoarabinomannan (LAM); should signal cytokine production through the mannose receptor (MR)	Treatment will result in TNFα and IL-6 production through interaction with the mannose receptor (MR)
HSA beads	Beads coated with human serum albumin (HSA); serves as a negative control for binding to MR or TLR2	Treatment will result in little to no TNFα and IL-6 production due to a lack of interaction with mannose receptor
LPS	Positive control for TNFα production through TLR2	Treatment will result in production of TNFα and IL-6
Cells pretreated with ManLAM	Macrophages pretreated with ManLAM beads for 15 minutes	Treatment will result in an increased amount of TNFα and

Beads	followed by LPS for 6 hours; serve to help determine if ManLAM causes a conformational change to the MR, augmenting TNFα production	IL-6 production due to a possible conformational change and interaction between the mannose receptor (MR) and TLR2
Cells pretreated with HSA beads	Macrophages pretreated with HSA beads for 15 minutes followed by LPS for 6 hours; negative control for ManLAM bead treatment for receptor interaction	Treatment will result in some TNFα and IL-6 production because of the positive control, LPS; however, HSA will not cause a conformational change in the MR, and thus will not cause increased amounts of TNFα or IL-6 production.
No Treatment	Negative Control; serves as a comparison for other samples	No TNFα or IL-6 will be produced due to untreated cells.

Table 1. Samples that were tested throughout the experiment and their purposes.

The treatments included positive and negative controls with the experimental conditions. ManLAM beads were coated with lipoarabinomannan (LAM) and should activate the mannose receptor. HSA beads are coated with human serum albumin (HSA) and served as a negative control since HSA beads are accepted as non-binding to the MR. LPS was a positive control for TNFα stimulation through TLR2.

Samples that were pretreated with ManLAM beads for 15 minutes followed by LPS for 6 hours were compared with cells that were pretreated with HSA beads for 15 minutes followed by LPS for 6 hours. Finally, the no treatment cells were used as a negative control for cytokine production, a comparison for other samples.

The cytokine production from these treatments was quantified through ELISA assays. The ELISA assays start out with an antibody bound to the bottom of the well. The sample, either the treated cells or cell media, is then added, which binds to the primary antibody if IL-6 or TNFα is produced in the sample (Figure 2). A secondary antibody then binds to the cytokine, if present, and a colorimetric reagent binds to the secondary antibody. The colorimetric reagent produces a color change depending on

the amount of cytokine production detected in the well. Larger amounts of sample will cause a stronger color change, indicating a higher presence of the cytokine being measured which can be calculated using a standard curve.

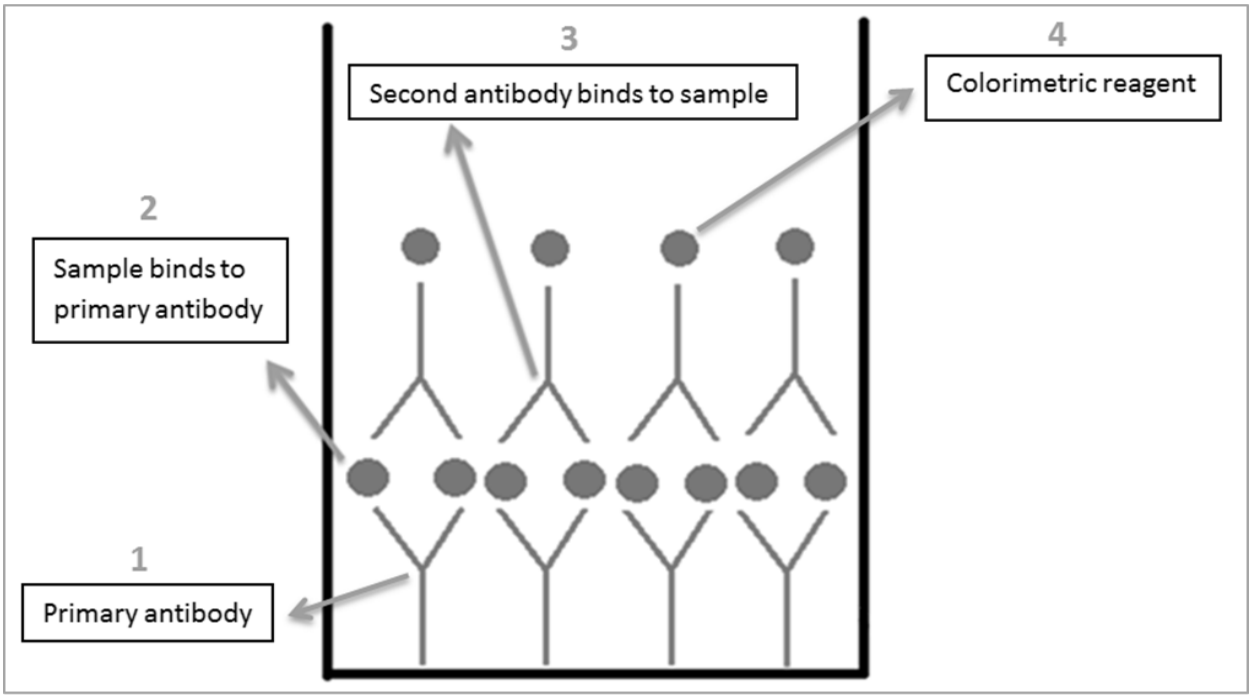

Figure 2. ELISA plate, well consisting of a primary antibody bonded to the sample, which then binds to a second antibody. This second antibody then binds to a colorimetric reagent. Larger amounts of sample will cause a stronger color change.

With the TNFα ELISA kit from Thermo Scientific, 50 µL of sample and then 50 µL of sample diluent were added to each well. The wells were then covered and incubated at room temperature for 1 hour. After the wells were washed 3 times, 100 µL of biotinylated antibody reagent was added to each well. The wells were incubated for another hour. After washing 3 times, 100 µL of streptavidin-HRP reagent was added to each well. The plate was incubated at room temperature for 30 minutes. The plate was subsequently washed 3 times, and 100 µL of TMB substrate was added to each well. Next, the plate was incubated at room temperature, in the dark, for 30 minutes. Finally, 100 µL of stop solution was added to each well, and the plate was read with a microplate reader at a wavelength of 450 nm to measure the optical density of each well. Standard curves were created using the same methods, using TNFα concentrations of 1000, 500, 250, 125, 62.5, 31.2, 15.6, and 0 pg/mL. These known

concentrations were created with serial dilutions. These methods were used to test TNFα production in relation the LPS concentrations.

IL-6 production was tested with the Human IL-6 ELISA Kit from Signosis, and the reagents were first prepared prior to starting the experiment using manufacturing instructions. First, 100 µL of sample, either cell growth media or the treated macrophage cells, was added to each well, and was incubated for an hour at room temperature with gentle shaking. After washing the sample a total of three times with 200 µL of 1x assay wash buffer, 100 µL of diluted biotin-labeled mouse anti-human IL-6 antibody was added to each well. This was then incubated at room temperature for one hour with gentle shaking. Then, the wells were washed and 100 µL of diluted streptavidin-HRP conjugate was added to each well and incubated for 45 minutes at room temperature with gentle shaking. The wash method was repeated once more, and 100 µL of substrate solution was added to each well. This was then incubated for 10 to 30 minutes before 50 µL of stop solution was added to each well. Within 30 minutes the color change from blue to yellow was quantified with a microplate reader at an absorbance of 450 nm. Standard curves were also created with known IL-6 concentrations were added in the place of samples by performing a serial dilution within the wells. The concentrations of IL-6 that were used included 4000, 2000, 1000, 500, 250, 125, 62.5, and 31.2 pg/mL. Similar methods were also used with two human TNFα ELISA kits from Signosis, which were used due to availability reasons.

Results

In order to verify successful TNFα production, macrophage cells were treated with varying amounts of LPS, a positive control. It was determined that as the amount of LPS stimulation increased, the amount of TNFα that was produced also increased (Figure 3).

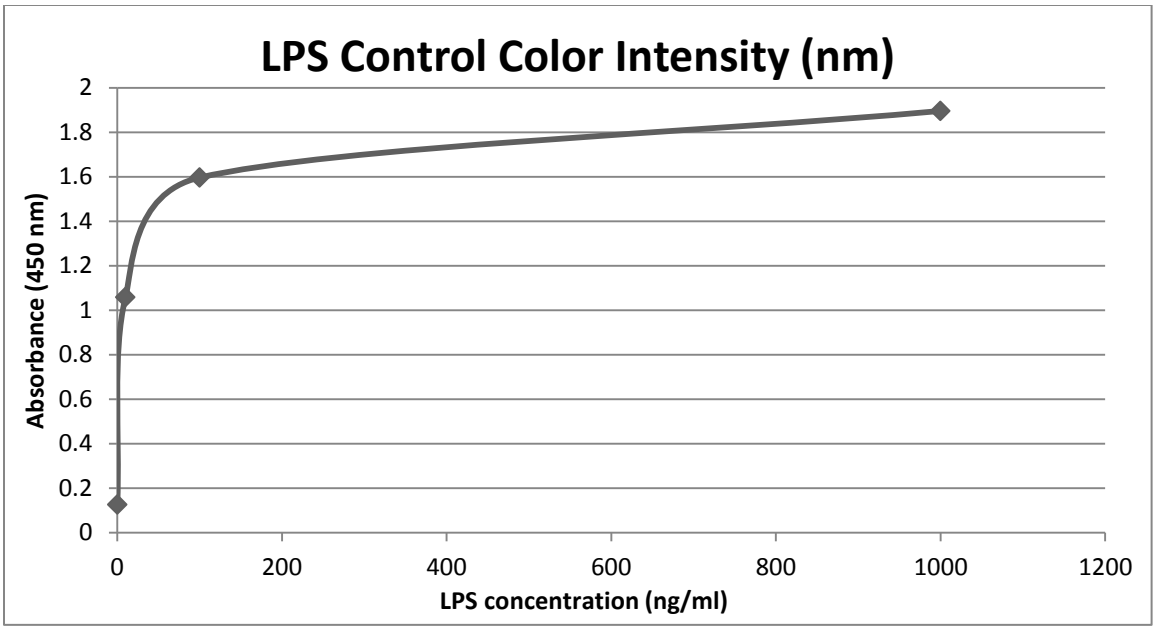

Figure 3. As the amount of LPS increased, the concentration of TNFα production increased; therefore, it was concluded that the concentration of TNFα was able to respond to the amount of LPS stimulation.

Following verification of TNFα production, other samples and controls were also tested for TNFα production. The amounts of TNFα produced for the samples ManLAM 20 beads/cell and LPS 100 µg/mL were compared with those for the samples HSA 20 beads/cell and no treatment. No significant difference was observed in the production of TNFα between the HSA treatment and the ManLAM treatment, despite the fact that the HSA treatment was a negative control for the binding of the MR and TLR2 and was thus not expected to result in significant TNFα production and expression. However, it was observed that the only sample that did not produce significant amounts of TNFα was the no treatment negative control (Figure 4). Through a one-way ANOVA analysis, the amount of TNFα production from the no treatment sample was significantly different from all of the other treated samples (p-value <0.01).

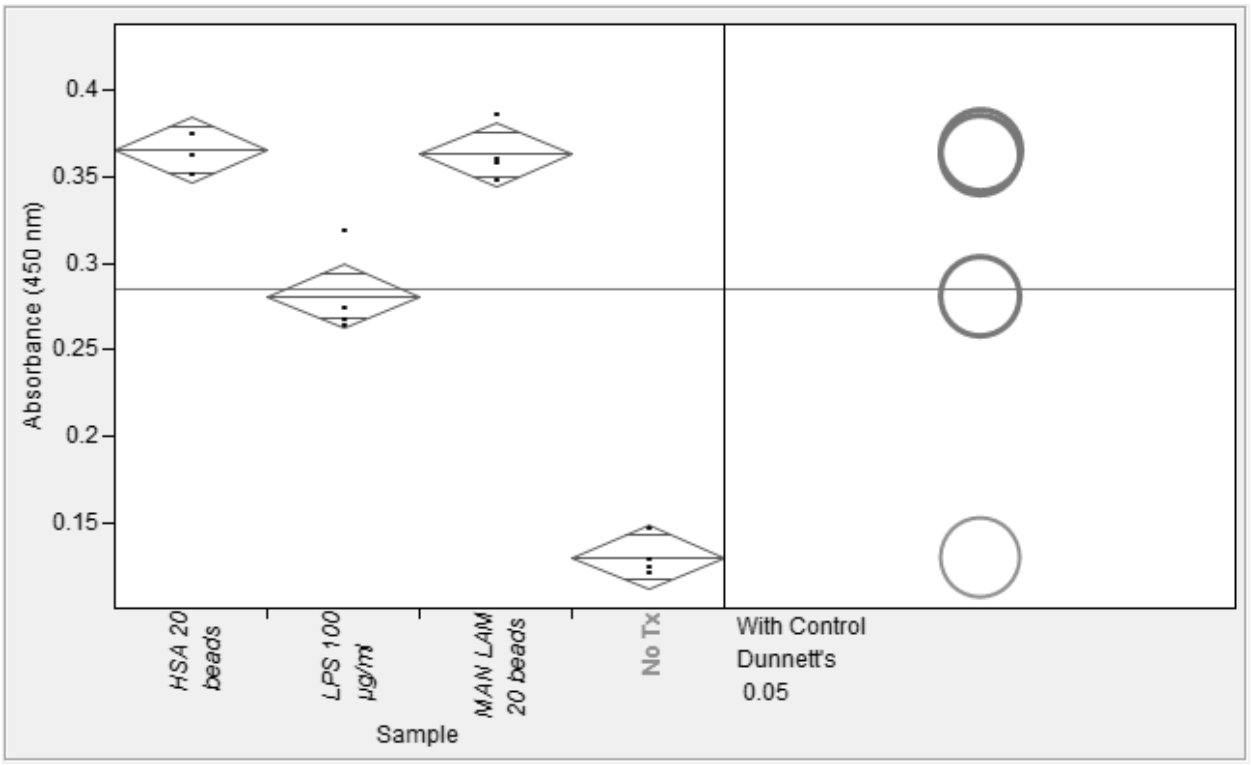

Figure 4. The ANOVA graph shows that the HSA and ManLAM beads were not significantly different from each other. This supports the idea that TNFα is not produced by activation of the mannose receptor, but instead, by another receptor.

In order to determine the factors that impacted the TNFα production from the HSA coated bead and ManLAM coated bead treatments and to evaluate the possibility of increased TNFα production caused by possible MR augmented TLR2 function, LPS samples pretreated with HSA coated beads or ManLAM coated beads for 15 minutes at 50 beads/cell were tested and compared with samples that were not pretreated. Because HSA beads do not interact with the MR, they should not augment TLR2 function through a conformational change. Therefore, they were used as a point of comparison to determine if ManLAM beads actually augment TLR2 function through first binding to the MR. The absorbance was measured for different treatments (Figure 5).

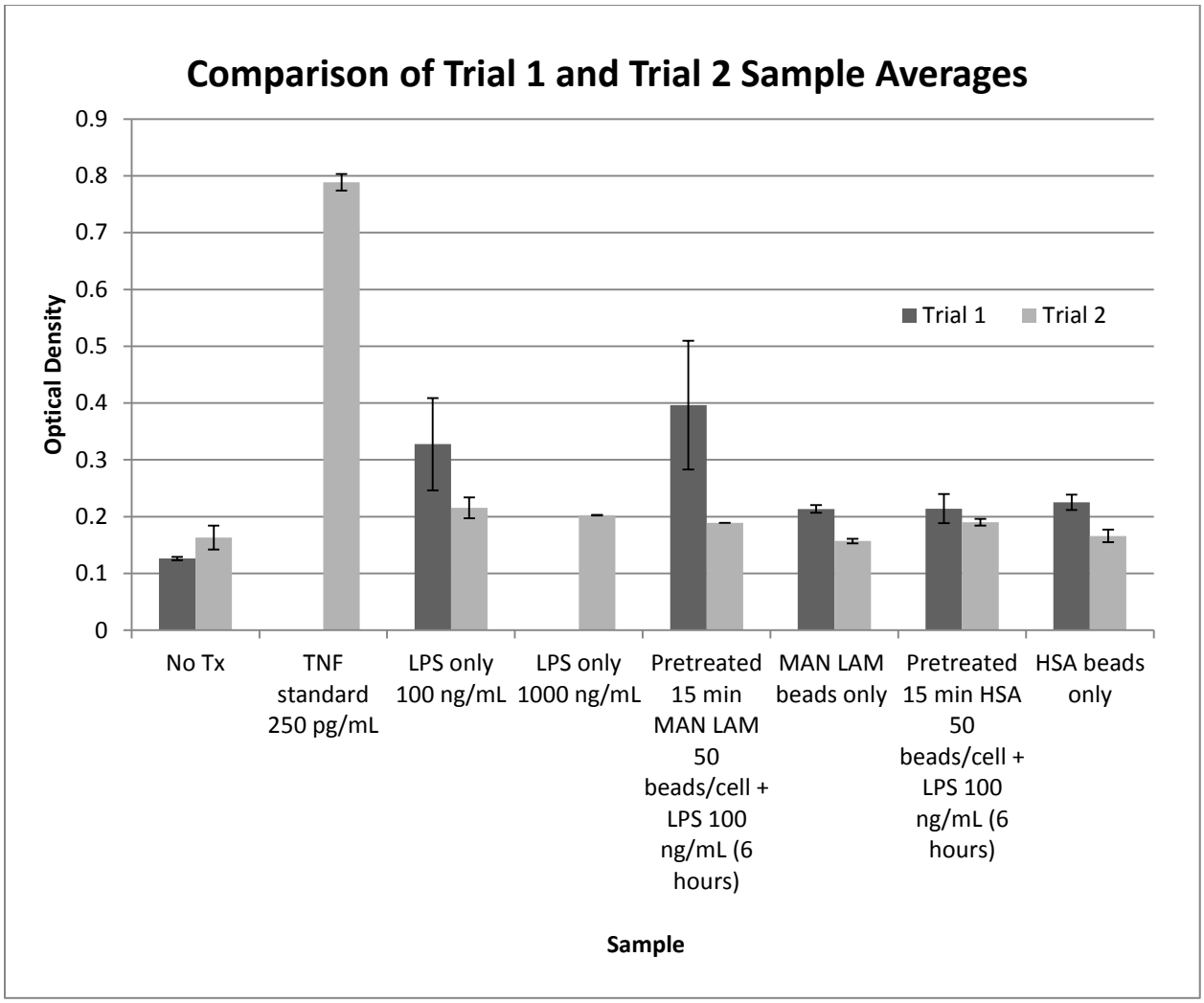

Figure 5. Trial 1 shows that TNFα production increased as the LPS and ManLAM concentration increased and was significantly different from no treatment (p-values <0.05). However, Trial 2 shows that the treatments yielded results that were not significantly different from no treatment (p-values >0.05).

The data collected from Trial 1 supported the hypothesis that TNFα production would increase with ManLAM pretreatment, which was thought to occur through MR augmented TLR2 receptor activity. Amounts of TNFα produced were significantly higher (p-values <0.05). However, the opposite was found to be true for Trial 2. Whereas the first trial showed significantly higher results for the treatments compared to the no treatment and HSA pretreated samples, the second trial produced results that were not significantly different from the no treatment (p-values <0.5).

To evaluate results from Trial 2, which were not significantly higher than the no treatment negative control, amounts of TLR2 and the MR were assessed with

fluorescence activated cell sorting (FACS) to determine if both receptors were present, as the receptors could only interact if both were present. The FACS showed adequate amounts of the MR, but only minimal amounts of TLR2 were present (Data not shown). It was predicted that TLR2 would interact with the MR through a conformational change; however, because the macrophage cells lacked high amounts of TLR2, it is likely that adequate interaction may not have occurred. This proposal served as a reason for the low production of TNFα in Trial 2.

Since cells with low levels of TLR2 produced low amounts of TNFα, the roles of both high and low TLR2 in the production of TNFα were studied. These tests were done to verify whether or not there was a direct relationship between concentrations of TLR2 and cytokine production. Furthermore, IL-6 was also tested with low and high TLR2 levels, after consideration of deSchoolmeester's study, which concluded that stimulation of the MR resulted in greater increases of IL-6 production than of TNFα production [1].

Despite the varying concentrations of TLR2 in the cells, generally low amounts of IL-6 were produced, though the no treatment control with high TLR2 produced greater amounts of IL-6 than any of the other samples. However, the difference between low TLR2 and high TLR2 for IL-6 production was not significantly different (p-value >0.05).

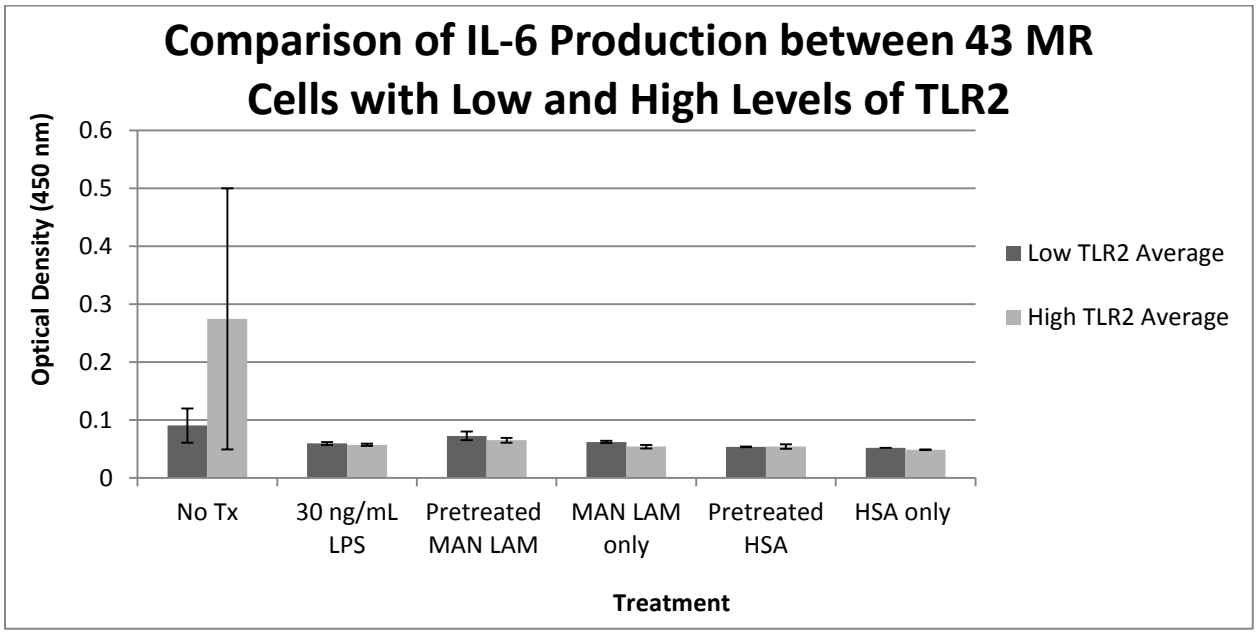

Figure 6. The difference between low TLR2 and high TLR2 for IL-6 production was not significant (p-values >0.05), resulting in no direct relationship between varying levels of TLR2 and IL-6 production.

The relationship concerning high and low levels of TLR2 was also investigated by studying the production of TNFα. The conditions with lower amounts of TLR2 seemed to generally produce larger concentrations of TNFα than the conditions with higher amounts of TLR2. However, the difference between low and high levels of TLR2 and TNFα production was insignificant (p-value >0.05); thus it was concluded that there was no difference between the low and high TLR2 conditions.

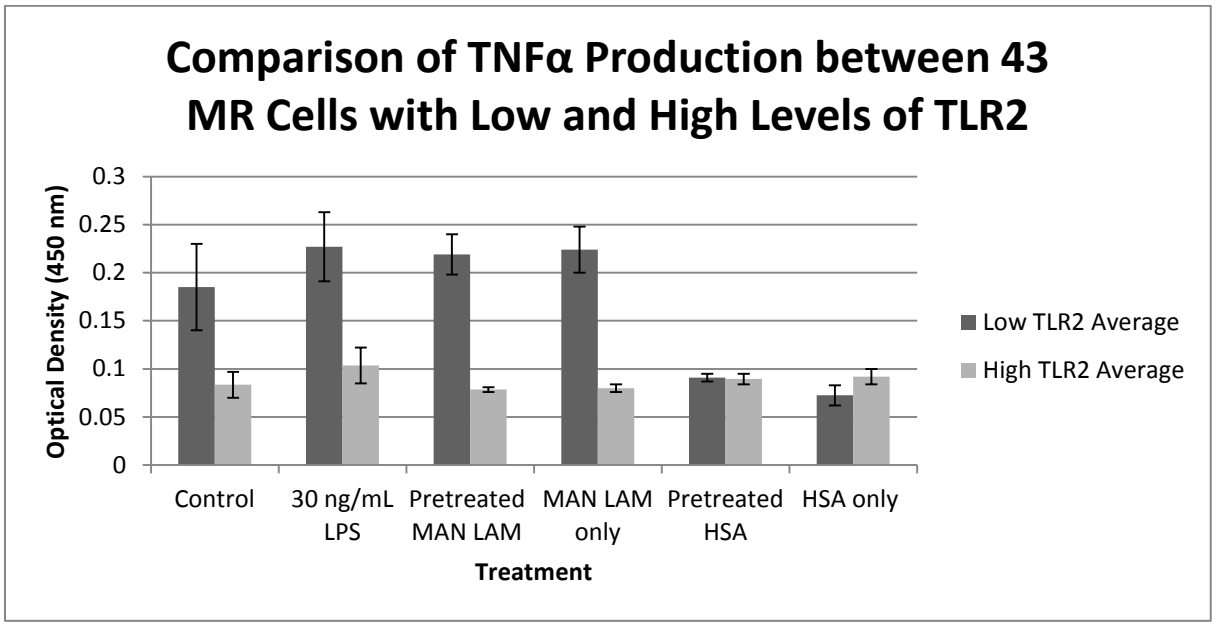

Figure 7. The low levels of TLR2 generally produced higher concentrations of TNFα than high levels of TLR2. However, the difference in TNFα production is not significant (p-values >0.05).

In general, low TLR2 levels had more TNFα and IL-6 production than high TLR2 levels. However, the increase in production for IL-6 with low TLR2 levels was far less than the increase in production for TNFα with low TLR2 levels.

Discussion

Contrary to previous research conducted by M. deSchoolmeester, the results obtained from the study showed that the binding of the ligands to the MR does not seem to play a significant role in TNFα or IL-6 production [1]. The amount of TNFα produced leveled off at a certain concentration of LPS, suggesting that at a certain point, the receptors reach full capacity.

Because it was verified that the amount of TNFα production did respond to the different amounts of LPS stimulation, cells treated under various conditions were tested. However, it was concluded that TNFα is not released through binding to the MR because HSA beads, as negative controls, and ManLAM beads produced about the same amount of TNFα. Instead, another receptor may account for the production of TNFα since HSA treated beads, which did not stimulate the MR, produced similar levels of TNFα when compared to the positive controls, which did stimulate the MR. It was hypothesized that primary binding to the MR would cause a conformational change of the MR, which would then provide the opportunity for it to interact with TLR2, augmenting TNFα and IL-6 production.

To test for the possibility of a conformational change in the structure of the macrophage, cells pretreated with either ManLAM beads or HSA beads were compared to those that were not pretreated. According to this idea, greater amounts of cytokine production would suggest the possibility of a conformational change. It was observed that TNFα production in Trial 1 for the ManLAM pretreatment was significantly greater than TNFα production for the no treatment control, which evidenced the possibility of a conformational change. However, in the second trial, it was observed that the TNFα production of the pretreated samples was not significantly different from that of the no treatment control.

The lack of TNFα production in the second trial prompted the acquisition of the FACS image, which pictured the quantities of MR and TLR2 in the macrophage. This picture revealed low levels of TLR2 in relation to the MR, which is highly unusual in macrophage cells. The low levels of TLR2 provided a possible reason for the low production of TNFα, as low levels of TLR2 may have prevented the necessary binding for the conformational changes of the macrophage.

This finding then led to the study of the effects of different TLR2 levels in macrophages, in relation to the MR and in relation to the production of TNFα and IL-6, as a previous study by deSchoolmeester had supported that increased amounts of IL-6 resulted from MR binding and stimulation [1].

Because it was originally hypothesized that the low TNFα amounts produced in response to samples pretreated with LPS were likely due to low levels of TLR2 on the

macrophages, it was also hypothesized that higher densities of TLR2 would lead to a greater production of TNFα and IL-6. When IL-6 was tested with high and low amounts of TLR2, the findings were similar to those for TNFα: there was no significant difference between the different amounts of TLR2, even though low TLR2 levels produced more TNFα and IL-6 than high TLR2 levels in general. However, this was based on the research conducted and may be prone to vary if more experiments are done, as they may reflect differing results of other studies. Unlike the results found in deSchoolmeester's study, more TNFα was produced than IL-6 in general [1].

Overall, it was concluded that the possible interaction of TLR2 and the MR does not play a significant role in increasing the production of either TNFα or IL-6.

For future studies, it would be ideal to repeat these experiments in order to verify these experiments and better understand the interactions between the MR and TLR2. Furthermore, it would be possible to study other potential receptors that may affect the function of the mannose receptor.

Acknowledgements

We would like to thank Dr. Virginia Shepherd and Ms. Sherell Vick for preparing cell cultures for us and giving us the resources needed to perform the experiments. We would also like to thank the School for Science and Math at Vanderbilt and especially Dr. Angela Eeds for providing us with the insight and opportunity for this project to be accomplished.

Work Cited

1. Matthew L. deSchoolmeester, Luisa Martinez-Pomares, Siamon Gordon, and Kathryn J. Else, "The Mannose Receptor Binds *Trichuris muris* Excretory/Secretory Proteins but Is Not Essential for Protective Immunity," *Immunology*, vol. 126, pp.246-255, May 2008.

2. Shoenfelt, Joanna, Robert J. Mitkus, and Rolf Zeisler. "Involvement of TLR2 and TLR4 in Inflammatory Immune Responses Induced by Fine and Coarse Ambient Air Particulate Matter." Journal of Leukocyte Biology (2009): 303-12.

3. Vigerust, David J, Sherell Vick, and Virginia L Shepherd. “Characterization of functional mannose receptor in a continuous hybridoma cell line.” BMC Immunology (2012): 13: 51.

A Possible Confirmation of a Planet Around Star KOI5475431

Benjamin Daniel Firth
Sullivan South High School, Kingsport

Abstract

One hundred sixty-five images were taken on November 7, 2012 of the star KOI5475431 with the intent of observing an exoplanet. After calibrating and analysing the data reference stars were chosen. A photometry function was then applied to the data. A drop in the brightness of the star was observed and provides good evidence that the exoplanet candidate was there.

Introduction

An extra-solar planet, or “exo-planet”, is any planet that orbits a star other than the Sun (Berta, 2013). Exo-planets are important because they allow researchers to test their ideas of how solar systems and planets form, to search for extraterrestrial life, and to study stars such as brown dwarfs and other low mass stars (Townsend, 2009).

Exo-planets may be detected in several ways: the Doppler technique, transits of the parent star, and eclipses (Wolf, 2007). The transit method was used for this project. This method works by measuring the light output of a star and looking for a slight dimming of the starlight as the planet crosses in front of the star (see figure 1). This method of detecting exo-planets only works if earth’s orbit is located in the same plane as the exo-planet’s orbit (Wolf, 2007).

This requirement greatly reduces the number of easily observable exo-planets, but since there are so many (5431 as of this writing) there is the possibility of a false positive. False positives can be caused by the target star being a variable star, starspots, or by a cloud passing overhead during the observation. The target star that was observed for this project was KOI5475431 (Kepler Object of Interest) and is located at the coordinates: Right Ascension 19h 54m 03.29s and declination +40d 38m 22.6s.

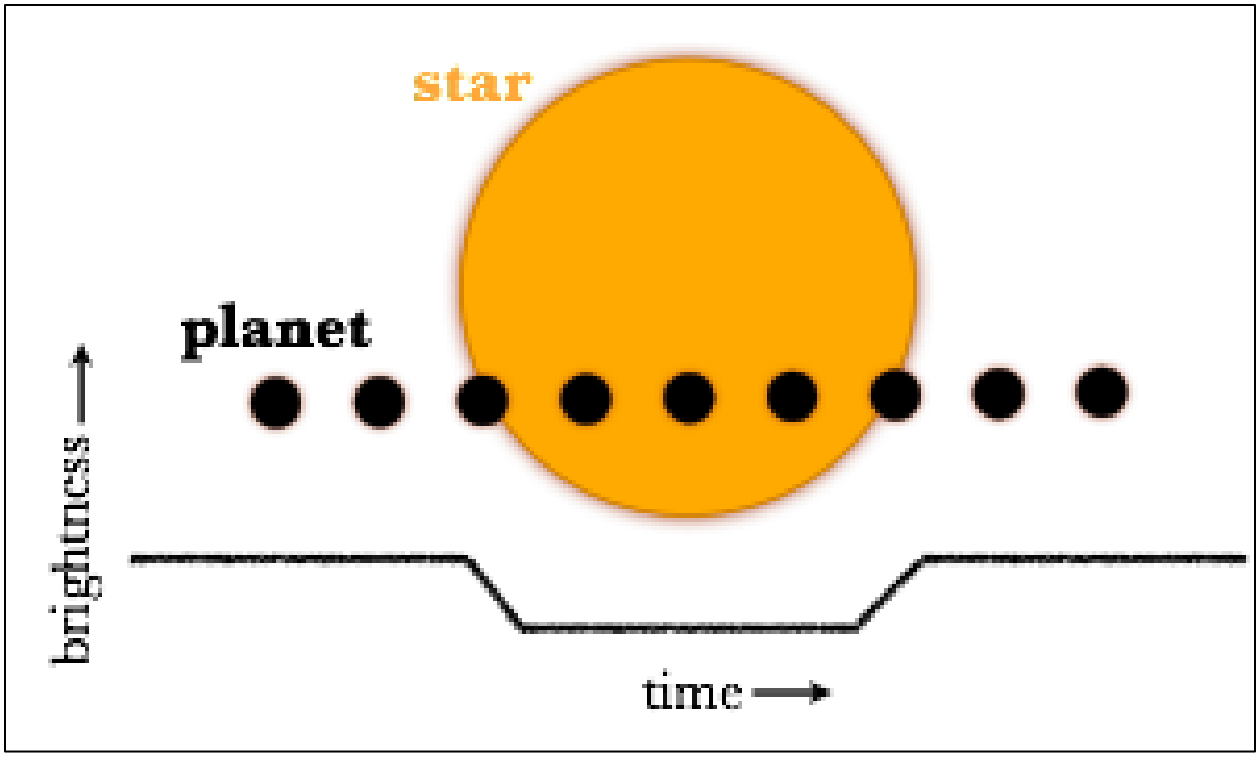

Figure 1. What a typical light curve looks like as a planet transits in front of a star (Wolf, 2007).

Procedure

The data for this project were collected using the 0.9 meter SARA telescope located at Kitt Peak, Arizona. SARA is the Southeastern Association for Research in Astronomy, which is a group of southeastern colleges which share in the operation of a 0.9-meter, f/7.5 telescope. Access to the SARA telescope was provided by East Tennessee State University (ETSU), located in Johnson City, Tennessee. Data collection required approximately 4 hours of observation.

Once collected, the data were processed using the photometry software *MaximDL*. First, the images were calibrated and aligned. Calibrating involves applying both dark and flat frames. Flat frames are images that are taken of a surface of a uniform brightness. This gives what is essentially an image of the telescope's optics which can be used to make allowances for vignetting and for dust on the detector or filters. In addition, flat frames can compensate for the different sensitivities of each pixel in the CCD (Sitko, 2007).

Dark frames are necessary because every CCD camera has differences in how its pixels respond to light. Dark frames are images which are taken with the telescope covered in order to block out all light. This provides an image of the hot and cold pixels on the CCD. Some pixels, known as hot pixels, always indicate that light is hitting them even if there is no light. Other pixels, known as cold pixels, always indicate no light no matter how much light hits the pixel. Both dark and flat frames are applied mathematically to the images during the calibration process (Sitko, 2007).

In addition to the above procedures, the images must be aligned with one another. Aligning is necessary because as the star moves across the sky it will not be in exactly the same pixel on the camera even though the telescope is tracking the star. The drop in brightness of the star during the transit is very small and so errors must be reduced as much as possible.

The data were taken using b and v photometric filters. A b filter transmits blue wavelengths (440nm) while a v filter transmits green wavelengths (550nm) (Fischbach, 2013). Using this information, the observed b-v value – which is a measure of the color index of the star. It is determined by subtracting the brightness taken with the b filter and the brightness taken with the v filter. The software package *Excel* was then used to subtract the two values.

Stars of similar apparent magnitudes were used as reference stars (apparent magnitude is how bright the star appears as seen from Earth). These reference stars were used in order to determine whether a dip in the light of the target star curve occurred when compared to the reference stars.

Then the sort function in *EXCEL* was applied to that data to find those stars that were closest in brightness to the target star. The chosen reference stars were of a similar color to the target star because as the target star moved closer to the horizon the light from the star has to pass through more of the earth's atmosphere. The light from a star is diminished because the atmosphere absorbs the bluer wavelengths of light more than the redder wavelengths causing a differential color shift in the star light (Flanders, 2008).

The six reference stars used were those closest in color to the target star. On data images the target star is labeled Obj1 and the six reference stars are labeled Ref1

to Ref6. Figure 2 shows KOI5475431 and the six reference stars. After selecting the stars, the data were saved as a .cxv file. The file was then opened in *EXCEL* and every five data points were averaged to make the graph more readable. Then the averaged data points were copied into *Logger Pro* to generate a graph. The error bars were calculated by separating the plot into three sections (before the transit, during the transit, and after the transit). The standard error was found for each category and then a weighted average was used to find the standard error for the entire plot. Then the graph from *Logger Pro* was copied into *Smart Notebook* to allow lines of best fit to be drawn. The percent drop in brightness was calculated by using the average of the brightness without the transit (B_{nt}) and the average of the brightness during the time of transit (B_t). The formula for the percent drop is $\log[(B_{nt}-B_t)/B_{nt}*100]$. The logarithm has to be taken because magnitude is a logarithmic scale (Dolan, 1989). The size of the planet is equal to the cross-sectional area of the star times the percent drop expressed as a decimal.

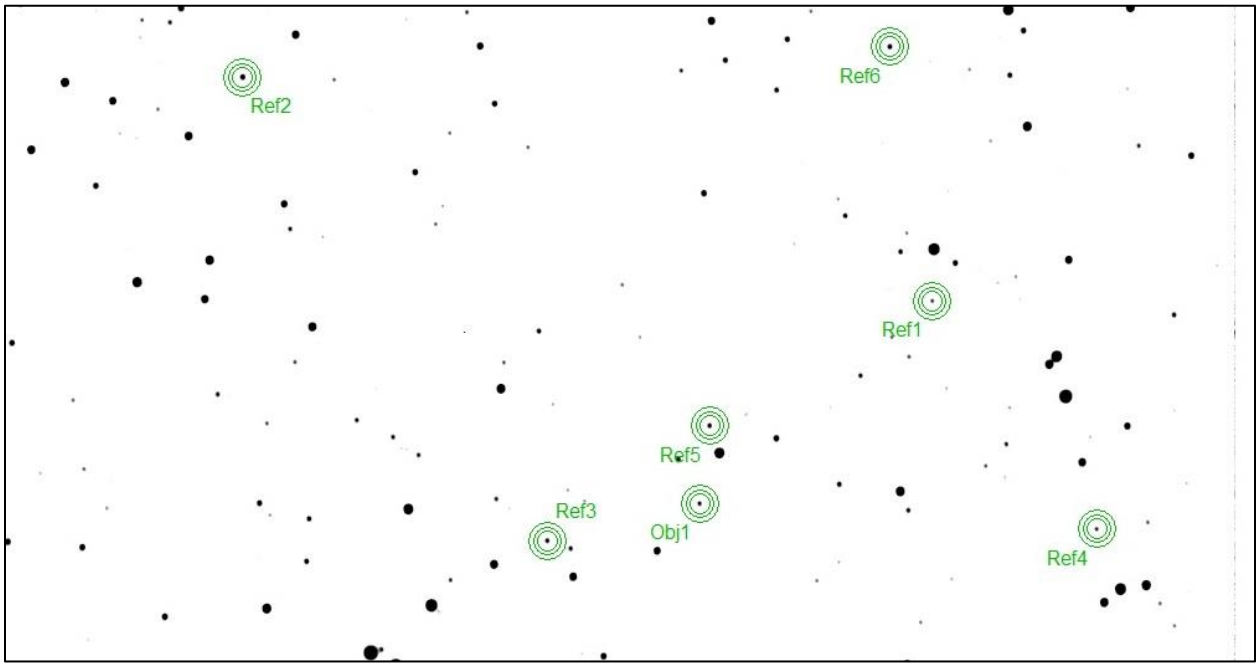

Figure 2 This figure shows the stars that were used. Obj1 (KOI5475431) is the star that was observed, and Ref1 to Ref6 are the six reference stars that were used.

Results

It is apparent that by looking at the plot that there is a dip in the light curve of KOI5475431 when compared to the reference stars (see figure 3). Percent drop was

calculated to be about 1.54% which indicates that there was a possibility of the planet transiting during that time. The error bars were calculated to be 0.00202 for the target star and 0.00220 for the reference star used in the diagram. The amount of time from the beginning of the transit until the end of the transit was about 1.8 hours. The planet's diameter-was calculated to be about 12 percent of the star's diameter.

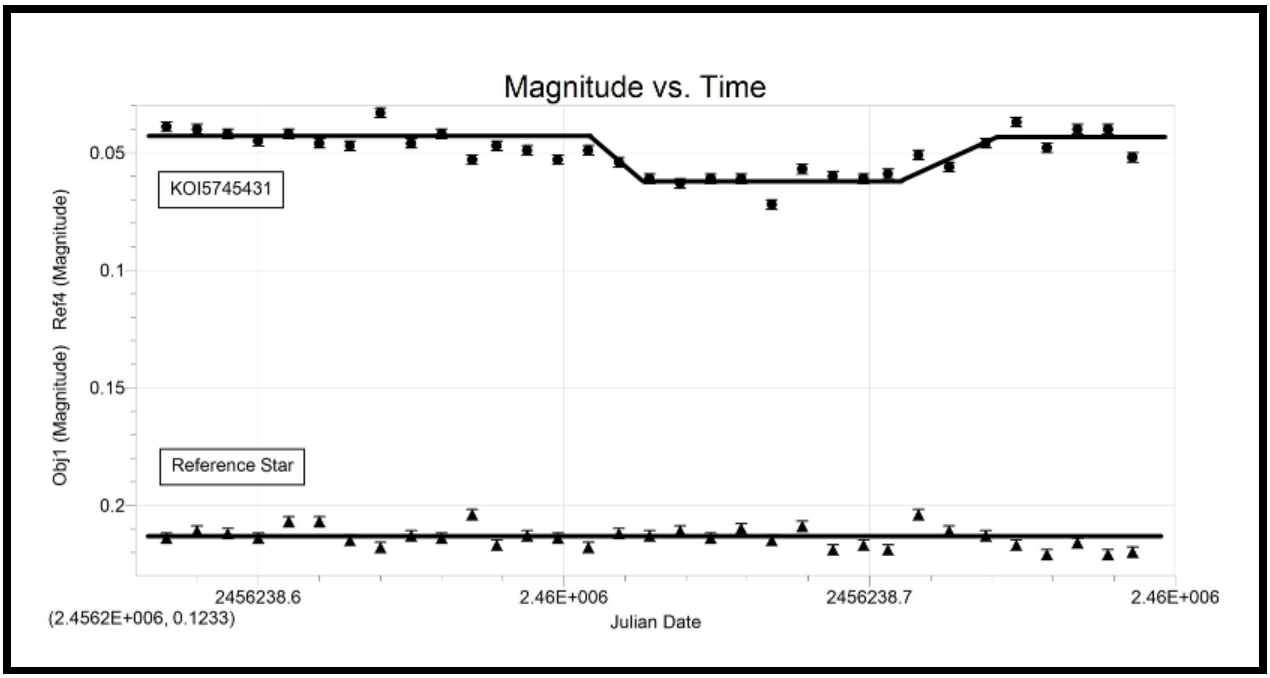

Figure 3 shows the light curve of the target star and one of the reference stars. The target star has the circular points and the reference star has the triangular points.

Conclusions

Based on the evidence, it can be concluded that there was a probable exoplanet transit during the time of observation. This does explain the drop in the light curve at the predicted time. Additional evidence is that the predicted size of the planet-to-star ratio is 10.6 percent compared to the observed value of 12 percent. The length of the transit also gives support because the predicted value was 1.72 hours and the observed value is 1.8 hours. These values agree well with those reported by NASA (NASA, 2013).

Work Cited

Berta, Zachory K. (2013) “The MEarth Project” http://www.cfa.harvard.edu/MEarth/Science.html. February 27, 2013.

Dolan, Charlie. (1989) “Stellar Brightness” http://www.astro.wisc.edu/~dolan/constellations/extra/brightest.html March 6 2013 March 6, 2013.

Fischbach, Jürgen. (2013) “Astronomy Filters” http://www.lot-oriel.com/files/downloads/andover/en/astronomyfilters.pdf Andover Corporation. March 4, 2013.

Flanders, Tony and Phillip J. Creed. (2008) “Transparency and Atmospheric Extinction” http://www.skyandtelescope.com/howto/visualobserving/19712459.html Sky and Telescope. March 4, 2013.

NASA. (2013) “NASA Exoplanet Archive” http://exoplanetarchive.ipac.caltech.edu/cgi-bin/ExoTables/nph-exotbls?dataset=cumulative March 6, 2013.

Sitko, Michael L (2007) “How to Use an Astronomical CCD Camera” http://www.physics.uc.edu/~sitko/AdvancedAstro/7-CCDuse/CCDs.pdf Department of Physics, University of Cincinnati. March 3, 2013.

Townsend, Rich. (2009) “The Search for Extrasolar Planets” http://www.astro.wisc.edu/~townsend/static.php?ref=diploma-2. Feb 21, 2013.

Wolf, Portia. (2007) “The Outer Planets: Extrasolar Planets” http://lasp.colorado.edu/education/outerplanets/exoplanets.php#detection Laboratory for Atmospheric and Space Physics University of Colorado at Boulder. February 27, 2013.

Acknowledgements

Thank you to Dr. Gary Henson of East Tennessee State University (ETSU) for operating the telescope and collecting the data. Thank you to Mr. Anthony Peters for helping with calculating the error bars for the light curve. Thank you also to Mr. Thomas Rutherford for helping with using *MaximDL* and *EXCEL* in addition to proofing my paper.

Natural Antibiotic Resistance in Cave Stream Bacterial Communities

Petra Byl, Diana Neculcea
Hume-Fogg Academic High School, Nashville

Abstract

Actinobacteria and penicillin fungi are common features on the walls of Mammoth Cave, a karst system in Mid-Southern Kentucky. These microbes create environmental pressure for antibiotic resistance; therefore bacterial cave stream communities in Mammoth Cave are prime candidates to test the effectiveness of man-made bactericidal agents on naturally resistant bacteria. Plate counts conducted using 10% tryptic soy agar rendered bacteria populations that ranged from 700,000 to over 2 million colony forming units per 100 mL of cave water. Antibiotic concentrations of 0.01, 0.1, 1 and 10 mg/L erythromycin, tetracycline, and ampicillin were used for dose-response tests and zone of inhibition studies. After quantifying colony forming units and screening zone of inhibition tests, it was determined that bacteria from Mammoth Cave produced a typical dose response when subjected to increasing concentrations of the antibiotics ampicillin and tetracycline. However when the cave-stream bacterial community was exposed to erythromycin at sub-lethal levels [0.01-1.0 mg/L], the number of colony forming units increased. Further investigation will need to clarify if this stimulation of colony formation was the result of a quorum sensing mechanism for erythromycin in the cave habitat.

Introduction

Antibiotics have been present in Earth's biosphere long before observation could be recorded and were generally assumed to be mechanisms of survival (D'Costa, 2006; Wright, 2010). For the most part, natural bactericides were thought to eliminate competitors that would otherwise consume a limited amount of resources (Baltz, 2008; Wright, 2010). However in the contemporary world, antibiotics have been manipulated chemically and are mass-produced to eradicate pathogens (Campbell, 2009). Subsequent overuse of laboratory synthesized antibiotics has led to a greater amount of resistance among bacteria populations, as well as provoked much concern in the medical community (Campbell, 2009; Thaller, 2010).

Recently, research in the Lechiguilla cave system supported the proposition that antibiotic resistance in sub-surface bacteria communities has occurs naturally without human interference (Bhullar, 2012; Brown, 2009). Therefore one could speculate that

bacteria found in remote sections of Mammoth Cave, Kentucky- another karst cave system, might demonstrate a similar phenomenon. Water samples collected from deep inside Mammoth Cave provided bacteria, which were endemic to a relatively isolated environment (Barr, 1976). The only energy sources carried into the cave system came from bat guano coupled with the base-flow and recharge of water (Barr 1976). The water remained generally free of synthesized contaminants because management practices, such as parking lot filters effectively prevented chemicals from leaching into Mammoth Cave (Diehl, 2012; Ryan and Meimen, 1996). Although Mammoth Cave was previously used for saltpeter mining and then became a tourist attraction, conservation acts have protected the natural cave ecosystem (Crothers, 2013). Tourists have restricted access to cave passages, and land use on the surface is carefully controlled by the National Park. This protection of the cave ecosystem reinforced the legitimacy of using Mammoth Cave as a site to sample bacteria unexposed to manufactured antibiotics.

Bacteria indigenous to the hydrologic flow path of Mammoth Cave provided a foundation to test multiple antibiotic resistance. Frequently if bacteria have exhibited resistance to one type of antibiotic they often have demonstrated resistance to other bactericides (Chapman, 2003). One of the main genera of bacteria in the remote regions of Mammoth Cave is the *Actinomycete*, which is known to produce several antibiotic compounds (Rusterholtz and Mallory, 1994). Given that cave bacteria have been repeatedly exposed to bactericidal agents produced from surrounding microbes, they therefore have increased selective pressure for resistance to natural and synthetic antibiotics (Rusterholtz and Mallory, 1994). Comparing the responses of sub-surface bacteria communities to synthetically and naturally derived antibiotics could reveal more information on antibiotic resistance in general.

These antibiotics were selected for evaluation- tetracycline, erythromycin, and ampicillin. In the context of medicinal use, tetracycline and erythromycin can both be prescribed for skin, urinary, or respiratory ailments, and function by attacking the pathogens' ability to synthesize protein. Tetracycline and erythromycin were first identified from actinobacteria and actinomycetes, the second of which has formed a biofilm in Lee's Cistern- a cavern that lies in the hydrologic flow path of Mammoth Cave

(Embry and others, 2012; Rusterholtz and Mallory, 1995). Thus bacteria sampled from Lee's Cistern were exposed to erythromycin. Another site sampled was Annette's Dome, which lied further upstream and had a less extensive visible community of actinomycetes (Barr, 1976; Rusterholtz and Mallory, 1995). Both Lee's Cistern and Annette's Dome were considered to be at the middle level of the four level cave system.

The two antibiotics, tetracycline and erythromycin were chosen to be part of this study because previous laboratory research has shown that the pathogen *Pseudomonas aeruginosa* exhibited biofilm formation and bacterial cytotoxicity when exposed to sub-lethal concentrations of tetracycline (Linares, 2006). Such morphological alterations deviated from the expected response and have supported the idea that antibiotics are used as a signaling agent within microbial communities (Keller and Surette, 2006). Yet, stimulation within a natural microbial community has not been described in the literature.

This study was split into three objectives. The first was to determine if antibiotic resistance existed in bacteria from Mammoth Cave, while the secondary objective was to characterize the extent of the cave bacteria's response to increasing doses of antibiotics manufactured for mass-production. Lastly, the final objective was to find if the location and microbial community inside the different caverns affected the bacteria's susceptibility to antibiotics.

Methods and Materials

Site description - The sampling sites were selected to represent different microbial communities in the cave system, Lee's Cistern with visible actinomycete growth and Annette's Dome with no visible growth.

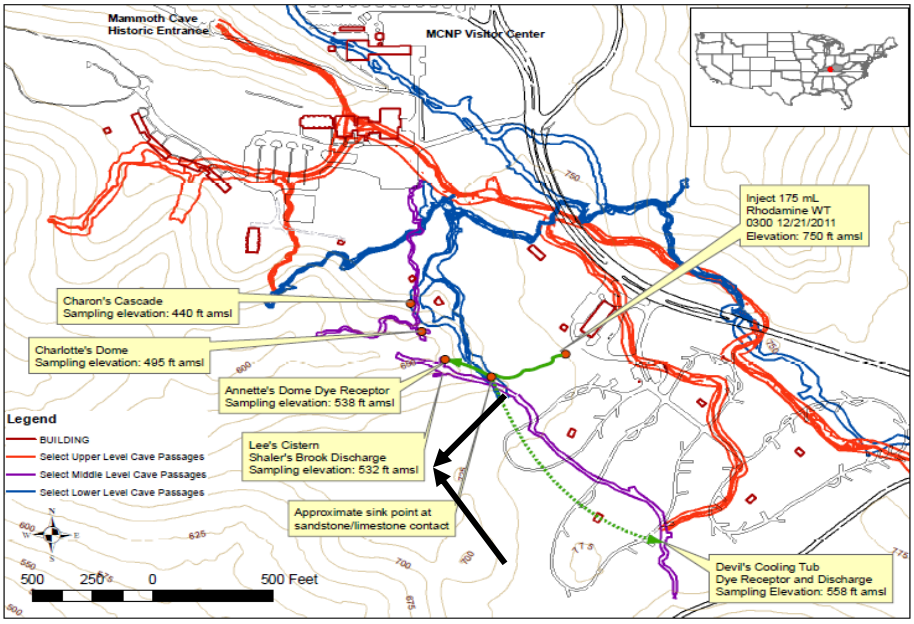

Figure 1. Arrows signify sampling sites. Cave samples were collected in Annette's Dome and Lee's Cistern for this study. (Map courtesy- Dr. R. Tommey, MACA NPS)

Flow path determination – Tracer studies were conducted, both on the surface and in the cave, in order to characterize flow paths. A 120-gram salt tracer was released in Annette's Dome during base-flow (discharge = 4.6 liter per minute). Salt concentration was measured every ten minutes, which determined how much tracer had moved through Lee's Cistern. The quantitative tracer equation from Palmer (2007) was used to calculate tracer center of mass. Center of mass equals half of the total tracer mass measured at Lee's Cistern (M_{out}). Approximately 119 grams of tracer were accounted by the load equation. Thus 99% of the mass released in Annette's Dome was observed in Lee's Cistern, indicating there was no loss of flow to any other passages.

$$M_{out} = V_f \, {}^{n}\Sigma_{i=1} \, Q_i \, (C'_i - C'_0) \, \Delta t_{i'}$$

M_{out} = mass of tracer recovered, in grams;

V_f = unit conversion factor (from sonde reading to grams per liter);

n = number of sampling intervals, equal to the total number of samples minus one;

i = the ith sampling interval;

Q_i = mean discharge during the ith sampling interval, cu. ft/sec, or, L/min;

C'_i = mean measured tracer conc during the ith interval, equal to the mean of 2 samples taken at the beginning & end of the interval, in mg/L;

C'_0 = background tracer concentration, measured at time of injection, mg/L;

$\Delta t_{i'}$ = duration of the ith sampling interval, minutes

A quantitative dye study in December of 2011 found that it took an estimate of 75 minutes for the tracer, released from the parking lot storm filter to cascade down to Annette's Dome, which is recognized as the beginning of Shaler's Brook (Embry and others, 2012). It took another 20 minutes for the dye to reach Lee's Cistern down gradient of Annette's Dome.

Water samples for microbial analysis were collected approximately every 2 to 3 weeks in the summer of 2012. Grab samples were collected during base flow using clean sterile 250 mL bottles. A first flush storm sampler (Diehl, 2008) was also used in Annette's Dome. The water samples were brought back to the laboratory in Nashville and stored at 5^{o}C until analysis was done.

Analysis included bacteria plate counts using 2% agar containing 10% strength Tryptic Soy nutrients (10% TSA). Previous work by Byl and others (2002) found karst groundwater bacteria grew better on low strength media than full strength TSA. Concentrations ranging from 0.00 to 10.00 mg/L on a base 10 logarithmic scale of tetracycline and erythromycin were mixed into the 10% TSA immediately prior to pouring the plates. The cave water samples were hand shaken for a minute to re-suspend the bacteria, and a 10 uL aliquot of raw water was placed on the agar. The cave water containing bacteria was evenly spread over the plate using a sterile glass rod. Inoculated plates were inverted and placed in an incubator at 25^{o}C. The bacteria

colonies were counted at 1, 2, and 3 days. The results are reported as colony forming units per 10 uL.

The second step of the analysis was to calculate the zone of inhibition caused by disks soaked with antibiotics tetracycline and ampicillin. Stock solutions were prepared, and then concentrations of 0.00, 0.10, and 1.00mg/L for each antibiotic were synthesized from the stock. Sterile qualitative filter paper (Whatman Grade #1) cut into 1x1cm squares were saturated in the various antibiotic concentrations and left to dry upon sterilized plastic sheets for 1 hour. In the duration of that hour, using a sterile loop colonies were gathered from bacteria grown on agar plates containing 1.00 mg/L of tetracycline from Annette's Dome and Lee's Cistern. The 2 selected colonies from Annette's Dome and Lee's Cistern were inserted into separate microcentrifuge tubes that held 1.00 mL of sterile distilled water, which was prepared via syringe filteration (Gelman Sciences). Next the bacteria were dispersed in the aqueous solution by hand shaking each microcentrifuge tube for 30 seconds. A 20 uL of the bacteria solution from Lee's Cistern was inoculated onto 2% agar plates with 10% TSA, preceded directly by the placement of the antibiotic disk in the center of each plate using sterile tweezers. The microcentrifuge tube was re-shaken before each inoculation of bacteria onto an agar plate, to ensure the bacteria were evenly distributed in the injection water. A replicate was created after the first set of bacteria from Lee's Cistern was inoculated onto agar plates. The same steps were repeated in inoculating replicate plates and establishing antibiotic screening tests using bacteria originating from Annette's Dome.

Results and Discussions

The bacteria population of Lee's Cistern and Annette's Dome exhibited minor resistance to tetracycline and much greater resistance to erythromycin. The microbial resistance to tetracycline qualified as a typical dose-response to antibiotics (Fig. 2). This was denoted when the concentration of the antibiotic increased, the number of bacteria decreased (Kane, 2004).

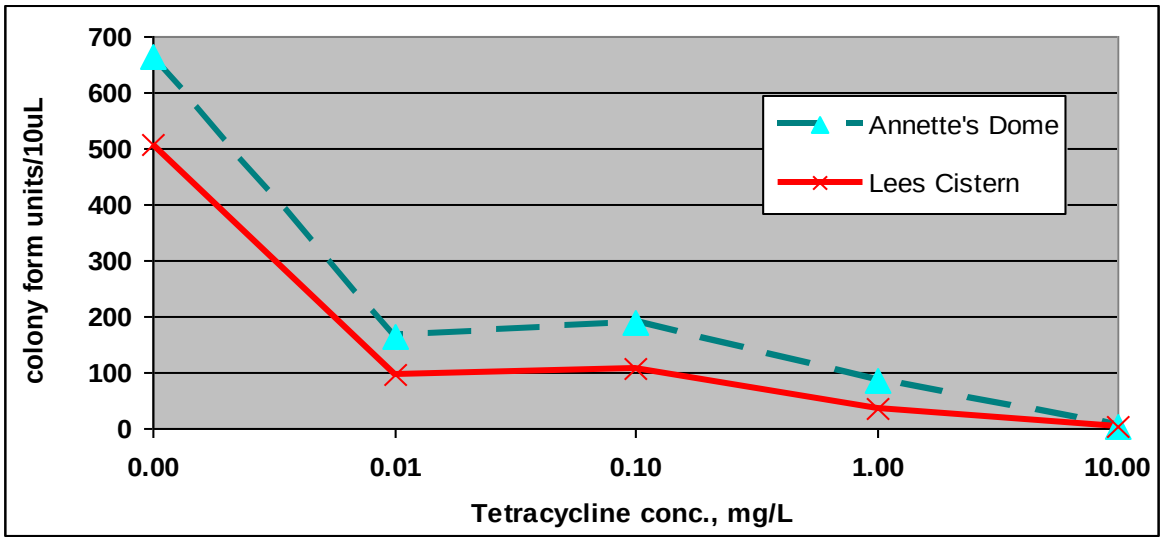

Figure 2. The response of bacteria sampled from Annette's Dome and Lee's Cistern to Tetracycline

In contrast to the tetracycline results, erythromycin stimulated cfu's (colony forming units) at low concentrations in both Lee's Cistern and Annette's Dome. The cfu stimulation was much greater in Lee's Cistern, where the population of actinomycetes was visibly much greater than in Annette's Dome (Fig. 3).

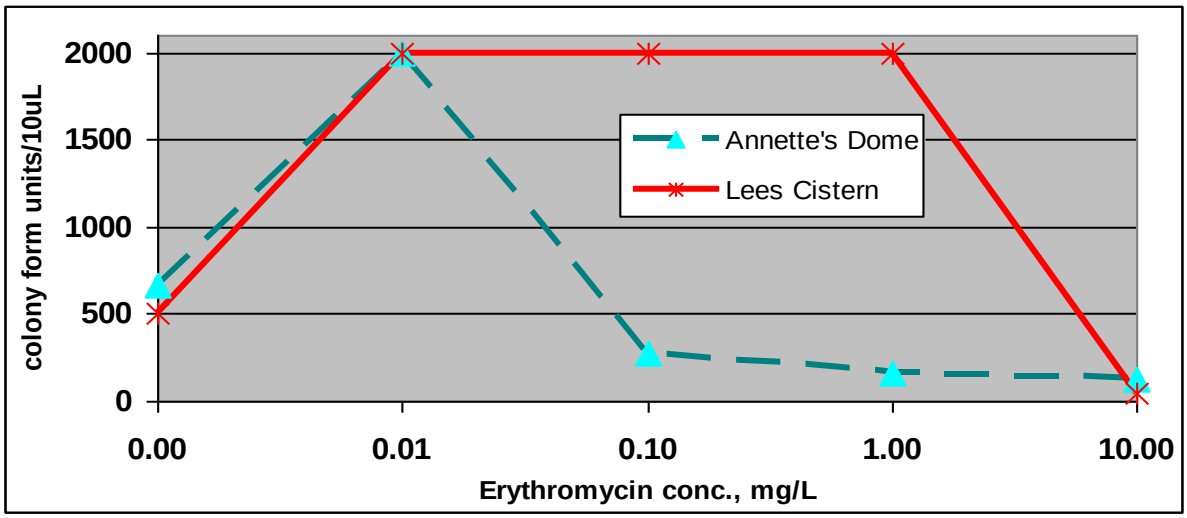

Figure 3. The response of bacteria sampled from Annette's Dome and Lee's Cistern to Erythromycin

The erythromycin dose-response test was repeated with a new sample from Lee's Cistern and more replicates. Bacteria from Lee's Cistern raised in the presence

of 0.1 to 10.0 mg/L erythromycin statistically (T-test) deviated from the control values at a p-value = 0.05 (Fig. 4). The white arrows symbolize statistically significant growth, while the black arrows indicate statistically significant reduction compared to the control plates with no erythromycin. An erythormycin concentration of 0.1 to 1.0 mg/L stimulated significant increases in cfu. The highest concentration, 10 mg/L, significantly decreased the cfu (Fig. 4)

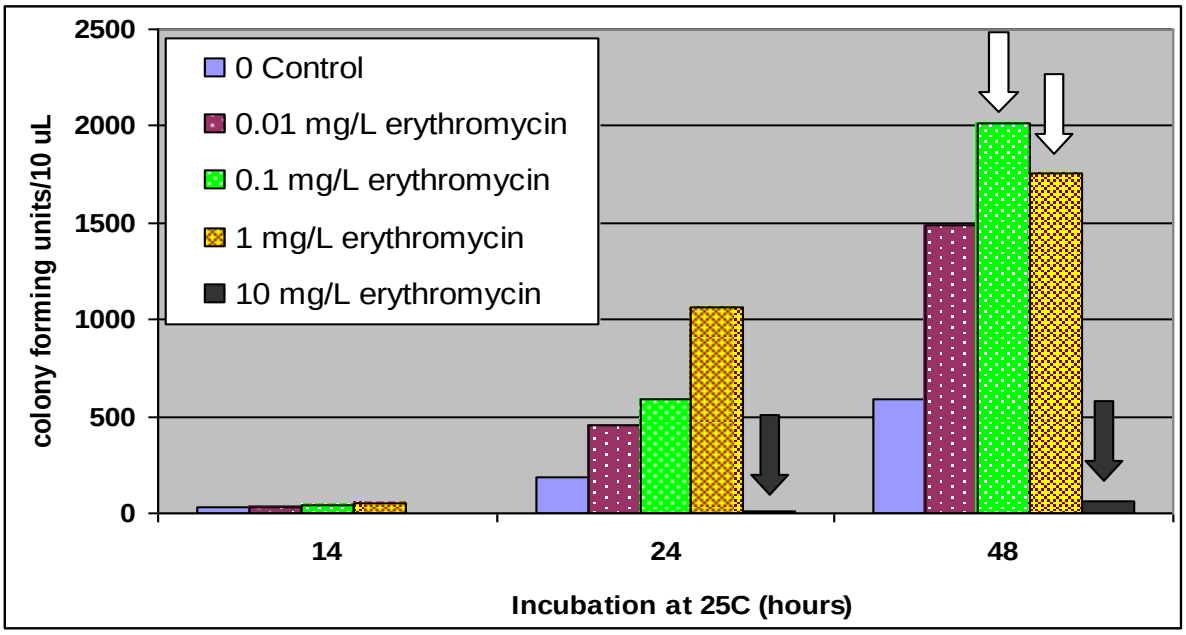

Figure 4. Bacteria from Lee's Cistern collected July 20, 2012 respond to erythromycin. Black arrows signified significant inhibition and white arrows a significant increase in the number of colony forming units (T-test, p=0.05).

The increase in cfu at low levels of eryhromycin corroborates the argument that certain antibiotics in microbial communities could be used as signaling agents rather than bactericidal agents (Linares, 2006; Keller and Surette, 2006). Actinomycetes present in Mammoth Cave could be responsible for regulation of the microbial community's growth inside wet sections of Mammoth Cave and especially Lee's Cistern.

Inhibition zones from tetracycline and ampicillin also support the premise that bacteria from streams in Mammoth Cave have multiple antibiotic resistance. Bacteria acquired from colonies growing on 10 mg/L tetracycline plates also displayed resistance to ampicillin (Fig. 5 and 6). Although bacteria from Annette's Dome and

Lee's Cistern expressed a higher susceptibility to tetracycline than ampicillin, for the most part disks saturated with 1.0 mg/L of either antibiotic was effective at inhibiting bacterial growth near the disk (Fig. 5 and 6).

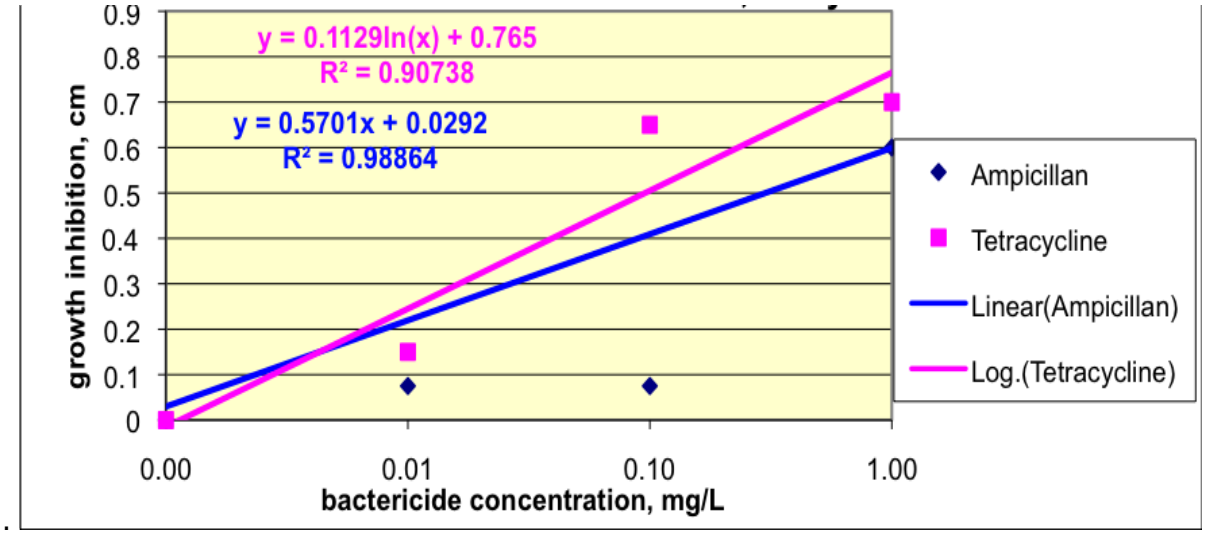

Figure 5. Bacteria from Annette's Dome on day 2, and their zone of inhibition caused by tetracycline and ampicillin along with the R -quared values of the data

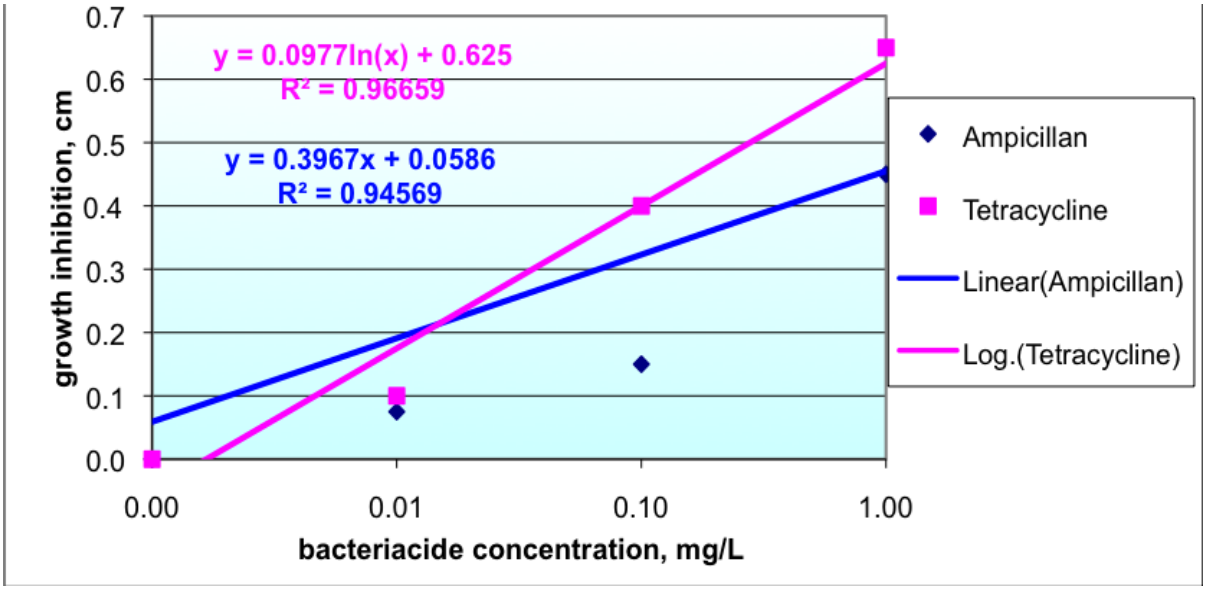

Figure 6. Bacteria from Lee's Cistern on day 2, and their zone of inhibition caused by tetracycline and ampicillin along with the R-squared values of the data

In summary, bacteria from a cave stream starting in Annette's Dome and flowing through Lee's Cistern did show signs of multiple antibiotic resistance, just as the investigators found at the Lechuguilla Cave (Bhuller and others, 2012). The antibiotic responses of bacteria collected from Lee's Cistern versus the bacteria from Annette's Dome have shown a significant difference in their reaction to erythromycin. This may be due to the difference in the bacteria and fungi on the cave wall of the two caverns even though they were located fairly close as demonstrated by the dye tracer study. In contrast, tetracycline and ampicillin produced typical dose-responses and did not stimulate an increase in the number of colonies. The results from this study support the theory that natural antibiotics, such as erythromycin, could be a signal released into the waters used to stimulate growth. Further investigations necessary to verify that hypothesis include characterizing erythromycin concentrations in the natural habitat.

Work Cited

Baltz, RH (2008). Renaissance in antibacterial discovery from actinomycetes. *Current Opinion in Pharmacology* 8: 557–563

Barr, T. C. (1976). Ecological Effects of Water Pollution in Mammoth Cave. Final Technical Report to the National Park Service, Contract No. CXSOOOS0204. archived at Mammoth Cave National Park, Division of Science and Resources Management p. 45

Brown, M. G., Balkwill, D. L. (2009). Antibiotic resistance in bacteria isolated from the deep terrestrial subsurface. *Microbial Ecology* 57: 484–493

Bhullar, K., Waglechner N., Pawlowski A., Koteva K., Banks ED, et al. (2012). Antibiotic Resistance Is Prevalent in an Isolated Cave Microbiome. *PLoS ONE* 7(4): e34953

Byl, T. D., Hileman, G. E., Williams, S. D., Metge, D. W., Harvey, R. W. (2002). Microbial Strategies for Degradation of Organic Contaminants in Karst U.S. Geological Survey. in Artificial Recharge Workshop Proceedings, G.R. Aiken and E.L. Kuniansky, (eds.) Open-File Report 02-89. Sacramento, CA, p. 61-62

Campbell, N. A., Reece, B. J., Urry, L. A., Cain, M. L., Waaerman, S. A., Minorsky P. V., Jackson. (2009). AP Edition Biology, Eigth Edition. San Francisco, CA, Pearson Education, Inc. ISBN: 978-0-13-135691/0-13-135691-7 p. 572-573

Chapman, J. S. (2003). Disinfectant resistance mechanisms, cross-resistance, and co-resistance. *International Biodeterioration and Biodegradation*, 51:271-27

Crothers, G. M., Pappas, C. A., Mittendorf, C. D. (2013). The History and Conservation of Saltpeter Works in Mammoth Cave, Kentucky. Proceedings of Mammoth Cave National Park's 10th Research Symposium, p. 103-109

D'Costa, V. M., McGrann, K. M., Hughes, D. W., Wright, G. D. (2006). Sampling the antibiotic resistome. *Science* 311: 374–377

Diehl, R., Toomey, R., Roland, V., Embry, I. West, A. (2012). Effectiveness of Stormwater Filters at Mammoth Cave National Park, Kentucky. Proceedings from the 22nd Tennessee Water Resources Symposium, Burns, TN. p. P29-P36

Diehl, T.H. (2008) A modified siphon sampler for shallow water. U.S. Geological Survey Scientific Investigations Report 2007–5282, p. 11

Embry, I., Roland, V., Painter, R., Toomey, R., Sharpe, Jr. L. (2012). Quantitative Dye Tracing—Development of a New Interpretative Method. Proceedings from the 22nd Tennessee Water Resources Symposium, Burns, TN. p. 1C-6 to 1C-16

Kane, A. S. (2004) Dose Response Concepts. aquaticpath.umd.edu/appliedtox/dose response

Keller, L. and Surette, M. G. (2006) Communication in bacteria: an ecological and evolutionary perspective. *Nature Reviews Microbiology*. 1383: 1-8. doi:10.1038

Linares J. F., Gustafsson I., Baquero F., Martinez J. L. (2006) Antibiotics as intermicrobial signaling agents instead of weapons. *Proceedings of the National Academy of Science* of the United States of America 103:19484-19489

Palmer, A.N. (2007) Cave Geology. Dayton, OH, Cave Books Publishing, an affiliate of Cave Research Foundation. ISBN-13: 978-0-939748-66-2. p. 454

Rusterholtz, K. J. and Mallory, L. M. (1994) Density, Activity, and Diversity of Bacteria Indigenous to a Karstic Aquifer. *Microbial Ecology*, Vol. 28, No. 1, pp. 79-99

Ryan, M., Meimen, J. (1996). An examination of short-term variations in water quality at a karst spring in Kentucky. *Ground Water*, 34:23-30.

Thaller, M. C., Migliore, L., Marquez, C., Tapia, W., Cedeno, V., et al. (2010) Tracking acquired antibiotic resistance in commensal bacteria of Galapagos land iguanas:no man, resistance. *PLoS One* 5: e898

Wright, G. D., (2010) The antibiotic resistome. *Expert On Opinion Drug Discovery* 5: 779–788

Acknowledgements

The authors would like to thank the staff at Mammoth Cave, Dr. Rick Toomey and Ms. Shannon Trimboli for field assistance. We also appreciate the assistance and guidance of Dr. Tom Byl, US Geological Survey and Tennessee State University; Dr. John Lee, Hume-Fogg Academic High School Biology; Ms. C. Suttle, Middle Tennessee State University, and support for supplies from the National Science Foundation.

Allelopathic Effects of the *Juglans nigra* (black walnut) on the Pea Plant

By Megan Gerstner and Katie Swaringen
Pope John 11 High School, Hendersonville

Abstract

In order to determine the extent of an inhibitor's effect on plant growth, pea plants were combined with a specific concentration of an allelopathic solution from the *Juglans nigra.* The hypothesis concluded that if the amount of the allelopathic concentration in the petri dish increases, than the lengths of the sprouting shoots will grow less than the shoots in a less concentrated petri dish. To test this hypothesis, five levels of concentrated *Juglans nigra* were used from levels zero to one hundred percent, each containing ten germinated peas. After 10 days, the sprouts had achieved a significant growth despite the presence of this chemical solution; however, there was a larger length in the pea plants with a lower concentration. In conclusion, the process of growth from the added allelopathic concentration was a gradual process, allowing the seed to show initial possibilities of survival, yet obviously affecting early on through the shortening lengths of stems.

Introduction

Allelopathy, first considered to be the chemical interaction between two organisms by H. Molisch in 1937, now branches off to several varying definitions (Hibbs & Shumacker, 1987). For the purpose of this experiment, allelopathy should be defined as any negative interaction, direct or indirect, of one organism on another. Currently, there exist three subsections of allelopathy determined as antibiotic, phytoncide, and kolines. While the first two of these particularly affect microorganisms, the focus will remain on kolines, or the reactions of two higher plants (Hibbs & Shumacker, 1987). In this case, the two tested organisms will be pea plants and their reactions to the allelopathic chemicals of the black walnut (*Juglans nigra*).

A common tree in the backyards of people across the world, the *Juglans nigra* survives in the midst of competition with surrounding vegetation because it produces the chemical inhibitor of juglone (Sternberg, 2004). Located in the husk encasing the black walnut, as well as the roots of the *Juglans nigra*, juglone is released into the soil around the potentially threatening plants which can either stint or diminish growth; however, it has been found in some experiments that a few species will continue to thrive despite the harmful allelopathic chemicals around them (Sternberg, 2004). Understanding these

characteristics of allelopathic life is essential for the prevention of the reduction of biodiversity which causes a lack of species in a specific space as well as their ability to reproduce and maintain a large population (Foy & Inderjit, 2001). Vegetables are largely affected by the allelopathic substances in comparison to common shrubs and larger vegetation, and by performing this experiment, the amount that these chemicals physically harm the survival of the pea plant will be observed (Sternberg, 2004).

In this experiment, pea plant growth will be observed in order to determine how the problems of differing concentrations of an allelopathic solution may alter the normal course of development with only water. In response to the problem, the predicted hypothesis presented is “If the concentration of the allelopathic solution increases, then the growth of the seeds will occur more slowly when encased in a petri dish with the same amount of seeds and solution.” The defined variables include the concentration of the juglone puree from black walnut seeds in the juglone and water solution as the Independent variable, while the Dependent variable is defined as the lengths to which the pre-germinated seeds grow.

Activated carbon has been shown to chemically inhibit allelopathic agents and negate their effects on certain plant life. In recent studies, plant biomass increased when interacted with allelopathic chemicals and activated carbon. Because the AC uses adsorption, the ability to condense the chemicals, and filtration, it easily neutralizes the allelochemicals and helps the growth of plants formerly susceptible to the effects of allelopathy (Luo, 2008).

Invasive allelopathic plants have been shown to limit the growth of native species and possibly even change the structure of the surrounding ecosystem. Unfamiliar allelochemicals within whole plant communities, while not majorly studied, could theoretically distort the natural composition or diversity of these communities (Orr, Roberts & Clay, 2005). However, not all results of these allelochemicals are necessarily detrimental to the overall environment. Applying strategies of allelopathy to agriculture and forestry, scientists have proven the positive effects in protecting the environment from dangerous bugs and diseases (Luo, 2008). Often times, the ability for these allelopathic chemicals to destroy these harmful factors is commonly referred to as crop rotation in which even ancient civilizations realized the benefit of leaving the ground to

replenish nutrients and allowing new plants to exert chemicals that would eliminate previous pesticides to crops (Luo, 2008). Because of this, plants are able to adapt to the threats around them and continue to grow, as well as help encourage the study of natural fertilizers for organic farming (Luo, 2008).

To calculate the effects of the *Juglans nigra*'s allelopathic chemicals on the growth of peas, the length of the germinating seeds will be counted per ascending concentration compared to seeds of lesser lengths in the solution. In an experiment formed in the American Journal of Botany, it is said that the process of germination will begin and become complete within a short period of time, usually "90% in one day and 95% in two days," therefore confirming that the effects of allelopathy on plant growth is observed rather quickly because it reaches the plant's system within hours (Nilsen, 1999). Besides the number of seeds germinating, the article also measures the length of roots during a growing period because it found data contrary to that which was taken about the germinating process. When studying the roots of a lettuce plant, the overall length of the roots was generally higher than the roots growing in only distilled water; something about the allelopathic chemicals stimulated to produce contrary results (Nilsen, 1999).

Methods and Materials

In order to make the *Juglans nigra* solution, a blender, black walnuts, water, and a knife were needed. Two black walnuts were cut so that only the husks were kept for making the solution. These walnuts were then blended into a puree with water added to gradually become a liquid. After the pieces were ground, the mixture was transferred to a large beaker so that it could sit overnight and allow the larger, unblended pieces of the husks to settle to the bottom. Once settled, cheesecloth was used to strain the solution from any unnecessary solids, which was then established as the fully concentrated allelopathic solution for the rest of the experiment.

Water and paper towels were used to help grow approximately 100 pea plant seeds in a large plastic bag. The peas were wrapped loosely in a paper towel soaked in water and allowed to sprout for 2 days. These peas were then removed and 50 of those which had sprouted were measured for length of each sprout. They were then evenly distributed among 10 petri dishes, 2 dishes used for each solution concentration. The

lengths of the peas placed in dishes with equal concentrations were averaged and recorded before solution was added.

Water, five beakers, a black marker, and the allelopathic *Juglans nigra* solution were needed in order to make the various concentrations of nutritional supplement for testing the growth of the pea plants in the petri dishes. One beaker was set aside with 100mL of water and another was set aside with 100mL of the initial *Juglans nigra* solution. The remaining three were left to create the concentrations which contained 25%, 50%, and 75% of the allelopathic solution. Each was filled with their prospective amount of *Juglans nigra* solution in mL, and then mixed with an amount of water to equal 100%. For example, the 25% was filled with 25mL of the allelopathic solution and 75mL of water. When all were created, each was labeled with its percentage of the black walnut concentration.

After the concentrations were made, paper towels were soaked in the differing solutions and then wrapped around the peas of each designated concentration. The peas were permitted to grow for the next 10 days, with extra solution added to each petri dish after the measurements on the fifth day. The measurements of the sprouts for each concentration were averaged and recorded with a measuring tape every day. The differences between the present day and the previous one were calculated and also recorded.

Data

Figure 1

Concentration of *Juglans nigra (%)*	Day 1 Avg Length (mm)	Day 2 Avg Length (mm)	Day 3 Avg Length (mm)	Day 4 Avg Length (mm)	Day 5 Avg Length (mm)	Day 6 Avg Length (mm)
0	7.05	10.05	15.4	20.91	27.85	31.55
25	8.4	9.1	14.9	17.8	21.2	23.4
50	12.7	16.45	21	25.2	27.35	30.4
75	18.4	20.5	26.5	30.1	31.1	32.4
100	20.1	23.8	28	30.7	28.8	32.2

Day 7 Avg Length (mm)	Day 8 Avg Length (mm)	Day 9 Avg Length (mm)	Day 10 Avg Length (mm)	Total Difference (mm)	Avg Increase per Day (mm)
36.95	41.93	53.85	56	48.95	5.47
25	26.43	26.73	28.85	20.45	2.27
35.75	37	39.4	41.98	29.28	3.25
36.5	40.3	38.4	40.2	21.8	2.42
34.4	32.8	34.8	34.2	14.1	1.567

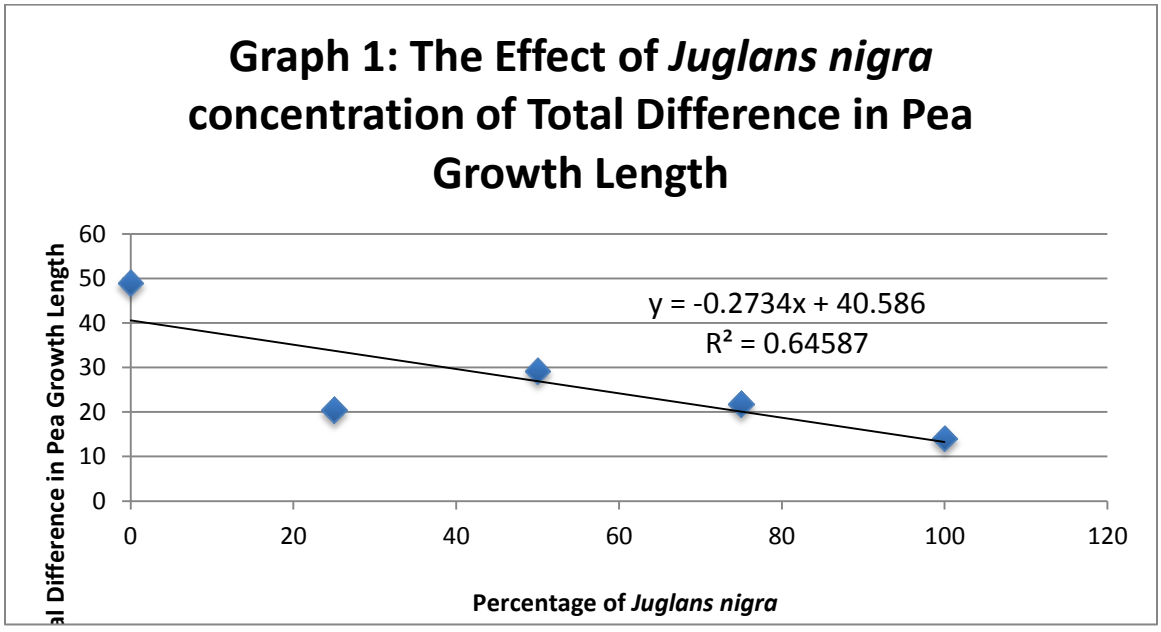

Figure 2

Figure 3

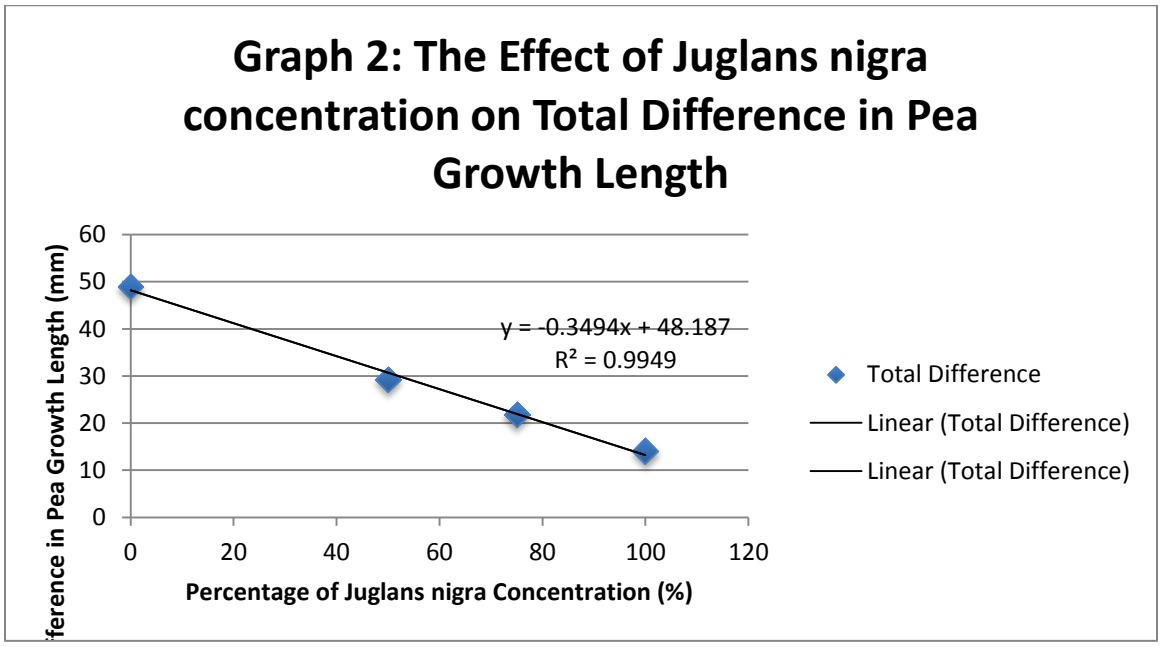

Figure 4

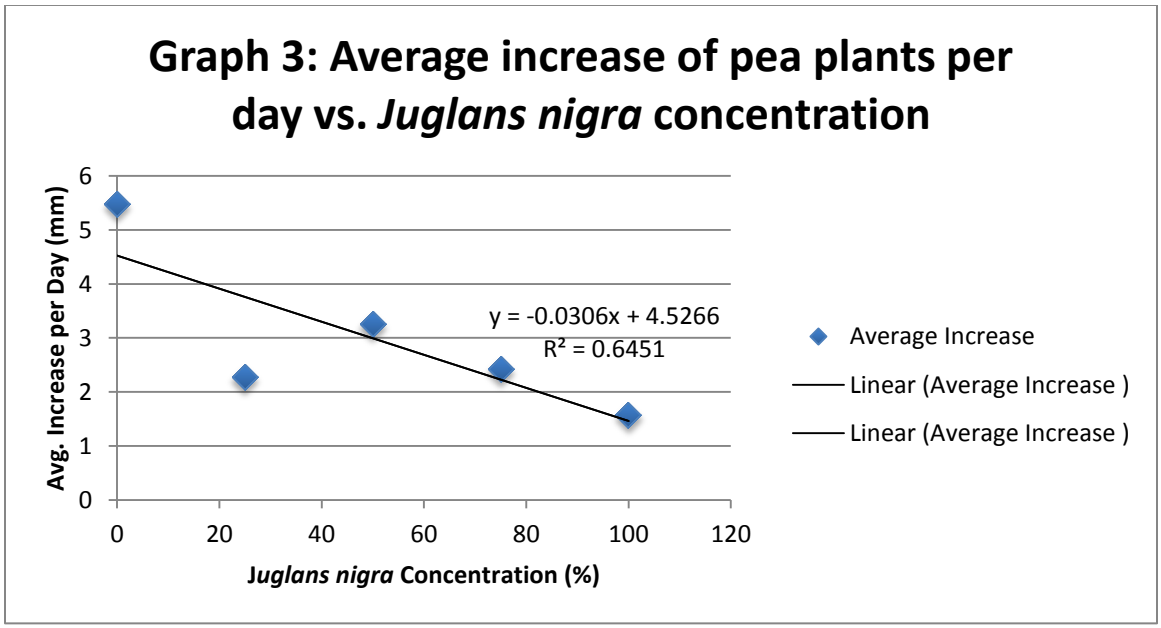

Analysis

After ten days of observation, the pea plants were found to have grown in any concentrated solution of the *Juglans nigra*. By the end of the ten days, the petri dishes containing 0% of the allelopathic solution grew to the greatest length and were recorded with the highest difference in length from Day 1 to Day 10. Generally, as the percent of *Juglans nigra* within the solution increased, the differences from the first and last days decreased, indicating those of highest percentage, 100% concentration, grew the least amount during this period. However, in opposition to the rest of the collected data, the peas in the 25% solution sprouted shorter stems, on average, than the 50 and 75% most likely due to an experimental error or variation compared to the rest of the pea plants. Despite the varying concentrations of the *Juglans nigra* solution in each petri dish, the peas still exhibited similar growth patterns within days of one another. Initially, the peas constructed tiny sprouts which grew straight from the opening and out to the left or right. A few days later these sprouts were joined by an additional growth to the opposite direction in which the primary sprout had already grown. A few peas began to rot or leak a chemical with an odor, in addition to some splitting directly in half or losing the encasing. By the end, even the less developed peas still began to grow tiny sprouts from the larger stems because the peas still developed with a stunted growth.

By the end of Day 5, the peas in 0% concentration were observed to have lost the outer shells and began to turn partially green with extra shoots sprouting from the center. On Day 8, more sprouts appeared once again in the 0% solution. The same day, the peas in 25% solution had finally begun growing new sprouts, but remained a brown color, probably stained by the *Juglans nigra*. The following day, Day 9, the peas in 0% grew even more sprouts shooting off of the original stem.

As hypothesized, the majority of the data showed that the peas within the lesser concentrated, and therefore less allelopathic, solutions developed much quicker and larger than those in the highly allelopathic solutions, particularly in the 100% concentration. While the average growth of the peas in 100% *Juglans nigra* was approximately 1.567mm per day, the growth in the 0% solution was recorded as 5.47mm per day. The remaining averages for 25%, 50%, and 75% fell within these two

parameters. The 50% solution grew the next highest amount at 3.25 mm per day, which is due to lab error. Such error could have occurred through faults in the data collection or in the process for distributing the solutions. Certain petri dishes received extra solution almost regularly to prevent dehydration. However, others were only given more solution less frequently. What should have been the fourth in efficiency of growth was the 75% solution at 2.42mm a day. Before the least productive growth of the 100% was the 25% solution which grew at a rate of 2.27 mm per day.

Therefore, while certain results were incompatible, the overall analysis and data suggests that the original hypothesis proves correct.

Conclusion

If the concentration of the allelopathic solution increases, then the growth of the seeds will occur more slowly when encased in a petri dish with the same amount of seeds and solution. The allelopathic *Juglans nigra* solution has the capacity to limit the growth of pea plants by interfering negatively with weaker species such as the pea plant (Foy & Inderjit, 2001). *Juglans nigra* concentration, as the controlled variable, influenced the amount of growth in the roots of the newly germinated plants. As proven through the data collected, the concentration of the black walnut solution varied inversely with the length of the seeds, eventually leading to the extermination of those in the solutions with greater concentration.

In a normal habitat, plant roots are exposed to dangerous chemicals from surrounding competitors and are able to survive if they can adapt to the new intrusion into the water supply. In an allelopathic habitat, however, seedlings are prevented from sprouting, proving detrimental to plant life and maturation because they are then unable to gain exposure to energy from the sun without the ability to grow beyond the soil. Though the first few days might demonstrate clear growth, it is important to note that the data collected in the first recordings might compare differently to the overall trend of restricted growth in the roots (Nilsen, 1999). This partially explains why the data recorded for the 25% *Juglans nigra* solution was skewed because the initial days do not have much influence in the result of the experiment. However, this does not disprove

the outcome of the entirety of the compiled data because this experiment dealt with a much less complex organism than that of a large tree such as other experiment (Nilsen, 1999) Therefore, the unimportant data must have been a result of the first three to four days, which allowed the 75% and the 50% concentrations to grow faster. In addition, the sample size of 10 peas per petri dish was exceedingly inadequate. To limit experimental error, groups should be enlarged to approximately 50 peas for each concentration and given longer than 10 days to grow. Other minor discrepancies that could contribute to flaws in the experiment would be that the seedlings were not equally spaced among one another in the petri dishes. If two coexisting pea plants were closer to each other than another pea in the petri dish, it is harder for the adjacent peas to find free space than the distant pea that does not have as much competition surrounding it (Tilman, 1994). Another factor that may have led to unpredicted data was that there were a few pea plants that rotted in their respective petri dish and quit growing at a rapid pace early on in the measuring period. By taking the average of the entire concentration of peas, that one pea can drop down the expected scores and lower the total average of growth.

In conclusion, the recorded data along with previous experiments provide evidence that certain allelopathic substances can be harmful to the surrounding environment. For example, farms require constant crop rotations in order to prevent the dry, allelopathic soil from destroying the crop. However, allelopathic plants such as the *Juglans nigra* have been found useful in uprooting weeds capable of devastating necessary plant life. Such allelopathic substances can prove beneficial for removing herbivores from a particular area to increase other plant growth, (Zeng, Malik, & Luo, 2008). So, while allelopathy in itself can be detrimental to susceptible plant life, once understood, allelopathic plants can theoretically be used to extend crop life and reduce weed interference.

Work Cited

Foy, C. L. & Inderjit. (2001). Understanding the role of allelopathy in weed interference and declining plant diversity. Weed Technology, 15.

Hibbs, E. T., & Shumaker, C. A. (1987). Intraspecific allelopathy. The American Biology Teacher, 49(1). doi:10.2307/4448411

Nilsen, E. T., Walker, J. F., Miller, O. K., Semones, S. W., Lei, T. T., & Clinton, B. D. (1999). Inhibition of seedling survival under rhododendron maximum (Ericaceae): Could allelopathy be a cause? American Journal of Botany, 86(11).

Inference of allelopathy is complicated by effects of activated carbon on plant growth. (n.d.). New Phytologist Trust, 412-423.

Orr, S. P., Rudgers, J. A., & Clay, K. (2005). Invasive plants can inhibit native tree seedlings: Testing potential allelopathic mechanisms. Plant Ecology, 181(2). doi:10.1007/s11258-005-5698-6

Sternberg, G., & Wilson, J. (2004). Native trees for North American landscapes.

Zeng, R. S., Mallik, A. U., & Luo, S. M. (2008). Allelopathy in sustainable agriculture and forestry. Springer.

Acknowledgments

This project would not have been successful without the assistance of Mrs. Jennifer Dye and her willingness to support the experiment throughout the year. She provided very useful advice, guidance, proper materials for making the allelopathic solution in the experiment, as well as the workspace to allow the collaboration between partners. It should also be noted to thank the Hopper and Gerstner families for their approval of growing the petri dishes in the dark places of their homes. Finally, Google provided the means of communication of the collected data through the website Googledocs.

Testing the Effectiveness of Luminol in the Dating of Skeletal Remains

Katherine Watson and Skyler Cochrane
Vanderbilt School of Math and Science, Nashville

Abstract

This research tests whether the luminol blood detecting reagent is an effective method of dating skeletal remains by analysis of chemiluminescence data. Analyses with luminol were conducted with sets of various bone specimens that had known recent and older ages: ≈3/4th of a month ± 2 months and 3 months ± 18 months old, respectively. The chemiluminescence values of bone samples, both with and without luminol, were determined and enhanced through the analysis of images taken of the chemiluminescent bone samples in Image J. The older enhanced bone set had a 97% coefficient of variance, while the recent enhanced bone set had 28% coefficient of variance. A high coefficient of variance from the older bone data indicates that the older bones were the most volatile in blood amount, explained by their exposure to the environment. A lower coefficient of variance from the recent bone data suggests that there was less variation between the bones, leading to the conclusions that their ages would be similar and that luminol is not dependent upon type of bone. From this, it was determined that luminol is not an efficient method of dating skeletal remains, as the results can be affected by environmental conditions.

Introduction

The techniques currently available for dating skeletal remains are all extremely expensive to perform and/or require bulky equipment that is difficult to transport. For example, the equipment for carbon dating includes things such as a furnace, stainless steel reaction vessels, auxiliary equipment, liquid scintillation spectrometer, etc [1]. Ideally, a viable new skeletal dating technique would be able to deduce a bone's age despite any various environmental factors that would typically cause interference, such as weather, temperature, or the medium in which it lies. This technique, in addition to it needing to be inexpensive, needs to be easily performable as well.

The research showed that the chemical luminol is a reagent commonly used as a blood detector [2]. The visible chemiluminescence of luminol is caused by a reaction between the iron in the oxygen-carrying protein hemoglobin, located in blood, and the luminol powder. The goal of this research is to test this chemical to see if it can be used to accurately date the age of skeletal remains based on analyzing the numeric value of its chemiluminescence and the coefficient of variance percentage that is gathered from

each set of data. For luminol to be an effective skeletal dating method blood amounts should vary based on age solely, therefore there should be little variation of blood amounts within the same age group of bones.

Different bone types were used in this experiment to ensure luminol chemiluminescence would not vary depending upon species and type. The bones of cow, deer, and sheep were used in this research, as well as the bone types: scapulae, femora, radii, and humeri. To compare whether or not luminol would actually work as a competent skeletal dating technique, different bones with known ages were used: ≈3/4th of a month ± 2 month old bones were used as the recent age and 3 months ± 18 month old bones were used as the older age. It was predicted that the older bones would be more volatile in blood amount than the recent bones because of their varying amount of environmental exposure (e.g. weather, temperature, etc.). The recent bones would not have any environmental exposure, causing their blood amounts to vary less.

Sample Name	Species	Bone
Older Bones: ≈3 months ± 18 months old		
1	Deer	Scapula
2	Deer	Scapula
3	Deer	Scapula
4	Deer	Scapula
5	Deer	Scapula
6	Sheep	Femur
7	Sheep	Femur
8	Sheep	Femur
9	Sheep	Scapula
Recent Bones: ≈3 weeks ± 2 months old		
10	Cow	Femur
11	Deer	Femur
12	Deer	Femur
13	Deer	Femur
14	Sheep	Scapula
15	Sheep	Radius
16	Sheep	Humerus
17	Cow	Femur

Table 1: *This chart displays all 17 samples that were used in this experiment and lists their species and bone type. Samples 1-9 were supplied by a processing plant, but were exposed to the environment for 3 months ± 18 months. Samples 10-17 were provided by various butchers within 1-2 days of being butchered.*

Table 1 displays the samples gathered for testing. Before the samples could be extracted, the bones went through thorough cleaning. All tissue, skin, and cartilage still attached to the recent bones were physically removed with scalpels and scrapers. The recent bones were then put into a water bath of 60°C to remove any excess skin and cartilage that could not be removed by physical means. This lower temperature is not high enough to mimic aging. The recent bones also had the ends sawed off and the bone marrow removed to prevent contamination. The older bones were sanded with coarse sandpaper to remove any lingering dirt from the environment in which they were found. Bone dust was extracted from each bone through the diagonal and vertical sawing on the shaft of the bone. Approximately three 50 mg bone dust samples were collected from each bone to use in luminol testing using the setup pictured in Figure 1 [3]. The setup, shown in Figure 2, was created for luminol testing in an attempt to keep the camera and test tube containing the bone dust stationary to prevent any skewing of chemiluminescence values. Three images were taken of the test tube in the setup: one with the test tube in the light, one in the dark with no luminol added, and one in the dark with 15 mL of dissolved luminol powder (Innovating Science) added to each bone sample extraction. Images were taken with a Sony Cybershot 12.1 megapixel camera on a high ISO setting of 3200 to enhance chemiluminescence

Figure 1: *The setup for the extraction of bone dust for luminol testing.*

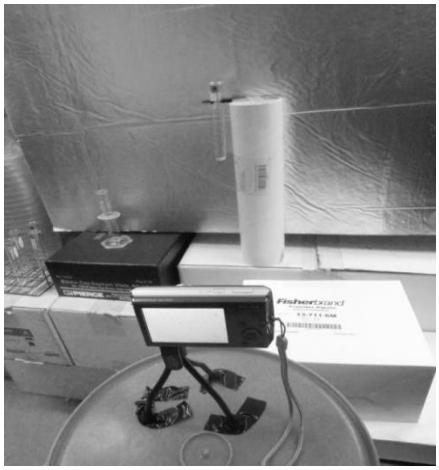

Figure 2: *The setup for image capture of the bone sample in the light, dark, and the dark with luminol.*

The nine images per bone sample were then stacked in ImageJ to be analyzed. The images of the test tubes in the light were used to select the appropriate area that could then be measured of both the images in the dark and with luminol added. Chemiluminescence measurements were taken of the samples in the light and dark without luminol and in the dark with luminol. The pictures were enhanced by changing the brightness/contrast setting to 3 and 65, as the chemiluminescence was barely visible. Ratios were calculated of the enhanced chemiluminescence values to the non-enhanced chemiluminescence values to ensure enhancement was constant. These included both ratios of the regular dark to the enhanced dark images and the regular luminol to the enhanced luminol images. To strictly calculate the chemiluminescence of each bone sample, the differences of the chemiluminescence values of the bone samples in the dark were taken from the chemiluminescence values of the bone samples with luminol in the dark to eliminate what chemiluminescence was already being emitted in the room without luminol.

The actual chemiluminescence values from the three trials from each bone sample were used to calculate the average chemiluminescence value per bone sample. Standard deviations for the recent and older bone samples were calculated using the averages of the recent and older bone samples. To test the volatility of the data, the coefficient of variance was calculated for the enhanced and natural older and recent bone samples using the standard deviation and averages of the groups of data.

Results

Bone Sample	Average Luminol Chemiluminescence (± Standard Deviation)	Average Enhanced Luminol Chemiluminescence (± Standard Deviation)
1	4.99 ± 2.54	30.70 ± 14.55
2	0.65 ± 0.70	4.15 ± 4.48
3	10.41 ± 6.35	50.50 ± 21.87
4	1.59 ± 0.40	10.65 ± 2.89
5	6.04 ± 0.09	37.69 ± 0.09
6	1.71 ± 0.95	10.73 ± 5.94
7	0.78 ± 0.77	5.11 ± 4.94
8	0.23 ± 0.17	1.45 ± 1.27
9	1.22 ± 0.39	8.05 ± 2.61
10	1.35 ± 0.70	9.14 ± 4.69
11	18.51 ± 13.58	69.29 ± 3.01
12	14.88 ± 0.08	65.66 ± 2.98

13	24.58 ± 12.21	75.56 ± 13.60
14	18.34 ± 3.23	73.20 ± 4.86
15	5.80 ± 0.34	35.14 ± 1.91
16	7.63 ± 2.20	54.45 ± 26.78
17	5.29 ± 1.44	33.11 ± 8.68

Table 2: *The averages and standard deviations of the chemiluminescence of our recent and older bone samples both enhanced and non-enhanced.*

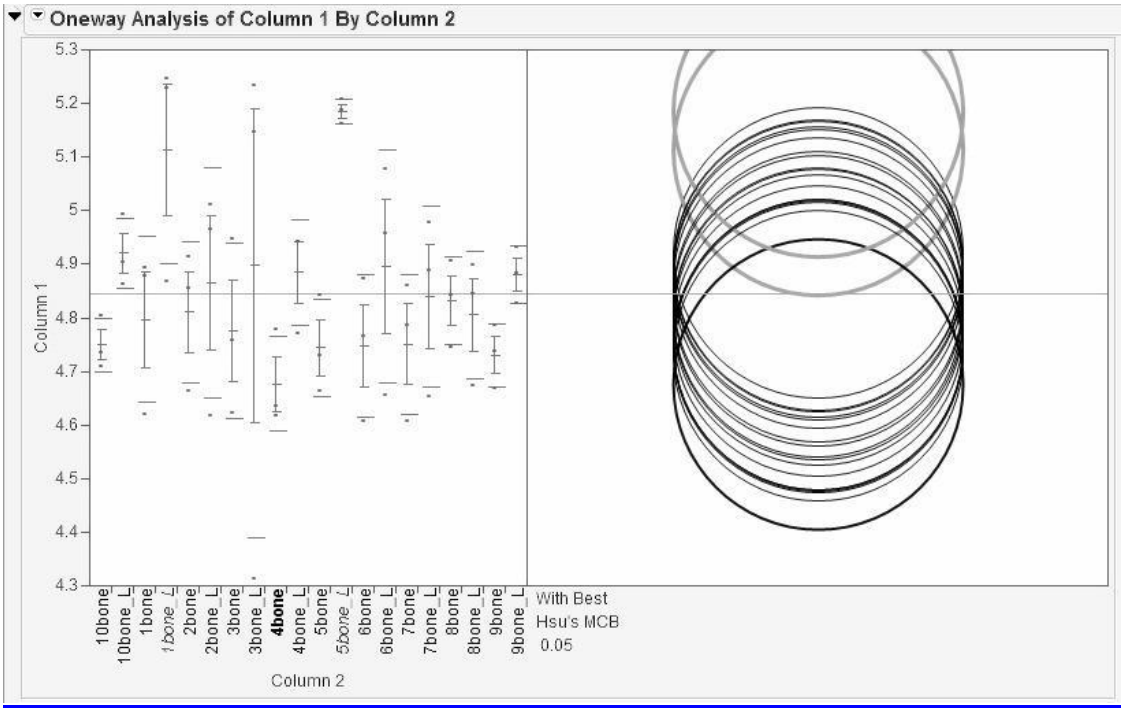

Figure 3

Level	vs. Max p-Value	vs. Min p-Value
5bone_L	.	0.0055*
1bone_L	0.8397	0.0206*
10bone_L	0.2412	0.3012
3bone_L	0.1867	0.3717
6bone_L	0.1851	0.3741
4bone_L	0.1599	0.4142
9bone_L	0.1520	0.4279
2bone_L	0.1243	0.4817
7bone_L	0.0875	0.5709
8bone	0.0783	0.5976
2bone	0.0568	0.6692
8bone_L	0.0528	0.6845
1bone	0.0461*	0.7112
3bone	0.0328*	0.7725
7bone	0.0213*	0.8359
10bone	0.0209*	0.8381
6bone	0.0206*	0.8400
5bone	0.0192*	0.8488
9bone	0.0149*	0.8767
4bone	0.0055*	.

Table 3

Figures 3 & Table 3: *A MCB analysis and a t-test of the ratios were performed on the set of older bones to determine their similarity. The results are displayed visually in* ***Figure 3****, and the numeric data is displayed in* ***Table 3****. This test shows the average ratio of each sample and compares them to the average of all samples displayed in* ***Table 3****.*

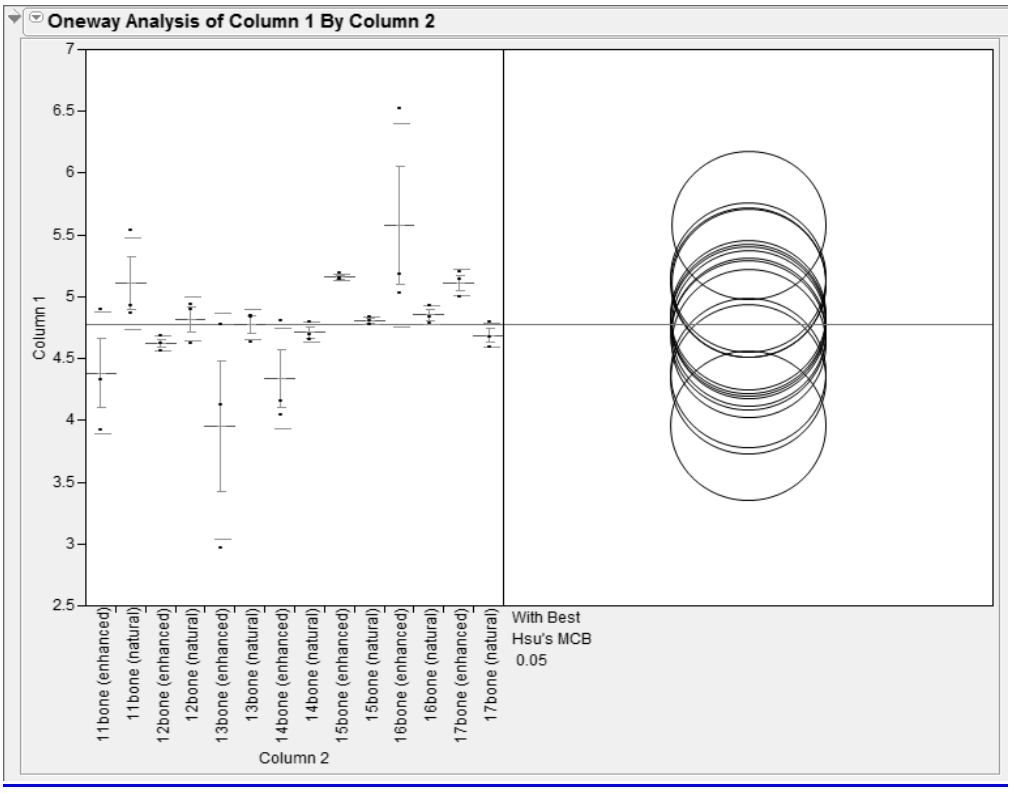

Figure 4

Level	vs. Max p-Value	vs. Min p-Value
16bone (enhanced)	.	0.0001*
15bone (enhanced)	0.4403	0.0039*
17bone (enhanced)	0.3765	0.0055*
11bone (natural)	0.3688	0.0057*
16bone (natural)	0.1084	0.0372*
12bone (natural)	0.0898	0.0461*
15bone (natural)	0.0815	0.0513
13bone (natural)	0.0682	0.0618
14bone (natural)	0.0462*	0.0897
17bone (natural)	0.0394*	0.1033
12bone (enhanced)	0.0250*	0.1493
11bone (enhanced)	0.0042*	0.4252
14bone (enhanced)	0.0029*	0.4954
13bone (enhanced)	0.0001*	.
Mean[i]-Mean[j]-LSD		

Table 4

Figures 4 & Table 4: *A MCB analysis and a t-test of the ratios were performed on the set of recent bones. The MCB analysis shows the average ratio of each sample and compares them to the average of all samples. The t-test results are displayed visually in Figure 4, and the numeric data is displayed in Table 4.*

Bone Group Type	Average ± Standard Deviation of whole group	Coefficient of Variance
Older	2.85 ± 3.85	134.93 %
Recent	13.58 ± 8.52	62.75 %
Old Enhanced	16.51 ± 18.44	111.68 %
Recent Enhanced	58.06 ± 20.37	35.08 %

Table 5: *This chart displays the overall average chemiluminescence, standard deviation, and coefficient of variance for each group of data. The coefficient of variance is the percentage of the standard deviation over the average amount of chemiluminescence*. (CoV= (STDEV/AVG) * 100%).

Conclusions

The technique that was used to enhance the images was tested by creating ratios to compare the values in proportion to each other, both before and after enhancing. The results are as follows: older dark (4.76 ± 0.10), recent dark (4.82 ± 0.19), older luminol (4.93 ± 0.21), and recent luminol (4.74 ± 0.68); the low standard

deviations showing little variation. The consistency of the ratios were also determined using a MCB analysis, shown in Figures 3 and 4, which compared the average ratio for each sample to the average ratio overall for the older and recent bones; and also a t-test, shown in Tables 3 and 4. The numbers turned out consistent across in the MCB analysis, shown by the averages of each ratio being similar to the average of all ratios, so it was determined to be a valid method that would not interfere with the results. However, while the variation between the coefficients of variance percentages in Table 5 from the older values to the older enhanced values is not that dramatic, the change between the recent natural and the recent enhanced is rather significant. This suggests that the enhancement technique used was not constant, which is also contradictory to the ratios that were previously mentioned. They suggested that the technique was plausible due to the fact that they were nearly identical after enhancement.

The older bone's coefficients of variance percentages being over 100%, shown Table 5, suggest that our initial hypothesis was correct, which was that the older bones would be much more volatile in blood amount than the recent bones due to exposure to the environment. The low coefficient of variance percentages in Table 5 for the newer samples suggests that the concentration of blood in a bone is not specific to any particular species or bone type. This was shown by the variety observed in our sample group, listed in Table 1. Also, the variance displayed by the older bones suggests that luminol is affected by environmental conditions rather that age. Thus, luminol is not an efficient method to date skeletal remains based on blood amount.

During the process of testing, there were several possible occurrences that had potential to skew the results and provide false data. One of which might have been a mechanical error in the setup that was created for the process of capturing the images necessary for analysis. Occasionally the camera would be knocked slightly so that the images did not always line up perfectly. Another potential error might have come from the luminol itself. Due to the nature of luminol, it tends to lose its potency after a short amount of time, and when it came to the testing of several of our samples, the luminol powder had been mixed for several weeks.

This project could be further expanded by adding not only more bones of different species, but also a greater range in ages as well as more bones in general.

Also, a better setup could be designed and used for the image-taking process. For now, based on the results gathered from this research, it can be concluded that the use of the numeric values gathered from the chemiluminescence reaction of blood and luminol is an ineffective method of dating skeletal remains.

Work Cited

1. Buzinny, Michael G. "Benzene Line: (Radiocarbon Dating Equipment)." Benzene Line: Radiocarbon Dating Equipment. SET UP. N.p., 2000. Web. 29 Nov. 2012

2. Watkins, M. Dawn, and King C. Brown. "A Comparison of Visual Enhancement Chemicals for the Recovery of Possible Blood Stains at the Crime Scene". Luminol vs. BlueStar® "Bluestar Forensics. N.p., n.d. Web. 29, 2012.

3. Frank Ramsthaler, Sarah C. Ebach, Christopoh G. Birngruber, Marcel A. Verhoff, Postmortem interval of skeletal remains through the detection of Intraossealhemin traces. A comparison of UV-fluorescence, luminol, Hexagon-OBTI®, and Combur® tests, Forensic Science International, Volume 209, Issues 1-3, 15 June 2011, Pages 59-63, ISSN 0379-0738, 10.1016/j.forsciint.2010.12.011

Acknowledgements

We would like to thank Dr. Jonathan Creamer and all of our instructors at The School for Science and Math at Vanderbilt who aided us in our research. We would also like to thank Lebanon Locker Company in Lebanon, TN, Porter Road Butcher in Nashville, TN, and Dr. Kevin Seale for their donations of bones.

The Effects of Angle of Attack on the Lift Created by an Airfoil

Lachlan Hassman and Eliza Gooding
St. Andrew's-Sewanee School, Sewanee

Abstract

Air travel is perhaps the most important industry in the modern day. It connects people of every country with the other 8 billion residents of Earth in an amazing way. Thanks to aeronautics, someone who would have previously had to take a boat from England to New York, a trek that could take months to complete, can now take a flight from JFK to London International in seven hours. What would have been a dangerous journey from the Pacific to the Atlantic, which could take many days and earlier many lives, can now mean only a 7 and a half hour flight from Charlotte-Douglas International to San Francisco. It is very important as a society to understand this technology which has changed our lives in such a huge way. This paper explores perhaps the biggest idea in aeronautics: lift. The purpose of the force of lift is to overcome gravity and allow the airplane to get off the ground and increase altitude. We describe the relationship between the angle at which a wing hits the airflow, or angle of attack, and the amount of lift it creates.

Introduction

Four seconds has not changed the world as we know it as much as it did on December 14, 1903. On a field in the Outer Banks of North Carolina, Wilbur Wright flew 112 ft. in the first powered aeronautical vehicle, the Flyer I. (Lawrence,2004) Aircraft have completely changed our world. Countries and communities are connected quicker and more closely than ever. Powered flight has had an impact on the world similar to the internet and inter-continental phones. We owe our way of life to powered flight, the pioneers who paved the way of the future, and the scientific principles that have allowed advancements in aeronautics.

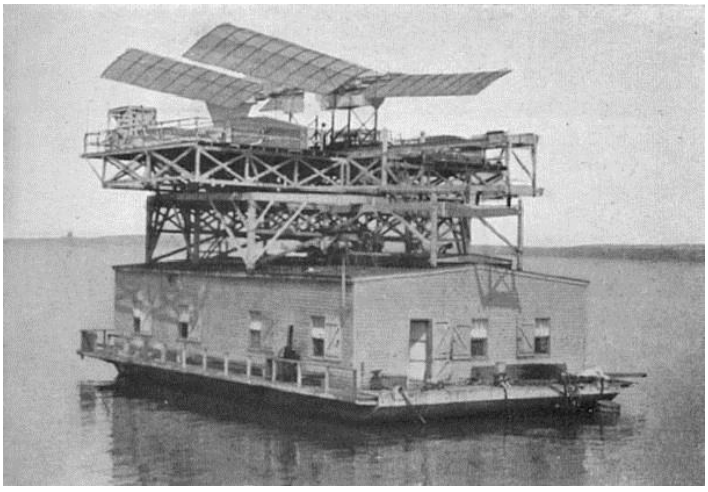

Figure IV The Aerodrome From NASA Langley Research Center

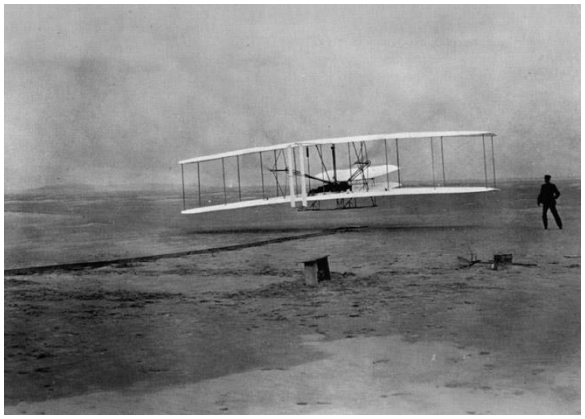

Figure VI The Wright Brother's Kite From www.aerospace web.org

A mere months before Wilbur flew, on September 7 of the same year, Samuel Langley launched his Aerodrome, a full scaled, motor-less aircraft which was launched by a catapult atop a barge. Due to a faulty catapult, it took a nose-dive right into the river. The Aerodrome was hailed as “a buzzard” and the barge the “Ark”. Scientists and historians have debated for the last century about whether or not it would have flown. They will never know, and Langley died four years later a broken man. His work on the Aerodrome was continued, and eleven years and many improvements later, finally flew (Lawrence, 2004). In those eleven years many advancements in the aeronautical field had been made. The Wright Brothers used kites to experiment with many basic principles of flight, such as lift, drag, and angle of attack.

Airfoils, the wings of the plane, and their angle of attack are important parts of the construction of any air machine. Airfoils, the wings, produce lift, the upward force which counteracts gravity. Angle of attack affects the amount of lift produced by the airfoil. The equation for lift is $L = C_l \times \frac{r \times v^3}{2} \times A$, where Cl is coefficient of lift, r is air density, a is area of the wing, and v is velocity (Rosen, n.d). Now this does not include anything about angle of attack, that comes when defining coefficient of lift, which is $Cl = 2 \times \pi \times y$, where y equals the angle of attack (Benson, n.d).

Figure VI- Lilenthal in mid-flight, 1895, notice the bird-like wings From the Library of Congress

Stall is a phenomenon caused by an increase in angle of attack past its crucial point, when it produces the most lift. Stall is usually reached when a plane attempts to climb to quickly (Benson, NA).

In 1901, Wilbur Wright recorded running into stall while flying his second glider. Five years earlier Otto Lilienthal died because of stall on August 9th. Hailed as the "Father of the Glider", he was doing one of his routine flights, his fourth of that day, when his glider stalled. He tried to correct it, but he died 36 hours after the crash. He is hailed for his last words, which inspired generations of future pilots, "sacrifices must be made"(Jakab,n.d).

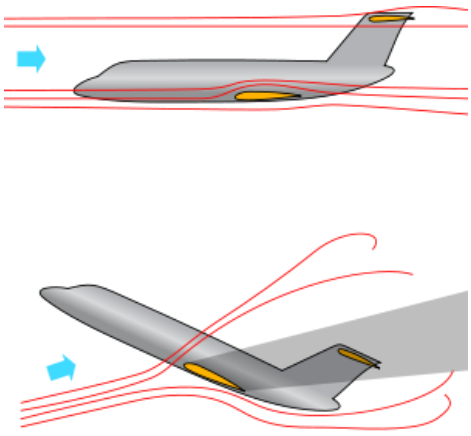

Figure VII- Above: normal flight, Below: stall From NASA Aerospace Research

This death of an earlier pioneer, as well as Wilbur's encounter with it, caused the Wright Brothers to design their plane in "canard" configuration(see Figure V), which is the set of "little wings" that made recovery from stalls easier and is said to have saved the pioneer's life multiple times (Jakab, n.d).

As angle of attack affects human life every day, but it is hardly thought about. As airplanes continue to progress and advance, it is important for humans to understand these principles that affect them so continuously. The hypothesis of this project, based on research and study is that as the angle of attack of a standard airfoil increases in controlled conditions, the lift will also increase.

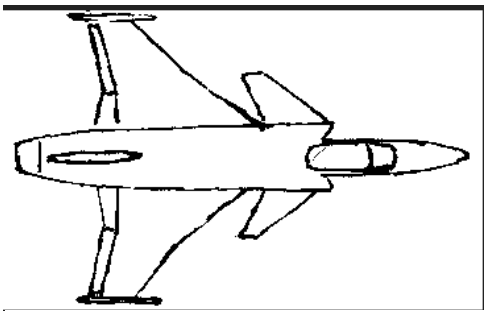

Figure VIII, Canard Configuration

Materials for the Wind Tunnel

Materials needed for the wind tunnel are 2 foam boards which are 7 in wide, 3 feet long, and at least 2 1/2 inch thick. We also needed 2 glass or acrylic panes that measure 7 inches wide and 3 feet long, 1 desktop fan with protective cage, an industrial trash bag,

duck tape, super glue, string. Also is a force reader that measures force in newtons. Lastly, extra metal rods or bamboo skewers are necessary**.**

Instructions for Constructing the Wind Tunnel

Cut slits 1 inch deep in the foam board 1 inch from either side of the board. Do this for both foam boards. Place dots of glue on the bottom of the slits, one about every 3 inches. Fit the glass panes into each slit as demonstrated in the figure below. Wait the directed time for the glue to set. Cut the trash bag to a width of 22 inches wide and a length of about 3 feet. Tape the bag to the inside of one end of the wind tunnel all the way around its perimeter. Make sure there are no gaps or holes in the seams. Tape the other end of the bag around the circumference of the desk fan, with the fan facing away from the tunnel, so that it sucks air out of the tunnel. Poke the rods into the foam boards half way through the tunnel. They should be half an inch in on either side, a quarter inch of either acrylic/glass pane. Drill a hole in the top foam board, directly about the rods and in the center. Create a pyramid with the bamboo skewers or extra rods, tall enough to hang the force reader over the top of the hole you just drilled. Hang the force reader down from the top of your pyramid. Attach a string to the other side of the force reader, and thread that through the hole into the wind tunnel.

Figure IX Finished Windtunnel

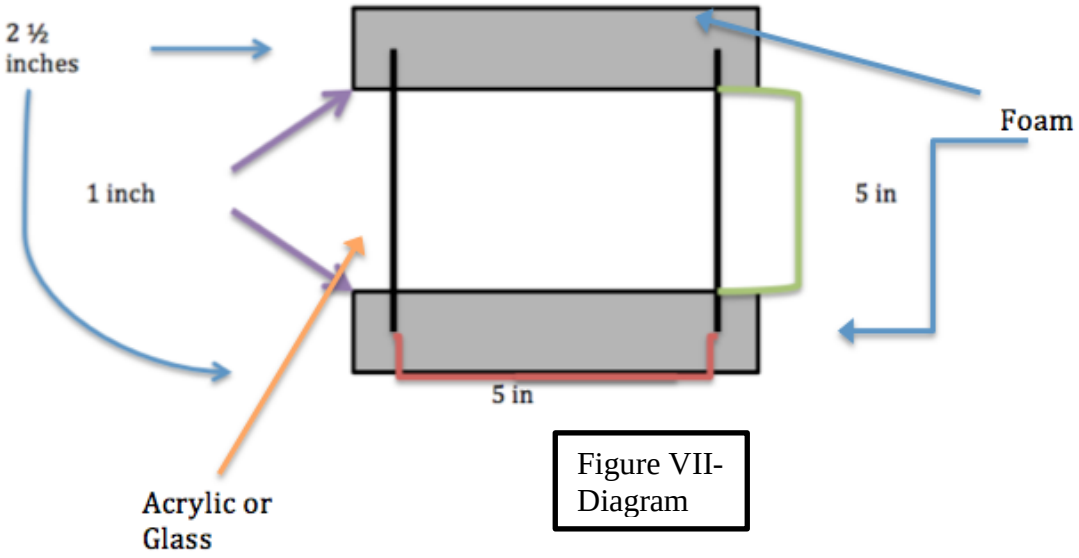

Figure VII-
Diagram

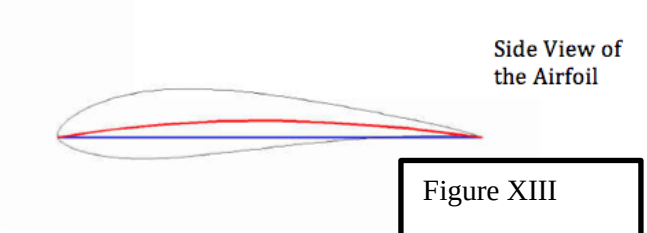

Figure XIII

Instructions for creating the Airfoils

Using a hot knife, gouge and/or file whittle down the small foam boards into identical airfoils, cutting out the diagram below to use as a guide for the side and cross section. It is very important the (A) the cross-section of the airfoil is exactly as shown in the diagram below (or scaled up), (B) that the airfoil is smooth and (C) that all the airfoils have the same mass and volume. Measure and check these both. Super glue the straws to the airfoil at different angles. These angles are 0 degrees, 5 degrees, 10 degrees, 15 degrees, 20 degrees, and 25 degrees from the wind- facing side of the airfoil.

Experiment Procedure

Start up the desk fan at its highest speed. Measure the wind speed with a reader. Record this data. This is the velocity. Place airfoils in the wind tunnel, with rods in the

middle, so that the airfoil can slide up and down without moving forward or backward. Attach the string from the force reader onto the airfoil. It should initially read a positive force, just because gravity is pulling the mass of the airfoil down. Start with the airfoil with the angle of attack of 0 degrees. Start the desk fan again and re-read the wind speed to make sure it is still the same. Read the force meter, record the change in force. Repeat steps 2 through 5 for the next 5 airfoils.

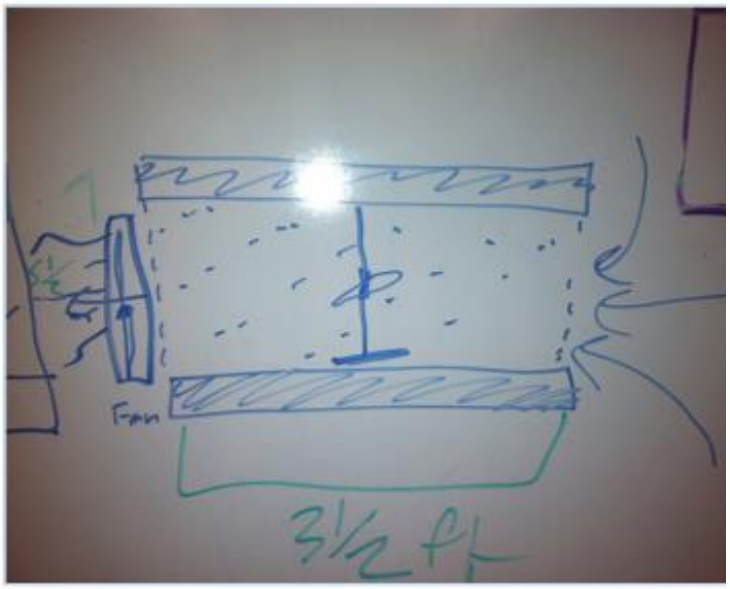

Figure IX- Early Sketch of Wind Tunnel Airflow

Table 1: Angle of Attack v Lift (n)

	T1 Lift (n)	T2 Lift (n)	T3 Lift (n)	T4 Lift (n)	T5 Lift (n)	Ave Lift (n)	% uncertainty
0	.004221	.004363	.005205	.0053	.006416	.0051008	43.03%
5	.0137	.01391	.01298	.01067	.01135	.012522	25.87%
10	.02174	.02429	.02375	.02797	.02723	.022499	27.69%
12	.03325	.03428	.03538	.03226	.0325	.033534	9.30%
15	.0037	.003701	.0029	.0025	.00225	.00301	48.2%

Table I- Results Table

Angle of Attack v. Lift Created

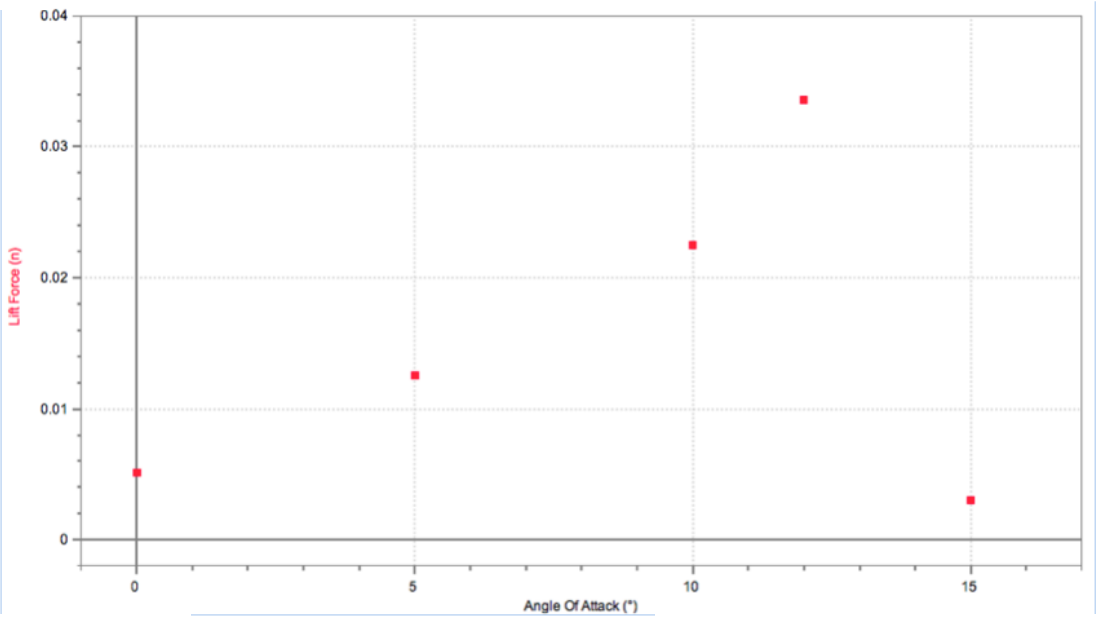

Figure XI

Figure XII-Expected Results Graph (*Aviation_History.com*)

Analysis

Table I is the results table. This is where the data was recorded, and from which the later graphs were made. Figure I demonstrates, the amount of lift created by the airfoil as the set angle of attacks varied. Notice that Figures I and III have similar shapes, with a steadily increasing slope until reaching a point of stall. The airfoils lift created increases at about 0.002223newton/degree of Angle of Attack, excluding fifteen degrees, the stall point. Figure XI shows a % of uncertainty graph. While the total line of best fit is nearly horizontal and zero, it should be noted that until the fifteen degree angle of attack point, the percent of uncertainty steadily decreases. It can therefore be concluded that as more lift is created, the airfoil steadies and experiences less turbulence.

Conclusion

The hypothesis of this paper is if the angle of attack increases, so will the lift produced. This hypothesis should be accepted because the data correlates to this. Figure X, the graph of results, suggests this because it has a positively increasing slope until it reaches a certain angle of attack, when the production of lift completely stops, much like the expected graph, figure XII. NASA agrees, it says that as the angle of attack affects the amount of lift created, and that when wing stall occurs all lift production completely stops (Benson, N.a). The percent uncertainty, as shown by Figure XI, decreases as more lift is created, until it reaches stall. This uncertainty is likely caused by disturbances in the linear airflow through the wind tunnel. Despite those effects, it was clearly demonstrated that the lift force does increase as the angle of attack is increased until the stall point.

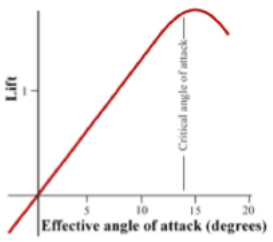

Figure XII-Expected Results Graph (*Aviation_History.com*)

Work Cited

Benson, Tom . "Geometry Definitions."*NASA*. N.p., n.d. Web. 23 Jan. 2013. <http://www.grc.nasa.gov/WWW/k-12/airplane/geom.html>.

Benson, Tom . "Modern Lift Equation." *Re-Living the Wright Way -- NASA*. N.p., n.d Web. 27 Jan. 2013. <http://wright.nasa.gov/airplane/lifteq.htm>

Benson, Tom. "Inclination Effects on Lift." *NASA - Title...*. N.p., n.d. Web. 27 Feb. 2013. <http://www.grc.nasa.gov/WWW/k-12/airplane/incline.html>.J. (n.d.). Which angle of attack generates the most lift. *The Complete Handbook of Science Fair Projects*, 41.

Jakab, Peter. "The Wright Brother Designing the 1900 Wright Glider." *The Wright Brothers*. Smithsonian National Air and Space Museum, n.d. Web. 27, Jan. 2013. <http://airandspace.si.edu/wrightbrothers/fly/1900/designing.cfm>.

Lawrence, Harry. *Aviation and the role of government*. Dubuque, Iowa: Kendall/Hunt Pub., 2004. Print.

Reyes, C. (2009). *RCadvisor's model airplane design made easy: the simple guide to*

designing R/C model aircraft or build your own radio control flying model plane. Albuquerque, N. M.: RCadvisor.com.

Rosen, J. & Gothard, L. Q. Bernoulli's equation.In *Science online*. Retrieved from http://www.fofweb.com/activelink2.asp?ItemID=WE40&SID=5&iPin=EPS0313&SingleRecord=True

Abstracts of Papers

Presented at the Annual Meeting
Belmont University
Nashville, Tennessee
April 19, 2013

Water Turbidity Has No Effect on Pheromone Communications in Aquatic Flatworms

John Franklin Crenshaw and Kathryn Pickrell
Hume-Fogg High School, Nashville

Abstract

Many aquatic organisms communicate via alarm pheromones that alert nearby conspecifics to danger when an organism is damaged and releases the chemical into the water. This experiment was conducted to determine if water turbidity via soil impedes the alarm pheromone response in *Dugesia tigrina* –brown planaria. Planaria were tracked in petri dishes for twenty minutes, and the alarm pheromone was introduced at the tenth minute. The experiment was conducted with tank water as the control, and with soil added to create turbidities of 10, 50, and 100 NTU. After the introduction of the pheromone the planaria fled the area, although some returned after a few minutes. There was no statistical difference between the avoidance behaviors of the planaria regardless of the turbidity level. It can be concluded that high soil levels in water do not prevent the reception of the alarm pheromone.

The Long-Term Effects of Airport Runoff on Urban Stream Quality and Habitability in Nashville, TN

Jansen Gibson, Thomas Metke, Sabrina Brewer, Christian Vera
School for Science and Math at Vanderbilt, Nashville

Abstract

In 2010, aircraft deicer runoff from Berryfield Nashville Airport resulted in a large-scale fish kill, including the endemic Nashville Crayfish. The effects of this pollution were studied at three sites along Mill Creek that received direct runoff, and compared to an unaffected proximal urban stream. Electrical conductivity, pH, dissolved oxygen, and nitrate concentration were recorded weekly for six months. Macro-invertebrates were collected and subsequently quantified according to EPA rapid bio-assessment protocol guidelines. The three sites that received direct pollution had a less diverse macro-invertebrate population, and fewer pollution tolerant organisms. The unaffected site facilitated a bio-diversity of 7.2 species per 100

organisms identified, whereas affected sites ranged from 1.2 to 6.0. Dissolved oxygen was only significantly different from the control after flowing through a re-oxygenation site. Nitrate concentration and pH were higher in these sites, as predicted by the dissociation of ethylene and polypropylene glycol. Stepwise multiple linear regression models were generated to predict bio-diversity and pollution tolerance based on the recorded water chemistry values with R^2 values of 0.96 and 0.91, respectively.

The Effects of Temperature on Insect Activity During Flesh Decomposition

Chloe Kilpatrick and Emily McRen
Pope John Paul II High School, Hendersonville

Abstract

The decomposition rate of the human body, often heavily affected by temperature and insect activity, can reveal crucial evidence about a person's death, especially in crime scene investigation. Four bone-in pork shoulders were exposed to varying temperatures and decomposed in order to determine the effects of temperature change on insect activity in decomposing flesh. The difference in insect activity determined the speed of decomposition in the specimen. The samples' initial and final weights were compared after the pork decomposed for four weeks, and insect activity was noted each week. The end of the experiment yielded a more complete understanding of how temperature increases decomposition rate by allowing insect population to develop more quickly.

Determining Plant Species by Use of an Android Application

Reeta Bandypoadhyay, Angelica Coleman, Young-Hun Kim, and Brennan Steele
School for Science and Math at Vanderbilt, Nashville

Abstract

Considering the fact that many different species of plants in Tennessee are unidentifiable by laymen, this project had a goal of designing an Android application to identify native and invasive species by use of image processing. Fifteen leaves from six species were collected and a total of fifteen geometric measurements, both absolute and ratio, were taken from pictures analyzed in ImageJ. Using Mathlab, the accuracy of these measurements was tested with image analyses of random samples, and accuracies of lighting differences were also tested. An application skeleton was created using Java in Eclipse. After testing, indirect sunlight yielded the highest accuracy, while direct sunlight yielded the lowest accuracy. Japanese Honeysuckle was the most significantly different and easiest to identify. Ratio measurements also yielded higher accuracies than absolute measurements. Additionally, an application skeleton encompassing three main activities was successfully created. The lighting results can be

explained by the presence of shadows, and ratio measurements likely yielded higher accuracies because of their non-spatial characteristic. Future directions include incorporating the designed image processing routine tested in Mathlab into the functional Android application. The final results from this project will provide a simple method for producing high accuracy image processing and plant identification.

The Good and Bad Effects of Fertilizer on Sunflowers

Taylor Cook
Northwest High School, Clarksville

Abstract

As found both in previous studies and an experiment personally done last year, fertilizer does have an impact on the growth of flowers, and more specifically sunflowers. However, if the same experiment was done again, though in different conditions and not as individual flowers, would the results be the same? This simple question led to the testing of the sunflowers again. The three main elements involved in plant fertilization are nitrogen, for a greater vegetation yield, potassium or potash, for a greater seed yield, and phosphorous, for stronger branches. This experiment did better than one completed the previous year. The results were better than the previous year, but over all, they were similar as far as which group did the best, the worst, and the two groups in between. The main thing that seems to be different, though only slightly is that the second group had the least number of plants that sprouted, and the third group had a couple less leaves on average than the first group.

The Effects of Lithium Chloride on the Feeding Habits of the Elimia Snail

Victoria Dolan and Jordan Lee
Pope John Paul II High School, Hendersonville

Abstract

Organisms as seemingly insignificant as snails can hold great value for ecosystems everywhere. Snails are important for many freshwater habitats due to their status as a source of food for other animals and their ability to break down organic matter such as algae. However, the snail's importance in the freshwater ecosystem could be increased through this experiment. By evaluating the amount of lettuce, a food source for snails, eaten in proportion with the amount of lithium chloride present in the lettuce, can determine whether snails can be bio-indicators for lithium pollution. Testing five different concentrations of lithium chloride, the data concluded that the more lithium chloride present in the food source, the less the snails would eat. Lettuce laced with lithium chloride was weighed before and after twelve hours amount ten snails to

obtain this data. This inhibiting of the feeding by the lithium chloride would force snails in nature to migrate from the lithium polluted areas in order to find food. As a result, the absence of snails in an ecosystem could act as a bio-indicator for lithium pollution.

Water Quality in Selected Watersheds in Benton County, Tennessee

Sam Hedge
Camden Central High School, Camden

Abstract

I will conduct the following experiment in which I will analyze the water quality of the discharge from the Wastewater Treatment Plant along three different streams located within Benton County, TN. Ramble Creek is located in the northern portion of the county, Cane Creek is located in the central portion, and serves as the primary watershed of the City of Camden, and Eagle C reek is located in the southern portion.

This testing will be conducted on a bi-weekly basis at the Wastewater Treatment Plant and at two different locations per selected creek; one near the source and the other, closer to the mouth, for a period of twelve weeks from August 23, 2012 until November 1, 2012.

I expect to discover three things after completing this experiment. First, I hypothesize that each creek will be cleaner closer to its source. Second, I anticipate that Cane Creek, which runs through the most densely populated area of the county, will be more polluted than either Ramble or Eagle Creek. Lastly, that the overall water quality of the discharge from the Wastewater Treatment Plant will be worse than that of any of the three creeks which I will be testing.

Biomass to Biofuels: New Sources to Make Ethanol in the Place of Corn

Rachel Baker
Camden Central High School, Camden

Abstract

The hypothesis of this study is that there will be a viable alternative for corn in the production of ethanol biofuel. Multiple sources will be used to obtain a wide and accurate range of information. Information from other scientific studies will be used to obtain knowledge of the information presented and to compare results to eliminate any potential bias. The sources of this information will be shown in the project data book. Through research, information will be obtained from various sources. Additional information will be calculated from an experiment where carbohydrates (sugar and starch) and cellulose levels will be recorded on a spreadsheet

data base. This recorded information will show which biomass has the most energy potential to ferment into useable ethanol biofuel. The information from the experiment will be compiled with the various source researched on a separate spreadsheet. Corn will be studied and used like a control group since it is currently the most used biomass for ethanol biofuel. All data will be compared to corn. This will show if the biomass is a probable source. Switchgrass and sugar beets will be studied tosee which biomass has the most potential to create an efficient ethanol product.

The Effects of High Chlorine on the Five Senses

Jada Hampton
Cleveland High School, Cleveland

Abstract

The purpose of this study was to see how serious the effect of swimming in high levels of chlorinated water has on the five senses. During the experiments seven teenagers were tested at a competition pool at the YMCA of Cleveland, TN. Sight, hearing, and touch were the most significant. All senses showed significant correlation of negative effects of swimming in chlorinated water.

.